Design of a Separation Process for Recycling Tritium and Helium-3 Mixed Gas

A Thesis
Presented in Partial Fulfillment of the Requirements for the
Degree of Master of Science
with a
Major in Nuclear Engineering
in the
College of Graduate Studies
University of Idaho
by
Jordan M. Argyle

Major Professor: Richard Christensen, Ph.D.
Committee Members: David Arcilesi, Ph.D.; Michael McKellar, Ph.D.
Department Administrator: Richard Christensen, Ph.D.

December 2018

Authorization to Submit Thesis

This thesis of Jordan M. Argyle, submitted for the degree of Master of Science with a Major in Nuclear Engineering and titled "Design of a Separation Process for Recycling Tritium and Helium-3 Mixed Gas," has been reviewed in final form. Permission, as indicated by the signatures and dates below is now granted to submit final copies for the College of Graduate Studies for approval.

Major Professor:	_____	_____
	Richard Christensen, Ph.D.	Date
Committee Members:	_____	_____
	David Arcilesi, Ph.D.	Date
	_____	_____
	Michael McKellar, Ph.D.	Date
Department Administrator:	_____	_____
	Richard Christensen, Ph.D.	Date

Abstract

Tritium, a radioactive isotope of hydrogen, and its decay product, helium-3, have enormous market value. Both gases are used in multiple applications which require these gases to be periodically replaced. Often, tritium-containing mixed gases are treated as nuclear waste when replaced rather than recycled, requiring the costly production of new gas. This work investigates an economical, scalable approach to recycling a gas stream containing mixed tritium/helium-3. Separation methods are discussed generally, followed by an examination of specific methods effective for separating tritium. An apparatus and process for conducting this separation is detailed, and the results of testing that apparatus are presented. A discussion of how to avoid the problems encountered using the apparatus leads to an improved, new separation system design. Simulation shows that this new system will be capable of economical, scalable recycling of tritium and helium-3.

Acknowledgments

When I began to work on this document in earnest and was preparing to perform experiments, almost every aspect of my personal, family, and professional life simultaneously developed crises. I learned to rely on and work with others, and to let go of unnecessary things. My family and committee provided support and understanding that allowed me to complete this work.

I would like to thank my advisor, Dr. Christensen, for helping me brainstorm solutions to setbacks and continuing to believe in me throughout the project. I would like to thank Larry for sharing his expertise throughout the project, and overseeing the construction of the system in my absence. I would also like to thank Alice for her unwavering support.

Dedication

Dedicated to my sweet wife, Ellie, who not only patiently raised our children and kept our home from falling apart while I toiled at school and work, but also essentially packed up and moved our entire house by herself. She was and continues to be an inspiration to me, and I am blessed beyond measure to have her in my life.

Dedicated to my God, who has supported and continues to support us by being directly involved in our lives and our finances. The strength, wisdom, and understanding that He has imparted have been and will continue to be essential to my life. Without Him, I could not have finished this work.

Table of Contents

List of Tables

List of Figures

List of Acronyms

Ar	argon
DAQ	data acquisition
ESA	energy separating agent
H	hydrogen
^{1}P	protium
^{2}D	deuterium
^{3}T	tritium
He	helium
^{3}He	helium-3
LabVIEW	Laboratory Virtual Instrument Engineering Workbench
LN	liquid nitrogen
MSA	mass separating agent
MOF	metal organic framework
Pd	palladium
P&ID	piping and instrumentation diagram
SOP	standard operating procedure
TC	thermocouple
TPBAR	Tritium-Producing Burnable Absorption Rod
ZrCo	zirconium cobalt

Chapter 1: Introduction

Hydrogen and helium isotopes find many industrial and nuclear uses, and are vital for scientific research. While extremely abundant in the universe, neither element is particularly plentiful on Earth. This is especially true of two very rare isotopes: hydrogen-3, which is radioactive, and helium-3. This thesis addresses a means of separating hydrogen from mixed gases, with an emphasis on hydrogen-3 and helium-3 separation and recovery for recycling. A brief discussion of the value and uses of hydrogen and helium isotopes is presented, as the methods investigated are applicable to other mixed gas streams containing these isotopes. An overview of the rest of the thesis concludes this chapter.

1.1 Hydrogen and Helium Isotopes

The most abundant form of hydrogen (H) has only a single proton in its nucleus, written ^{1}H, and is referred to as protium (^{1}P). ^{1}P makes up about 99.98% of all H in nature, and about 75% of all matter in the universe. On Earth, it is mostly bound up in chemical compounds, including water and biological molecules. Over 50 metric tons (556 million liters[1]) are produced each year through a few different means, noted by Miller [1], and used primarily in chemical processes such as refineries [2]. Nuclear engineering applications of ^{1}P include as an ion source for accelerator experiments and as a means of slowing neutrons through scattering interactions; in addition, it is important in magnetic resonance imaging analysis.

Almost all of the remaining 0.02% of natural H has a proton and neutron in its nucleus, written ^{2}H, and is referred to as deuterium (^{2}D). While ^{2}D exhibits chemical behavior nearly identical to ^{1}P, the extra nucleon imbues it with significantly different nuclear properties, including much lower neutron interaction rates and a different magnetic resonance signature, with applications in chemistry, physics, biology, and nuclear engineering [3, 4]. The primary source of ^{2}D on Earth is water consisting mostly of ^{2}D (referred to as heavy water), which is extracted from ocean water utilizing the slight mass difference between deuterated and protiated water. ^{2}D is consumed on the order of tons per year by chemical production, research, heavy-water nuclear reactors, and other industries [5].

For nuclear applications, water containing almost entirely ^{1}P, referred to as light water, can be used in nuclear reactors to slow neutrons to energies where fission is more likely. However, light water also absorbs a significant fraction of the neutrons produced, requiring more fuel atoms in the core, which is typically achieved through fuel enrichment. While heavy water slows the neutrons less abruptly, it has an absorption probability over two orders of magnitude lower than light water, allowing for the use of natural uranium in the reactor. ^{2}D also has some advantages in nuclear fusion technologies.

A third isotope of H, with a proton and two neutrons in its nucleus (written ^{3}H), was discovered in 1939 at the University of California, Berkeley, due to its characteristic radiation release [6]. At the time, it was noted to release very short-range radiation as it decayed to a form of helium. It was created by bombarding $^{2}D_2$ gas with ions of itself. Later referred to as tritium (^{3}T), it was found to also be produced through other nuclear reactions, notably $^{1}n + {}^{6}_{3}Li \longrightarrow {}^{4}_{2}He + {}^{3}_{1}T$. Acting nearly chemically identical to the other H isotopes, and due to the low risk presented by the low energy (5.68 keV) radiation produced, ^{3}T was used as a tracer in biological and water-filled systems by substituting lighter isotopes of H.

[1] At 101.325 kPa and 0 °C, where 1 mole occupies 22.4 L. Note hydrogen is diatomic (H_2)

^{3}T has a half-life of 12.32 years, making it a useful means of providing small amounts of power to systems for around 20 continuous years. A prominent example of such an application was in self-illuminating indicators and exit signs used for emergency lighting in many buildings. These signs load around 20 curies (2.08 mg) of ^{3}T into phosphor-coated glass tubes [7]. As the gas releases beta (β) electrons, they strike the phosphor and produce photons, similar to how cathode ray tube television sets operate. Today, there are tens of thousands of these signs that have reached the end of their useful life, and now must be recycled to recover the gases inside or stored as radiological waste. They are replaced with new signs lit by electrical components (*e.g.*, LEDs) or which have a fresh loading of ^{3}T.

^{3}T and ^{2}D are also particularly useful in the study and application of nuclear fusion, both for peaceful power production and for nuclear weapons because it releases far more energy than other H reactions and has a higher probability of occurring (see Table 1.1). While peaceful power production is still in active research facing difficult scientific hurdles in controlling the reaction for an extended time, weapons require less careful control and were reduced to practice over 50 years ago. Weapon stockpiles have been drastically reduced since the end of the Cold War, reducing ^{3}T consumption for weapons applications. Fusion power research, on the other hand, is actively growing, and is expected to consume more ^{3}T in the near future.

Table 1.1: *Energy release and probability for various fusion reactions. The number of each reaction needed to equal the energy produced from a single ^{2}D-^{3}T fusion is noted in the last column [8, 9].*

Reaction	**Energy Release (MeV)**	$\sigma_{max}{}^a$ **(barns)**	$\epsilon_{max}{}^b$ **(keV)**	$\mathbf{E}_{D+T}/\mathbf{E}_{Reaction}$
p + p	0.42	4.4×10^{-25}	100*	41.90
D + p	5.49	–	–	3.21
D + D	4.03	0.096, 0.11^c	1250, 1750	4.37
D + T	17.6	5.0	64	1
T + T	11.3	0.16	1000	1.56
D + ^{3}He	18.3	0.9	250	0.96
T + ^{3}He	12.1 (51%), 14.3 (49%)^d; Average 13.178	–	–	1.45, 1.23; Average 1.34
D + ^{6}Li	22.4	–	–	0.79

a. Maximum measured fusion probability; * = no maximum given; – = no value of any kind given;
b. Center-of-mass energy where maximum probability occurs
c. Resulting in T + p, resulting in α + 2n
d. Resulting in ^{4}He + p + n; combined results of ^{4}He + D and ^{4}He + n + p

New ^{3}T production today is nearly exclusively performed in operating fission reactors through two major reactions. The first, ^{1}n + ^{2}D $\longrightarrow$ ^{3}T, occurs in heavy-water reactors when ^{2}D absorbs a neutron, and is currently the only commercial source of ^{3}T. A typical Canada Deuterium Uranium reactor (CANDU, the most widely used heavy-water design) can produce about 130 g (483 L) of ^{3}T per year. Extraction of ^{3}T from the heavy water requires processing at a facility dedicated to that purpose known as a Tritium Removal Facility [10]. Only two such facilities are in operation worldwide as of 2018. The

second reaction adds Tritium Producing Burnable Absorption Rods (TPBARs) containing enriched ^{6}Li into light-water reactors for 18 months of irradiation. While the exact amount of ^{3}T produced from each rod is not disclosed, it can be assumed to be less than 12 g per rod. This figure comes from the fact that the 2.8 kg (10,400 L) per year needed by the United States government to maintain its nuclear weapons cannot be fully met using 240 rods [11]. In addition to new production, significant quantities are recovered from retired nuclear weapons, and, combined with the production from TPBARs, will provide sufficient ^{3}T for the remaining weapons until around 2025 [12].

Approximately 23% of the known matter in the universe is made of helium (He) with all terrestrial He having two protons and two neutrons in its nucleus, written ^{4}He. Helium also has another stable isotope with two protons and one neutron, helium-3 (^{3}He), which is the decay product of ^{3}T. As an inert gas, He is useful for creating a local, non-reactive atmosphere, and is one of the best heat transfer fluids among elemental gases. It is also the coldest practical cryogenic fluid, with ^{4}He liquefying at 4.2 K (-270 °C) and ^{3}He at a full degree lower (3.2 K). Many scientific applications requiring extreme precision, such as superconductors and low-frequency-wave telescopes, utilize liquid He as a coolant, with liquid ^{3}He specifically being used for the most demanding applications [13]. ^{3}He also reacts with neutrons to produce ^{1}H and ^{3}T, generating a 764 keV gamma (γ) ray in the process. This allows ^{3}He to be a primary component of neutron detectors for security and accountability [11]. After the terrorist attacks in the United States on September 11, 2001, most of the global ^{3}He supply was consumed for neutron detectors positioned at ports and borders throughout America.

Global demand for all He is around 30,000 tons (168 million L) per year [14], while demand specifically for ^{3}He is around 10,000 L (1345 kg) per year, though this demand is highly erratic. On Earth, ^{4}He is produced primarily from the alpha (α) decay of radioactive elements such as uranium, thorium, and radium, and extracted from underground reservoirs, such as natural gas deposits, at a rate of about 80 billion L (10,800 tons) per year. ^{3}He is primarily produced from the decay of ^{3}T and has no natural terrestrial source. Both stable isotopes of He are currently in short supply with the shortage expected to become critical within 20 years unless some alternative production methods can be found [13].

This shortage has pushed the market value of these gases to extraordinary highs, with ^{3}He selling for between 100–2,000 USD/L (750–15,000 USD/g) and ^{3}T selling for as much as 81,000 USD/L (300,000 USD/g, 2017) [11]. An estimated annual ^{3}He demand of 8 kg (60,000 L) places the annual value of meeting demand at 6–120 million USD/year, and meeting the full 2.8 kg annual demand for ^{3}T would be worth 840 million USD/year. ^{3}T production has continued to be slow in recent years. After use it is frequently stored in a repository as radioactive waste rather than recycled. Since ^{3}T decays into ^{3}He, indefinitely storing ^{3}T is a waste of both of these precious gases. With the number of reactors capable of producing ^{3}T reduced by decommissioning, recycling has grown in importance for meeting demand.

Adding to shortages for regular use, ^{3}T and ^{3}He do not store well as the extremely small nuclei of these gases allow them to diffuse through metals and many other materials that would be used to contain them. Even though many processes that use these gases make efforts to recover these leaked gases, some amount is always lost. Because they are such light gases, once they are released into the atmosphere, they escape into space and are lost. They also tend to convert into other elements during normal use: ^{3}T is continually transformed into ^{3}He through radioactive decay, and ^{3}He is transmuted into ^{3}T when

used as a neutron detector. These slow, continual losses mean that new production is always necessary to allow for the gases to be regularly replenished for a given task, especially if a high purity of the isotope is required.

As previously mentioned, self-illuminating signs, such as building exit signs, are a meaningful possible source of ^{3}T and ^{3}He, with tens of thousands of these signs reaching the end of their useful lifetime each year. They are currently collected (at a fee of several hundred USD per sign) by a disposal company and buried as radioactive waste. Each sign at end of its life has approximately 0.675 mg of ^{3}T and 1.40 mg of ^{3}He, meaning large volumes of these signs would need to be economically processed to make recycling a viable means of meeting demand. Nearly pure ^{3}He with traces of ^{3}T can also be recovered from neutron detectors using the same means.

Additional future sources of ^{3}T include fusion work, advanced fission reactors, and increasing the number of reactors that process TPBARs. Of note, advanced reactors using lithium salts can produce sizable amounts of ^{3}T, currently considered by some to be a major problem. If a simple means of harvesting it could be devised that would also function well in these reactors, this "problem" could become an additional revenue stream for the reactor operators. If the separation methods prove flexible enough, it could benefit other sources of H, including high-temperature chemical reactors that must separate hydrogen from a complex chemical mixture. In short, a simple, largely passive means of removing H would benefit many industries, but the benefit would be most pronounced with ^{3}T recovery.

1.2 Purpose

The purpose of this thesis, and the project connected with it, is to investigate different low-cost, largely passive methods for ^{3}T/^{3}He mixed gas recycling with high recovery rates. A secondary purpose is to identify methods that would aid in separating any isotope of H from various production processes. A bench-top system implementing one or more of these separation methods will be described, and data from basic system validation will be presented. General research procedures will be discussed, as will the ease of creating a ^{3}He incubator that prevents significant ^{3}T leakage for the years required to make sizable quantities of ^{3}He.

Chapter 2 discusses different separations processes and their operational theory. Chapter 3 includes rationale for deciding on specific separation methods for testing and a description of the design process for a bench-top system to test those methods. Chapter 4 details the experimental setup and methods, explores the results of running the system, and discusses the lessons learned during this project, which are used to design an improved system for future use. The work concludes with Chapter 5, summarizing the significance of this research and detailing the experimental work that will need to be conducted in the future to verify the underlying principles.

Chapter 2: Separation Methods and Principles

"Separation" refers to a process by which individual components of a chemical mixture are extracted, typically with the goal of producing or removing at least one pure or useful component. Examples include the production of salt by evaporating seawater, the concentration of alcohol by distillation, and the cleaning of combustion exhaust by filtering particulates and scrubbing carbon dioxide before releasing the gas. While making a mixture of chemical species from separate chemical species (components) is a spontaneous process that requires no energy input, the separation of such a mixture is not spontaneous and does require energy [15]. Separation methods are measured by the purity of separation and the rate of separation. The preferred separation method for a given mixture is generally the process that requires the lowest energy input to obtain the highest purity product at the fastest rate.

Separation methods consist of independent steps, referred to as unit operations. While the parameters of a given unit operation will vary in specifics depending on the components of the mixture to be separated, the basic design principles, approach, and equations for the unit operation are always the same [16]. Unit operations exploit differences between the physical properties of the components in a mixture, which could include volatility, solubility, tendency to react to certain other chemicals, physical size, electric charge, response to external force fields, *etc.* A single unit operation often does not achieve an adequate degree of separation or result in the desired product, requiring repetitions of unit operations or inclusions of new ones. As a result, industrial separation systems are often complex and consist of dozens to hundreds of unit operations to perform the desired separation.

2.1 Types of Unit Operations Used in Separations

A separation system is designed to transfer mass between the different steps of the process. A basic mass transfer equation is generalized using words by Wankat [16] (Eq. 2.1).

$$Mass\ transfer\ rate = (reaction\ area) \times (mass\ transfer\ coefficient) \times (driving\ force) \tag{2.1}$$

The reaction area is typically related to the form of the separating agent, with strategies to increase this area including the use of porous materials or powders and performing reactions in gaseous form. The mass transfer coefficient is typically a property of the materials utilized in the unit operations. The driving force can be any energy imbalance, including concentration and pressure gradients, electric or gravitational fields, or chemical potentials, and can usually be actively controlled during the separation process (*e.g.*, if the driving force is a concentration gradient, the pressure of the system can be increased to increase the concentration and steepen the gradient). Because each unit operation transfers mass differently, an overview of the main methods will be presented that will follow the overview provided in the first chapter of Seader [15]. After this overview, methods specifically useful for hydrogen (H) separation methods will be explored in more detail. A summary of the separations method categories is provided in Table 2.1.

Table 2.1: *Summary of separation methods. Only a sub-set of these methods are useful for H/He separations.*

	Method	Unit Operations	Selection Criteria	How Achieved
1	Boiling/ Condensing	Partial condensation or vaporization, Flash vaporization	Species differ widely in volatility	Vapor condensed by removing heat or increasing pressure; liquid vaporized by adding heat or reducing feed pressure with throttling valve or turbine
2	Other phase transition operations	Drying, Evaporating, Crystallization, (De)Sublimation	Removal of solvents, purification, concentration, or fine control over phase transition cannot easily be otherwise achieved	Typically, the addition or removal of heat, though controlling the position of the heat transfer is especially important for crystallization
3	Pure ESA[a] distillation	Simple distillation	Application of Operation 1 does not provide sufficient separation	Multiple "stages" where counter-currently flowing liquid and vapor phases come in contact
4	Simple MSA[b] distillation	Extractive, Absorption, and Stripping distillation	Relatively small volatility difference between components of interest	Miscible MSA acts as a solvent increasing volatility or an MSA with high solubility for components is added to absorb it from the mixture
5	Complex MSA distillation	Azeotropic distillation, Liquid-liquid extraction	Vapor is difficult to condense or components of a vapor differ widely in solubility in a solvent	MSA becomes part of mixture, altering the volatility or other property of some component(s)
6	Porous membrane processes	Dialysis, Filtration	Mixture components differ widely in physical size	Fluid feed is introduced to one side of a membrane that prevents components larger than the membrane gaps from passing through
7	Nonporous membrane processes	(Reverse) Osmosis, Pervaporation, Gas permeation	Mixture components differ significantly in transport properties (*e.g.*, physical size, ionic charge, solubility, *etc.*)	Fluid feed is introduced to one side of a membrane that exploits physical properties of components to selectively transport them across
8	Sorption	Absorption, Adsorption, Ion exchange	Mixture components are at relatively low concentrations, and chemically interact with the solids	Mixture flowed through a bed of high surface area solids that selectively remove the components which interact with them
9	Non-electric fields	Centrifugation, Thermal diffusion	Mixture components respond differently to external forces	Force field is applied to the mixture either mechanically (*e.g.*, rotation) or by other means
10	Electric fields	Electrolysis, Electrodialysis, Electrophoresis	Mixture components either respond to electric fields differently, or can be ionized to different degrees	Electric field is applied to the mixture, altering how components migrate and causing separation

a. Energy separating agent (ESA); *b*. Mass separating agent (MSA)

2.1.1 Phase Creation or Addition

Additional phases can be created through the addition or removal of energy, which Seader calls an energy separating agent (ESA). Pure ESA unit operations include those that only result in phase changes, with partial vaporization, partial condensation, and flash vaporization (grouped as Method 1 in Table 2.1) being prime examples. Partial vaporization involves forcing some components of the mixture to boil, creating a gaseous phase. That vaporization can be achieved by adding heat or rapidly reducing the pressure to put some components of the mixture into a supersaturated state, leading to rapid boiling. In the case where the reduction of pressure is primarily used to cause the vaporization, the process is referred to as flash vaporization. Partial condensation is achieved by increasing pressure or removing heat to condense out components of a gas and create a liquid. These unit operations partition components of the mixture in inter-phase mass transfer, resulting in a vapor enriched with respect to the components more easily vaporized, and the liquid enriched with respect to less volatile components of the mixture [15]. Gravity is usually used to separate the denser liquid from the vapor.

Other processes that can be pure ESA include drying, evaporating, crystallization, sublimation, and desublimation (grouped as Method 2). These differ from the unit operations of Method 1 because these processes typically produce a relatively concentrated final product that can be directly extracted, rather than producing different phases enriched in one of the mixture components. For example, in drying, the liquid is evaporated, and the solids left behind are the desired product. In evaporating, the product is the vapor. In crystallization, the product is a solid that is removed from solution via cooling or evaporating the solvent. Sublimation and desublimation involve phase transition between gas and solid without a liquid phase. While these phase transitions can be achieved purely through the use of an ESA for some products, they often require the use of another chemical, usually acting as a solvent. These extra chemicals added to the process are referred to by Seader as a mass separating agent (MSA) [15]. MSAs are perhaps best understood in the context of distillation.

Distillation is the most widely utilized industrial separation process (Table 2.1, Method 3), and connects multiple repeated unit operations together, typically in a column. It is employed when a single unit operation does not separate the components enough, or multiple separation steps are needed. Each unit operation step, referred to as a stage, contacts counter-currently flowing liquid and vapor phases, producing a vapor that is increasingly enriched with respect to the more volatile species in the mixture as it flows up the column, while the liquid is increasingly enriched with respect to the less volatile species as it flows down [15]. Large sections of many textbooks on separation (*e.g.*, Seader [15] and Wankat [16]) are dedicated to the parameters of this process. Only a brief overview will be provided here, as distillation is not particularly useful for the separation of H and He.

In distillation, the feed mixture usually enters at a middle stage. The portion above the feed is referred to as the enriching or rectification section, while the portion below is referred to as the stripping section [15]. To ensure that both vapor and liquid are present throughout the process, some vapor is condensed into liquid (typically at the top of the column) called reflux and liquid is heated (typically at the bottom of the column) in a reboiler to produce a vapor termed boilup. However, if needed, boiling and condensing sub-stages (called interboilers and intercoolers, respectively) can be inserted into other

portions of the column to optimize product isolation.

When the volatility difference between the components is small, a MSA can be added that typically acts as a solvent to increase the difference. This process is called extractive distillation. For vapor that is difficult to condense or for capturing components of the vapor, a liquid MSA, referred to as an absorbent, can be added to dissolve components of the vapor. This process is called absorptive distillation. To separate liquid mixtures, a vapor MSA can be added that functions much like an absorbent in a process called stripping. These simple MSA distillation methods are grouped together in Method 4 of Table 2.1.

More complex MSA unit operations include azeotropic distillation and liquid-liquid extraction. In azeotropic distillation, the volatility of a component is modified by adding a MSA that forms an azeotrope with some components of the mixture. An azeotrope is a mixture that has the same proportions of components in the liquid and gas phases (*i.e.*, composition does not change when boiled), making it impossible to separate the components of the azeotrope by ESA distillation at constant pressure [17]. Since azeotropes often have lower boiling points than their individual constituents alone and because they have different boiling behavior, they are a useful method for extracting otherwise difficult chemical species [15]. Pressure changes or an MSA separation technique can usually be applied later to separate the components of the azeotrope. Liquid-liquid extraction is used widely when components of the mixture are not thermally stable, and uses MSA(s) as solvents to remove components of the mixture without needing to produce a vapor. These more involved MSA methods are grouped as Method 5 in Table 2.1.

While there are many variations of distillation tailored to meet the needs of thousands of unique separation processes, the overview above is sufficient for this work. Some difficulties that may be encountered in applying the above methods include:

- Considerable amounts of energy must be input, especially for phase transitional operations.
- Phase transitions can alter concentrations to the point where solubility limits are exceeded and components of the mixture can precipitate onto the equipment in the system. A common example is the scale and crud buildup in the flash vaporization of seawater. Such deposits can clog openings, alter flow paths, and hinder instrumentation.
- Nearly all MSAs add complexity to the separation process, as additional unit operations are required to separate the MSA from the desired product.
- Some MSA is lost from the system during operation and must be resupplied, adding another feed stream to the process. This lost MSA poses a contamination risk to the desired product, and increases cost.

However, MSAs make it possible to separate mixtures that otherwise could not be separated, and are an invaluable tool to separation engineers.

2.1.2 Barriers or Membranes

Membranes are thin structures with large surface area that allow preferential mass transfer [18]. The driving force for membranes is generally concentration or pressure gradients, though electric potential is also often used for ionic mixtures. They can operate on differences in the physical size of components, in which case they are termed porous membranes, or on differences in the solubility of the mixture

components in the membrane material, referred to as dense or nonporous membranes. Many membranes combine pore size with electric charge or other driving forces to enhance the membrane's ability to limit unwanted mass transport, referred to as selectivity.

Porous membrane processes (Table 2.1, Method 6) include filtration and dialysis. Filtration employs pores or gaps in a membrane to allow molecules smaller than the pore size to pass through, and prevents molecules larger than the pore size from passing. Filtration can range from scales large enough to only retain large particles in the mixture to small enough to operate on individual molecules. When retaining molecules 20 to 10,000 nm, the process is referred to as microfiltration, from 1 to 20 nm as ultrafiltration, and down to 0.1 nm as hyperfiltration. For reference, sodium atoms have an effective molecular radius of 0.1 nm, sucrose of 0.44 nm, hemoglobin of 3.25 nm, and a human hair is 45,000 nm in diameter [19]. Occasionally, the atomic spacing in crystalline solids are utilized like a filter. Referred to as molecular sieves, they perform a molecular sieving unit operation and are not considered to be part of filtration unit operations in the literature. Dialysis is similar to filtration, in that larger components of the mixture are held back due to pore size. However, dialysis also utilizes a concentration and pressure gradient to pass small solute molecules through the pores or gaps in the membrane, leaving the insoluble and nondiffusible particles behind.

Nonporous membrane processes (Method 7, also called dense membrane processes) include osmosis and reverse osmosis, pervaporation, gas permeation, and liquid membranes. Osmosis, like dialysis, utilizes concentration gradients, but functions across a semi-permeable membrane that operates using principles beyond simple component size filtration. The most common additional selector is ionic charge. Reverse osmosis utilizes pressure to force mass transfer against the concentration gradient, thus transferring in a direction opposite of typical osmosis operations. Pervaporation is reverse osmosis, but components are transported after they are evaporated. This is one of the most effective means of separating azeotropic mixtures, and requires significantly lower pressures than reverse osmosis [15]. Liquid membranes can be formed from surfactant-containing mixtures at an interface between two fluid phases, or by filling the micropores of a membrane with a fluid. The liquid dissolves or allows the passage of specific components of the mixture, which then flow along the concentration gradient. Gas permeation is of most interest to H/He separation, and will be discussed in more detail below. In this process, specific constituents of a gas mixture are absorbed or dissolve into the membrane, and can diffuse through it along a concentration gradient.

2.1.3 Solid Agents

Solids used in separations usually take a granular, powdered, or porous packed form to maximize surface area (see Eq. 2.1). They are either the active separator themselves or act as an inert support for a thin layer of the separating material. They selectively absorb, adsorb, or react with components of a fluid mixture, binding them while allowing other components to flow through. These processes are collectively referred to as sorption (Table 2.1, Method 8).

Sorption involves a chemical interaction between the solid and component(s) of the mixture in which the component(s) form chemical bonds with and are immobilized by the outer surface of the solid. In **ab**sorption, the immobilized species is able to diffuse into the bulk of the solid to form a solid solution

and/or causing phase transitions throughout the solid, while in **ad**sorption, the immobilized species does not meaningfully diffuse into the bulk and is confined to the surface. It should be noted that liquids can also be used as an absorbent. Adsorbents are usually employed to remove components at low concentrations. Ion exchange is similar to adsorption, but also involves an ionic exchange reaction where an ion is stripped from the exchange medium and replaced with an ion in the mixture that has a higher charge affinity. Sorbents eventually saturate, and need to be regenerated to again become active. The regeneration removes the captured molecules, and reverts the sorbent back to functional form. For ion exchange sorbents, this is accomplished by flushing the medium with a concentrated solution of the original ion. For non-ion exchange sorbents, one of four methods is typically employed:

1. Vaporizing sorbate with hot purge gas, referred to as thermal-swing adsorption;
2. Vaporizing sorbate by reducing pressure, known as pressure-swing adsorption;
3. Stripping sorbate with an inert purge gas without requiring a temperature or pressure change; and
4. Displacing sorbate using a fluid containing a more strongly adsorbed species.

2.1.4 External Field or Gradients

Differences in how components of the mixture interact with force fields can be exploited to cause separation. Centrifugation, for example, artificially increases gravity by rapidly rotating the mixture to separate components by mass. Thermal diffusion applies a temperature gradient to change fluid densities and concentrations, leading to molecular diffusion. Other force fields, including magnetic fields, can also be used. These are grouped together as Method 9 in Table 2.1.

There are several methods developed using electric force fields. Electrolysis decomposes molecules by passing an electric current through them with the best known example being water which breaks down to gaseous hydrogen and oxygen ($2\,H_2O_{\,(l)} \longrightarrow 2\,H_{2\,(g)} + O_{2\,(g)}$). Electrodialysis uses membranes that carry a fixed charge, preventing the migration of components of a like charge. Electrophoresis applies an electric field to the mixture and exploits the varying migration speeds of different components. Positively charged species migrate to the cathode, while negatively charged species migrate to the anode. Additional MSAs can be added to change how individual species behave, leading to a versatile process. These electric field processes are grouped as Method 10.

2.2 Hydrogen Separation Techniques

Of the methods presented above, only a subset are useful for extracting H and separating tritium (^{3}T) and helium-3 (^{3}He) mixed gases. In particular, membrane, pressure- and temperature-swing adsorption, and cryogenic separation methods are employed (cryogenic distillation is a variant of Method 3 from Table 2.1) [20]. These three will be discussed below as they pertain to H separations. Though other exotic options, such as laser-induced separation exist [21], they will not be discussed here as they are not currently commercially viable. Additionally, research investigating the behavior of protium (^{1}P) and deuterium (^{2}D) also applies to ^{3}T, as the isotopes of H chemically behave in nearly identical ways. The primary chemical difference between the isotopes is reaction rate, as the isotopes differ in size.

2.2.1 Membrane Separation

Membranes transport mass using a combination of five basic principles, illustrated in Fig. 2.1:

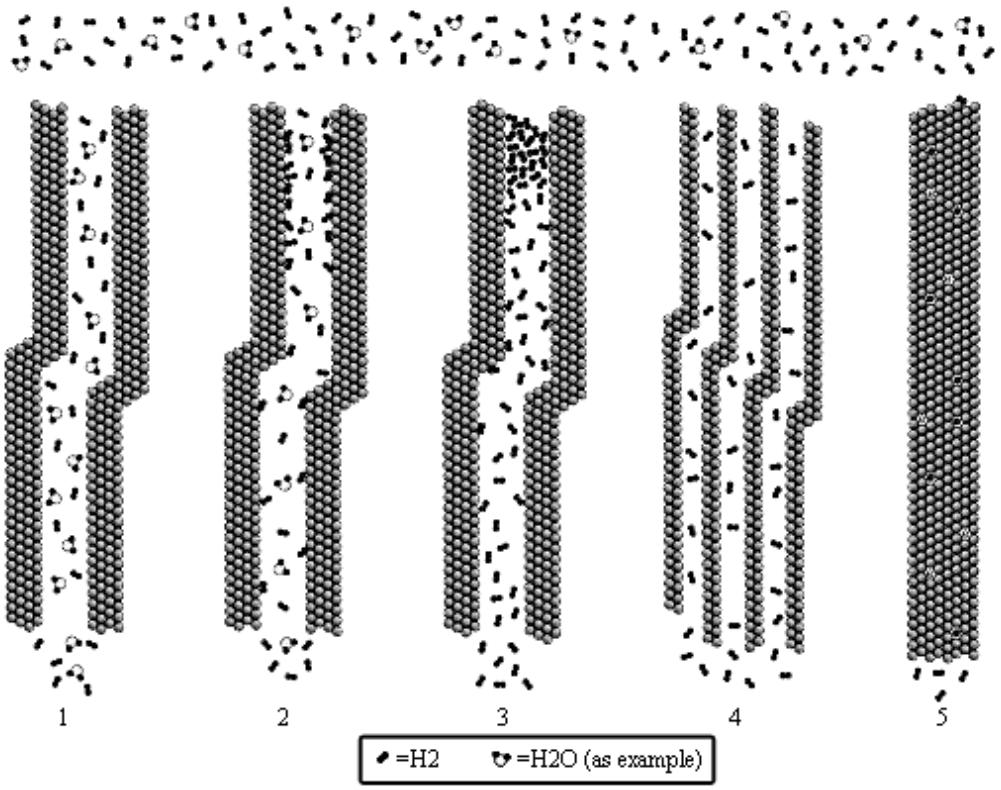

Figure 2.1: *Illustration of the main five H membrane separation mechanisms: (1) Knudson diffusion, (2) surface diffusion, (3) capillary condensation, (4) molecular sieving, (5) solution diffusion, after [22].*

1. **Knudsen diffusion**—interaction with the membrane wall. The diameter of the pore is smaller than the mean free path of the gas to be separated, so the molecules interact with the wall more than other gas molecules. If the pores are rough on a molecular level, or the molecule chemically interacts (adsorbs) to the wall, the speed of diffusion can differ greatly from diffusion reacting mostly with other gas molecules (*i.e.*, from Brownian motion) [23].
2. **Surface diffusion**—adsorption and inter-solid transport on the surface. Different molecules can be adsorbed into the surface and be transported through the solid. The molecules have low solubility in the membrane material, and are transported via thermal motion to the other side of the pore due to concentration gradients. Quantum tunneling effects have also been demonstrated [24].
3. **Capillary condensation**—formation of liquid in the pore. The vapor-phase particles adsorb the walls of the pore to form a base layer that attracts additional incoming vapor particles until a meniscus is formed at a liquid-vapor interface across the pore. Because the interactive forces (*e.g.*, van der Waals) between gas molecules are higher in the confined space of the pores, this condensation occurs below the saturation temperature [25].

4. **Molecular sieving**—size-exclusion principle. Components of the mixture smaller than the size of the pores in the membrane can pass through the pores, while larger components cannot pass. This largely mechanical process depends on the molecular kinetic diameter, which is a representation of the effective size of the atom or molecule as it interacts with other atoms. The kinetic diameter is typically larger than the atomic/molecular radius because it measures electron cloud interaction range [26].
5. **Solution-diffusion**—transport through the solid bulk. This transport depends both on the solubility and the mobility of the molecule in the solid. Similar to surface diffusion, it is typically related to thermal motion and is influenced by quantum effects [27].

Membrane performance is most often discussed in terms of flux and selectivity. Flux, written with the symbol J, is the total transport of a component through the membrane, measured in mass or mole per unit time per unit area (*e.g.*, $\mathrm{mol\,s^{-1}\,m^{-2}}$). It is governed by Ficks' first law:

$$J_H = -D_H \nabla C_{(x,\ y,\ z)} \tag{2.2}$$

where D_H is the diffusion coefficient for H and the differential vector operator acting on the concentration, $\nabla C_{(x,\ y,\ z)}$, is the three-dimensional equilibrium concentration in Cartesian coordinates, which, because we are mainly interested in the steady-state flux across the membrane itself, simplifies to a single dimension [22]. Permeability to component i, written ρ_i, is a fundamental material property that is unaffected by thickness and takes the form of the Arrhenius equation:

$$\rho_H = K\ e^{-(E/RT)} \tag{2.3}$$

where K is the preexponential factor constant (dependent on material), E is the activation energy, R is the gas constant, and T is the absolute temperature [27]. Selectivity, or separation factor, is the ratio of how much of two different components transport through the membrane, and is defined as:

$$\alpha_{i,j} = \frac{\rho_i \Delta P_i / P_i^f}{\rho_j \Delta P_j / P_j^f} \tag{2.4}$$

where $\alpha_{i,j}$ is the separation factor of component i from j, $\rho_{i/j}$ represents the permeability for the components, and $\Delta P_{i/j}$ is the difference in partial pressures of each component between the feed (retentate) and product (permeate) sides of the membrane ($P_{i/j}^f - P_{i/j}^p$) [22].

The design of a typical membrane test system is illustrated in Fig. 2.2. Distinguishing features include an internal vessel (blue walls) capped by a membrane that is fed with a to carry any transported gas to a chromatograph to determine concentrations. A feed gas charges the outer vessel (red walls). Any gas that escapes the outer vessel enters a third vessel (black walls), through which a purge gas is flowing to prevent the buildup of H outside the main vessel. The vessels are inside a furnace to provide the energy necessary to accelerate transport through the membrane. Pressures across the membrane are controlled by sweep gas flow rate and the pressure of the feed gas.

Membranes can be classified by their construction material, since their mode of operation (and,

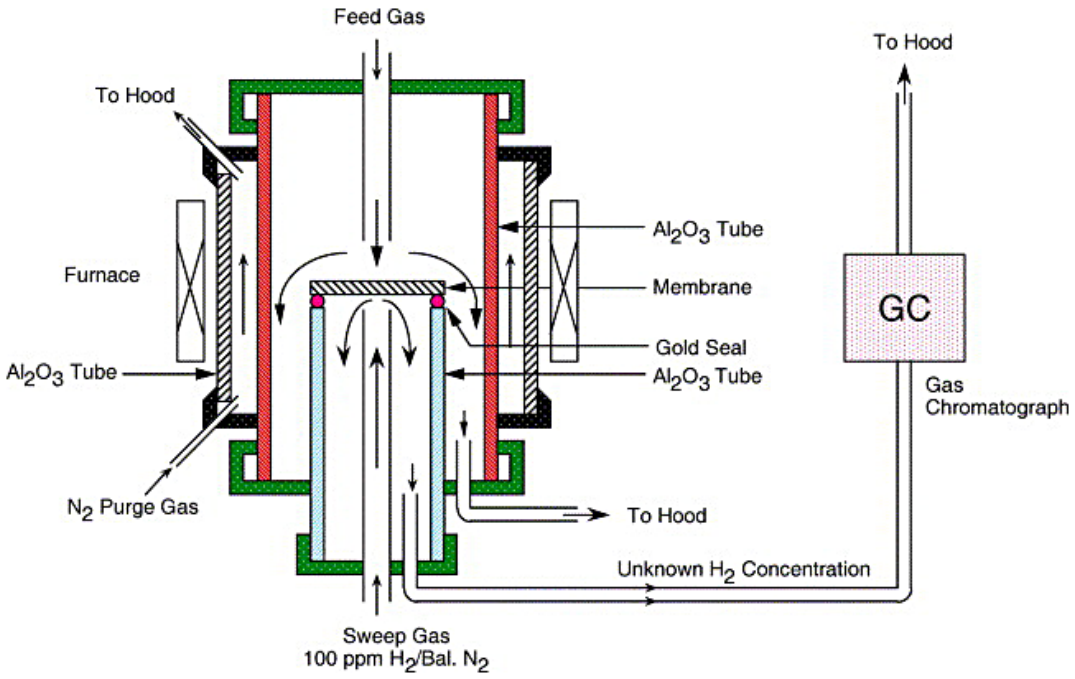

Figure 2.2: *Diagram showing a typical setup for a laboratory-scale system for testing membrane performance; drawing from [28].*

therefore, governing mathematics) is different for each material. Of these materials, metallic membranes are the most well-studied, thus more effort will be devoted to their explanation.

2.2.1.1 Metallic Membranes

Metallic membranes are typically dense sheets or films of various pure metals and alloys through which H can diffuse. Pure metals with particularly high solubility and permeability include palladium, vanadium, niobium, tantalum, β-phase titanium and β-hafnium. Pure metals usually suffer from changes in chemical structure and unit cell dimensions as they form hydrides, causing damage over time. Alloying elements such as aluminum, cobalt, chromium, gallium, or molybdenum have been shown to mitigate these changes and improve long-term performance of many of the permeable pure metals [29]. Metallic membranes offer high selectivity, as larger molecules cannot diffuse through them, and can be operated at higher temperatures which further accelerate H transport. The fundamental transport mechanisms involved are illustrated in Fig. 2.3.

Because the concentration in gas is strongly correlated to pressure for non-porous membranes, and because mass trasport through a membrane is only concerned with one spacial dimension, Eq. 2.2 can be simplified to Sievert's law:

$$J_{H_2} = \frac{\rho_{H_2}(P^n_{H,feed} - P^n_{H,perm})}{L} \tag{2.5}$$

where L is the membrane thickness [27]. The exponent n, referred to as "the n value," relates the dependence on pressure. If the rate-controlling step is the bulk metal diffusion of atomic H, then an n

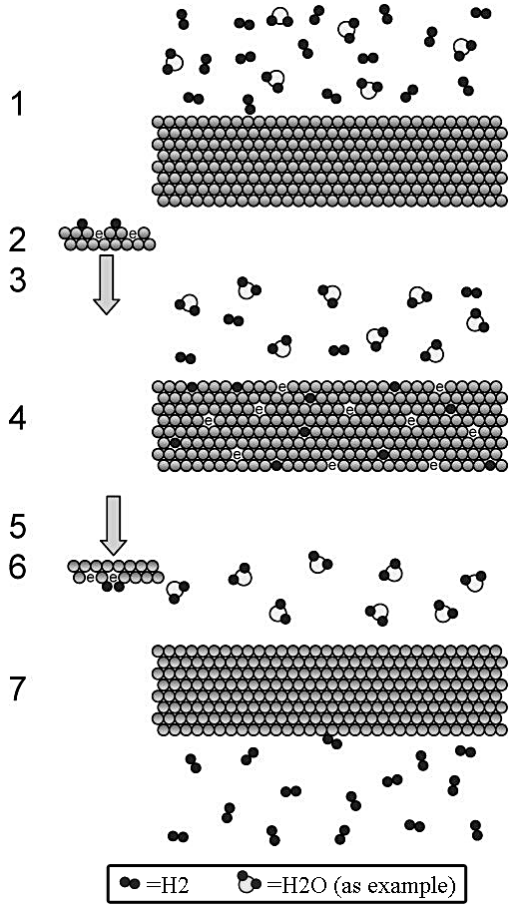

Figure 2.3: *The seven-step diffusion mechanism in dense metal phases: (1) movement of a mixed gas from feed stream onto the feed side of the membrane surface, (2) dissociation of H_2 into ions (H^{+1} and electrons, e^{-1}), (3) adsorption of H^+ ions onto membrane bulk, (4) diffusion of H^+ and e^- through membrane, (5) desorption of ions from membrane bulk to the membrane surface on the product side, (6) re-association of H^+ and e^- into discrete H_2 molecules, and (7) diffusion of H_2 from the membrane surface into product stream; drawing from [22].*

value of 0.5 is expected [30]. When the concentrations of the gases on the surface of the membrane are not known, Henry's law is used:

$$S = \frac{C_{gas}}{P_{gas}} \tag{2.6}$$

where S is a constant relating the vapor pressure of a nondissociative gas to its solution phase, C_{gas} is the concentration of the gas, and P_{gas} is the partial pressure of that gas.

Metallic membranes can be classified as pure (single element), crystalline, or amorphous. Pure metallic membrane properties are summarized in Table 2.2, and are a function of the lattice structure, lattice defects, and reactivity toward H or other components in the feed gas [22]. Membranes from palladium (Pd) have been studied extensively for H separation for various favorable characteristics, but as it is comparatively expensive (1–30 USD/g), greater interest recently has been placed on using the more abundant and less expensive tantalum (0.08–0.80 USD/g), niobium (0.025–0.30 USD/g), and vanadium

(0.30–0.60 USD/g, from [31]; for finished Pd, cf. [32]), among others. These metals suffer from slow dissociation/re-association, and so research has focused on modifying the surfaces to catalyze this reaction. Often, alloying the pure metals mitigates these problems.

Table 2.2: *Pure metal membrane interaction properties. Higher H solubilities and lower activation energies lead to higher permeation rates (H flux, J_H), while stable hydride formation leads to lower permeation rates and increased risk of embrittlement; table from [22].*

Crystal Structure	**Metal**	**Hydride Composition**	**H solubility (H/M @ 27 °C)**	**Hydride ΔH formation** ($\mathrm{kJ\,mol^{-1}}$)	**H permeability** ($\mathrm{mol\,m^{-1}\,s^{-1}\ Pa^{1/2}}$)
fcc[a]	Ni	Ni_2H	$\sim 7.6 \times 10^{-5}$	-6	7.8×10^{-11}
	Cu		$\sim 8 \times 10^{-7}$		4.9×10^{-12}
	Pd	PdH	0.03	+20	1.9×10^{-8}
	Pt	PtH	$\sim 1 \times 10^{-5}$	+26	2.0×10^{-12}
bcc[b]	V	VH_2	0.05	-54	1.9×10^{-7}
	Fe	FeH	3×10^{-8}	+14	1.8×10^{-10}
	Nb	NbH_2	0.05	-60	1.6×10^{-6}
	Ta	Ta_2H	0.20	-78	1.3×10^{-7}
hcp[c]	Ti	γ-TiH_2	$\alpha \sim 0.0014$	-126	
			$\beta \sim 1.0$		
	Zr	ZrH_2	< 0.01	-165	
	Hf	HfH_2	$\alpha \sim 0.01$	-133	
			$\beta \sim 1.0$		

a. fcc = face centered cubic; *b.* bcc = body centered cubic; *c.* hcp = hexagonal close packed

Further discussion of the most mature of the H separation membranes, Pd, is warranted, as any viable alternative material must at least meet its performance. Pd benefits from the ability to naturally catalyze the dissociation/re-association reactions of H at its surface, leading to H permeability as high as 2.2×10^{-5} $\mathrm{mol\,m^{-1}\,s^{-1}\ Pa^{1/2}}$ with α_{H/N_2} as high as 40,000 [33]. The permeability for a Pd membrane increases as temperature increases (see Fig. 2.4), with practical getting temperatures topping out around 900 °C [29]. However, it cannot survive extended use because its performance rapidly degrades when its surface is lightly contaminated. Additionally, as it is used and forms hydrides in its bulk, its unit cell lattice parameter increases from 0.3890 to 0.3895 nm for the α phase (0.13% increase) and to 0.410 nm for the β phase (5.4% increase). While this increase may appear small, it can lead to strain in the Pd and recrystallization that changes bulk and grain boundary properties.

Alloying elements have been added to improve these qualities, with silver and ruthenium demonstrating markedly improved performance in both solubility of H and mechanical properties, and copper and gold offering improved solubility and resistance to surface deactivation in the presence of contaminants

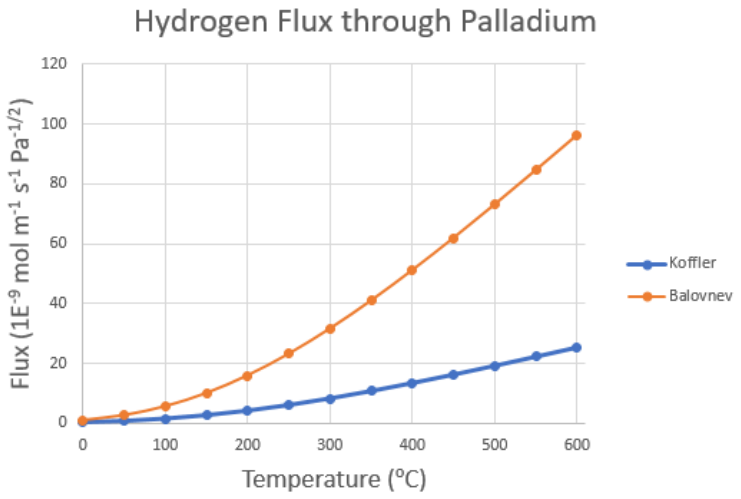

Figure 2.4: *Change in hydrogen flux through a Pd membrane from 0–600* °C*. Steward notes that the work of Koffler et al. seemed to be based on a more reliable data analysis and was therefore more preferred; equations noted in [29].*

[27]. Lessons learned from alloying Pd were carried over to alloying other metals as well. Alloys aim to maintain the body centered cubic structure in Group IV (zirconium, titanium, hafnium) and Group V (vanadium, niobium, tantalum) metals, as they are best suited to H permeation. Zirconium, molybdenum, ruthenium, and rhodium have been shown to suppress embrittlement, while copper, nickel, silver, and iron have been shown to reduce the negative effects of gas impurities (*e.g.*, H_2S, CO_2, and H_2O) [22]. The best performing, non-Pd alloy reported by Ockwig is $V_{85}Ni_{10.5}Al_{4.5}$ with a permeability of $5\text{–}7 \times 10^{-7}$ mol m^{-1} s^{-1} Pa$^{1/2}$.

While alloying has shown improvements in permeability and stability, the alloying elements also add possible interactions between the H and the chemical or structural defects they cause in the membrane and could lead to H trapping. The trapped atoms reduce total H flux and can degrade the alloy. One option to mitigate these problems for both Pd and other metal alloys is to create micrograin or nanograin alloys, as diffusion rates along grain boundaries are typically faster than through the grains themselves. Results have been mixed [22].

Another option for pure metallic membranes is to create an amorphous structure *i.e.*, a metal with a disordered atomic-scale structure. Amorphous metal membranes typically exhibit better mechanical and structural properties than crystalline membranes, and can be stabilized in alloy form, avoiding the need for defect-free film growth on the surface. In addition to better mechanical and corrosion performance, they also often exhibit higher H solubility. Such membranes are also much more flexible and homogeneous than their crystalline counterparts, making it easier to create catalytic surface coatings. Amorphous metal membranes, however, still require research, as none yet exceeds the performance of Pd alloys. Significant research has gone into developing these types of membranes; while they are still an area of active research, amorphous metal membranes will not be investigated further here (for additional information, see [22]).

Metal membranes, particularly Pd, are the standard for H separation. However, they tend to be

reactive to many types of molecules which potentially could be part of a mixture with H. Additionally, metal membranes generally suffer from degradation over time and often require costly materials in their construction, prompting the investigation of alternative materials.

2.2.1.2 Inorganics and Carbon

Inorganic membranes include combinations of silica, zeolites, oxides, and glass, with the most developed material options being silica and zeolites.

Silica membranes are easy to make, scale nicely, are inexpensive to produce, and are not susceptible to H embrittlement. They have a network of connected micropores approximately 0.5 nm in diameter and can accommodate separations of small molecules. They generally consist of a selective membrane layer connected to a structural support substrate via an intermediate layer [33]. Typically, a mechanically stable, porous, non-selective substrate such as aluminum oxide is chosen to provide structure to the membrane. The intermediate layer is made by dip-coating the substrate in nanopartical dispersions, typically of alumina, silica, or zirconia, followed by drying and calcination. This process is often repeated with graded particle size to form a uniform cover, as shown in Fig. 2.5. Then, the selective membrane is attached to the intermediate layer in one of two processes.

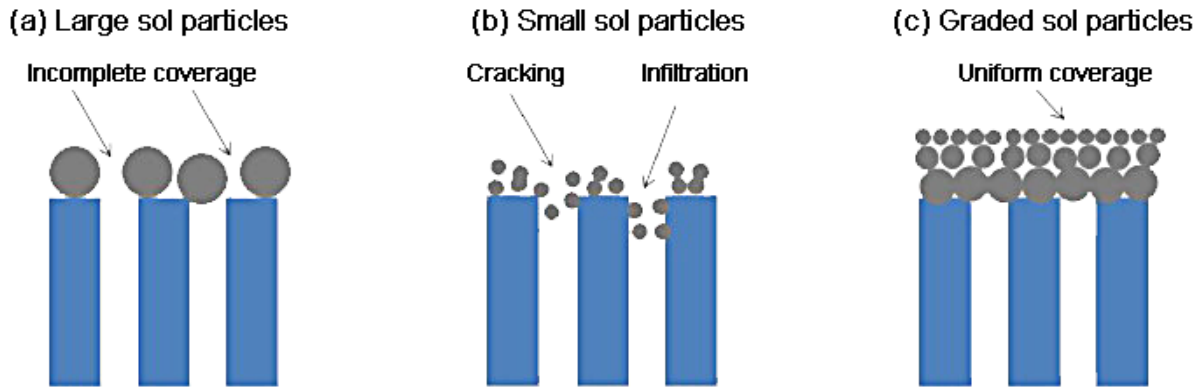

Figure 2.5: *Diagram showing why graded particles can achieve a uniform coating. The blue represents the porous metal with gaps on the surface. Attempts to coat the metal surface with the intermediate or membrane layers often result in pinhole leaks, gaps, or cracks in the coating as shown in (a) and (b). These coverage diagrams apply to both membrane attachment processes; drawing from [33].*

In the first, known as the sol-gel method, a colloidal silica solution is spread on a substrate, polymerized, and dried through careful control of pH, temperature, mixing, and time [33]. Chemical interactions between silicate monomers and molecules used in the solvent affect pore size, structure, and stability, making the chemistry as important as the processing. The second, more effective method is known as chemical vapor deposition. Reactive chemicals are vaporized and flowed past the substrate, gradually depositing on the surface. For both processes, inorganic oxides (*e.g.*, TiO_2, ZrO_2, Fe_2O_3, Al_2O_3, and NiO) have been added to improve the stability of silica membranes to steam. It should be noted that chemical vapor deposition of silica membranes have achieved a H_2/N_2 permeance ratio of 1,000, and another formulation achieved a H selectivity of 100% without loss of permeability [22].

Microporous silica membranes are low cost, offer high stability and high performance, but lack systematic studies of operational stability and will likely suffer from pores closing during use (referred to as densification), phase transformations, and structural disintegration at elevated temperatures and high steam pressures [33]. Because they contain ceramics, rapid pressure fluctuations will likely not be possible with such membranes. However, they do offer a promising non-metallic membrane.

Zeolite membranes, another inorganic membrane type, combine pore size and molecule shape selectivity with inherent mechanical, thermal, and chemical stability for a membrane that can be used in long-term separations [22]. Zeolites are inorganic framework structures made of TO_2 units where T represents an atom that can form tetrahedral structures (silicon, aluminum, boron, germanium, *etc.*). The shape and distribution of pores can be tuned by adjusting the number of T atoms in the ring that makes up the pore, accomplished by the choice of zeolitic phase(s). This tunability makes zeolites versatile molecular sieves, though viscous flow through the grain boundaries is another important transport method, as shown in Fig. 2.6.

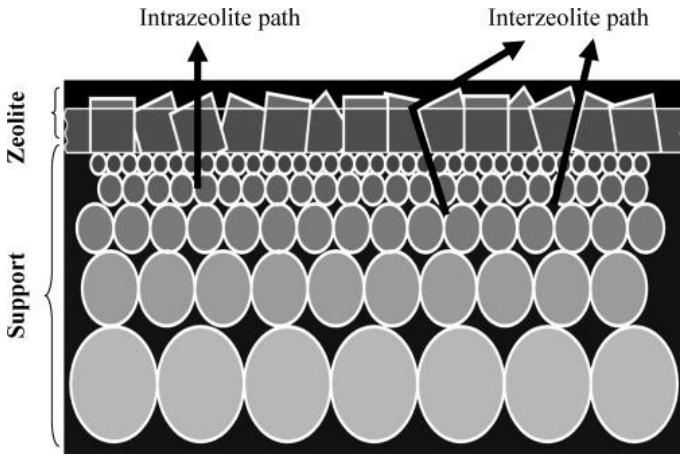

Figure 2.6: *Representation of possible permeation pathways through a zeolite membrane on a nonselective oxide support (e.g., Al_2O_3). The intrazeolite path consists of five steps: (1) adsorption from the feed stream to zeolite external surface, (2) diffusion from surface to inside of zeolite channels, (3) diffusion in zeolite channels, (4) diffusion from zeolite channel to external surface, and (5) desorption from external surface to gas phase. Interzeolite path is dictated mostly by gas component size. Not to scale; figure from [22].*

At present, it is difficult to exclude intercrystal pores in the zeolite films. When the intercrystal pores, also referred to as nonzeolite pores, are larger than the zeolitic pores, the membrane suffers a significant decline in separation efficiency [22]. The type of zeolite, the synthesis procedure, and the calcination conditions affect the number and size of such pores. Fig. 2.6 notes the steps of transport that are possible in zeolites, but the actual mechanism depends on the gas adsorption properties of the zeolite. If the gas does not adsorb, it may directly enter the pores of the zeolite from the gas phase. In such situations, smaller, highly mobile molecules tend to permeate at a much greater rate than the larger, less mobile molecules.

2.2.1.3 Other Membrane Types

Carbon membranes are H rejective membranes that are prepared from organic polymers that are converted to pure carbon by treatment at high temperature in an inert atmosphere [22]. Films, hollow fibers, and capillaries have been prepared. They benefit from the ability to finely adjust the pore dimensions and distribution by selectively adjusting the chemical pretreatment, using different precursors, and through simple thermochemical treatment [22]. Because of this, they make for useful molecular sieves. This fine tunability is important because it has been shown that different isotopes of H can be separated by molecular sieving [26].

Unfortunately, carbon membranes suffer from extreme brittleness and are 10–1,000 times more expensive than polymer-based membranes because they are primarily made from polyimide. Thus, much research is focused on improving their capabilities and substituting construction material for something less expensive (*e.g.*, polyacrylonitrile). These types of membranes are not ready for commercial applications.

Polymeric membranes can be porous or nonporous. Porous ones operate mostly on pore size diffusion, including Knudsen and surface diffusion, capillary condensation, and molecular sieving. Nonporous, or dense, polymeric membranes operate by solution diffusion. There are also ionic and ion exchange polymers, though those usually prevent H from crossing and selectively pass certain constituents, such as carbon dioxide.

The primary benefit of polymeric membranes is their low cost and great chemical flexibility. However, they generally have limited mechanical strength, are sensitive to deformation, cannot operate at temperatures much above 100 °C, and are susceptible to various chemicals which are often in mixtures with H. These weaknesses preclude the use of polymeric membranes for commercial H recycling.

2.2.1.4 Hybrids or Composites

The final category for membranes is hybrid or composite structures. This category includes metal-coated silica systems, cermet, and complex zeolites. Metal coatings on silica layers can utilize the selectivity of those metals through a very thin layer, and benefit from the transport properties of the silica system to produce membranes with many of the benefits of metal membranes at a much lower cost. Argonne National Laboratory produced several cermet (ceramic-metal composite) membranes expressly for high H flux and selectivity. Their membranes consisted of 40–50 vol% of metal or alloy dispersed in a ceramic matrix to achieve permeabilities as high as $5.36 \times 10^{-6}\ \mathrm{mol\,s^{-1}\,m^{-2}}$ [28]. They were Pd in Y_2O_3-stabilized ZrO_2. Synthetic zeolites have been shown to be able to separate isotopes of H (and mixed H_2 molecules, such as $^1P^2D$) via molecular sieving at cryogenic temperatures [26, 34]. Hybrid membranes are not commercially available, but hold promise to be a viable replacement for Pd membranes with comparable performance.

2.2.2 Adsorption Separation (Getters)

Membrane materials are capable of adsorbing H, though as a membrane the desired behavior is to transport the adsorbed H through the membrane thickness. Studies have looked at using this adsorption

for storing H instead, particularly for storing ^{3}T. Other materials, including heavy metals, binary alloys, carbon-based compounds, and metal organic frameworks (MOFs), have also been investigated, though currently metal- and metal alloy-based systems hold the most promise. When used for storage, these materials are referred to as getters. For most getters, metal hydrides are formed (MH, MH_2, or MH_3), binding the H. These hydrides are typically of lower energy, allowing the H to be liberated again by adding enough energy, generally in the form of heat. Each of the material groups will be briefly discussed in Sec. 2.2.2.2. However, the fundamental operation of all getter materials is largely the same. They immobilize H by one of two methods [35]:

1. By dissociative chemisorption of gaseous H and diffusion of atomic H in the solid matrix (absorption). For this process, the rate determining step is generally reported to be the internal diffusion or the growth and nucleation of the hydride phase (the β phase for getter metals).
2. By physical adsorption of H on the getter, forming a strong bond confining H mostly to the surface. The rate limiting step here is usually the dissociation of the H_2.

Both require appropriate temperature and pressure to operate effectively.

Getters are of interest for H separation because are capable of reversible uptake and immobilization of H isotopes by forming hydrides. This allows getters to store large amounts of gas in small volumes when compared to traditional H storage methods involving compressed gas or cryogenic storage. In most cases, if the getter has been properly prepared, the hydriding reactions require "tens of seconds" to acheive 70–80% completion, and are essentially complete within minutes [36]. When released, the H is typically of very high purity, making getters one of the least involved means of purifying the gas. The getters experience an effective H vapor pressure above them which, if maintained, allow the getters to continue to hold the H for years under proper conditions. For many getters, the vapor pressure remains low even at room temperature, while others require cryogenic temperatures for long-term storage.

As with any technology, there are some unfavorable features that must be designed for [35]:

- All known getters must be activated before they will capture H. This activation consists of exposing the getter material to high temperatures (typically 400–600 °C) under vacuum followed by H exposure at high pressure. The material must go through several hydriding cycles (charging with H and releasing it) before it is fully activated into a free-flowing powder that will readily adsorb H.
- Once activated, the powder not only adsorbs H, but also reacts with oxygen, nitrogen, moisture, oxides, and other species in side-reactions that can reduce or destroy the adsorptive capacity of the getter. These reactions can be reduced somewhat by treating the surface to make it more selective (*e.g.*, fluorination pretreatment with a KF solution or HF, a process shown to increase matrix surface area and increase reaction selectivity).
- As already discussed in Sec. 2.2.1.1 above, materials expand on hydriding, and upon dissociation can be left with altered adsorption and thermal conductivity properties, suffer decomposition, or segregate into separate elements. If a getter system fails to accommodate these changes, it could lead to large mechanical stresses on the bed walls, loss of effectiveness, and fine particulates dispersed throughout the system.
- While modeled on equilibrium conditions, in reality these conditions are rarely met, and the getters

typically adsorb less than models would suggest and do not release all that they have adsorbed.

- The hydriding reaction is exothermic, releasing large amounts of heat, and dehydriding requires large amounts of heat (around 30 $\mathrm{kJ\,mol^{-1}}$ [37]). For scale, in a study investigating requirements for getter use in vehicles, it was estimated that the getter beds would require 700 kW of cooling during the hydriding reaction, and would require similar heating rates for release [38]. For reference, the 700 kW needed for H capture or release is equivalent to 938 horsepower, meaning the release energy could not be supplied by a typical internal combustion engine. Larger getter beds would have higher heating/cooling requirements.
- Related to heating, getters function best as powders, which have very low effective thermal conductivities, typically in the range of 0.5–2 $\mathrm{W\,m^{-1}\,K^{-1}}$ [35]. The use of high conducting materials such as copper or aluminum balls or expanded graphite fibers as additives have been shown to increase the effective thermal conductivity to about 10 $\mathrm{W\,m^{-1}\,K^{-1}}$ [38], though they reduce the storage capacity by weight. Other methods include using high conducting metals as structural frames, flowing the gas to induce convection, and creating compacts with high conducting materials.
- Chemical kinetics are generally poor, and it is possible to form explosive reaction mixtures with oxygen and moisture.
- Even though they store large amounts of H in a small volume, the H to getter mass (referred to as gravimetric storage capacity) is low because the getters are significantly more massive than the H.
- Getters are currently very expensive and require difficult operating conditions.

The basic equations that are used to model this behavior are not as simple to generalize as for membranes, and will be presented below. Bhattacharyya performed a literature review, and simplified the equations using assumptions that were common among many researchers, noted below [35]. Table 2.3 lays out the necessary variables for understanding the equations.

Assumptions:

1. The gas and getter are in thermal equilibrium (*i.e.*, the same temperature for solid and gas).
2. The getter is isotropic and uniform (*i.e.*, thermal conductivity, density, specific heat, and porosity are the same in both radial and axial directions).
3. Gas behaves as an ideal gas, with density expressed as in Eq. 2.14.
4. Thermal properties of the solid do not significantly change with extent of hydriding.
5. The relationship between equilibrium pressure and temperature can be related through the Van't Hoff law (Eq. 2.15), and the kinetics of hydriding and dehydriding can be expressed through Arrhenius-type rate laws (Eq. 2.10 and 2.11 respectively), with constants specific to the getter and particular H isotope combination being considered.
6. Gas velocity in the porous region can be expressed by Darcy's law (Eq. 2.12).
7. Heat loss can be incorporated in the wall boundary condition by the use of an overall heat transfer coefficient when coolant temperature remains almost constant. Otherwise, the coolant requires a separate energy balance equation.

The system of equations below are used to model transport into a getter, including the reaction rate and the mass of H collected. Material balances for the gas and getter are followed by energy balance and

Table 2.3: *Nomenclature for getter equations; adapted from [35]*

A,B	Van't Hoff constants for equilibrium temperature-pressure relation, demensionless and K^{-1}, respectively	m_s	mass of the solid, kg
C(t)	density of the solid at any time, $kg\,m^{-3}$	P	instantaneous H pressure, Pa
C_{pg}	specific heat capacity of the gas, $J\,kg^{-1}\,K^{-1}$	P_{eq}	equilibrium pressure of H over metal hydride, Pa
C_{ss}	density of fully hydrided or saturated solid, $kg\,m^{-3}$	R	universal gas constant, 8.314 $J\,mol^{-1}\,K^{-1}$
d_p	diameter of catalyst, m	T	absolute temperature of gas/solid (see assumption 1 above), K
E_a	activation energy of the hydriding reaction, $kJ\,mol^{-1}$	T_s	absolute temperature of the solid, K
E_d	activation energy of the dehydriding reaction, $kJ\,mol^{-1}$	t	time, s
H	enthalpy of hydriding reaction, $J\,mol^{-1}\,K^{-1}$	V_s	volume of solid in the getter bed, m^3
K	permeability, m^2	v_g	superficial velocity of gas in the porous bed, $m\,s^{-1}$
k_a	frequency factor for hydriding reaction, s^{-1}	ϵ	void fraction in the hydride bed, dimensionless
k_d	frequency factor for dehydriding reaction, s^{-1}	μ	gas viscosity, Pa·s
k_e	effective thermal conductivity of the porous solid, $W\,m^{-1}\,K^{-1}$	$(\rho C_p)_e$	effective specific heat capacity of the H-metal hydride system, $J\,kg^{-1}\,K^{-1}$
M_g	molecular weight of H isotope, $g\,mol^{-1}$	ρ_g	gas density, $kg\,m^{-3}$
$\dot{m}$	reaction rate, $kg\,m^{-3}\,s^{-1}$	∇	differential vector operator $(\delta/\delta x,\ \delta/\delta y,\ \delta/\delta z)$

rate equations, which are followed by fundamental equations and laws used to obtain various parameters. The material balance for H is:

$$\epsilon\frac{\delta\rho_g}{\delta t} + \nabla\cdot(\rho_g\nu_g) = -\dot{m} \tag{2.7}$$

Material balance for the solid is:

$$\frac{dm_s}{dt} = V_s\dot{m} \tag{2.8}$$

The combined energy balance, based on assumption (1), simplifies to:

$$(\rho C_p)_e\frac{\delta T}{\delta t} + (\rho_g C_{pg})(v_g\cdot\nabla T) = \nabla\cdot(k_e\nabla T) + \dot{m}\Delta H \tag{2.9}$$

The rate equation for the hydriding step is:

$$\dot{m} = k_a \; e^{-(E_a/RT_s)} \; ln(\frac{P}{P_{eq}})(C_{ss} - C(t)) \tag{2.10}$$

and for dehydriding:

$$\dot{m} = k_d \; e^{-(E_d/RT_s)} \; (\frac{P - P_{eq}}{P_{eq}})C_{ss} \tag{2.11}$$

Darcy's law is:

$$v_g = -\frac{K}{\mu}\nabla P \tag{2.12}$$

where K, the permeability, comes from the Kozeny-Carman equation:

$$K = \frac{d_p^2 \; \epsilon^3}{150(1-\epsilon)^2} \tag{2.13}$$

Gas density from the ideal gas law is expressed:

$$\rho_g = \frac{M_g P}{RT} \tag{2.14}$$

Finally, Van't Hoff's law is:

$$ln(P_{eq}) = A - \frac{B}{T} \tag{2.15}$$

2.2.2.1 Design of a Getter System

The design of a typical getter test system is illustrated in Fig. 2.7. The full system has the getter in an inner vessel surrounded by a heater. A thermocouple sits in the powder to measure the powder temperature. This tank is valved off from other measurement instruments and reservoirs of feed gas. The close-up of the getter vessel shows filters, heat transfer mechanisms (copper blocks holding the powder and copper beads mixed into the powder), an inlet on the annulus outside the getter block, and an outlet through the center of the getter block.

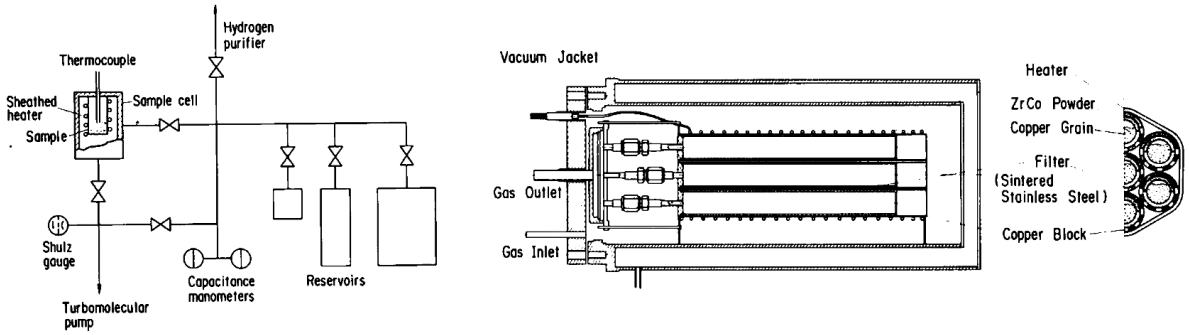

Figure 2.7: *Left: Diagram showing typical setup for a laboratory-scale system for testing getter performance. Right: Detail of the inner vessel design and loading; diagrams from [39].*

Bhattacharyya elaborated that getter beds are typically double containment to lower permeation

losses and to improve recovery of permeated hydrogen [35]. These vessels are typically stainless steel type 316L cylinders, and often include heat transfer (such as copper plates) and permeation barriers (such as oxide layers or coatings) to reduce permeation. Getter powder is typically confined between steel or ceramic screens with mesh/pore sizes around 2–5 µm. These screens allow gas access to the getter while trapping the majority of fine particulates generated by hydriding/dehydriding cycling of the getter, preventing system contamination.

Horizontal configurations typically have multiple tubes holding the getter arranged in an array, like in Fig. 2.7, while vertical systems are usually a getter vessel inside an outer vessel acting like a jacket. The annulus between vessels can be used to provide cooling by flowing an inert gas, or the heating from the exothermic hydriding reactions can be controlled by limiting the amount of H introduced at any one time. For long term storage, the annulus can be filled with another scavenger to further limit H gas escape. Often, the primary vessel is divided into sectors using copper strips, which helps ensure even loading and provides heat removal.

The beds are typically designed for a known amount of H, which will continue to be adsorbed until the equilibrium pressure (effective vapor pressure) is achieved. The size of the bed should be sufficient to allow for an even application of heat from heating rods, coils, or tape on the vessel. Total diameter should be large enough to accommodate ports for inlet, outlet, and instrumentation, generally placed on top of the closure. Vessel length and diameter ratios, which affect the total external surface area, are determined by the outer surface temperatures during charging and the heat produced via radioactive decay of ^{3}T (0.324 $\mathrm{W\,g^{-1}\,m^{-1}}$) [35]. ^{3}T inventory can be taken by passing an inert gas stream (generally He) through the bed, and measuring the temperature rise. If such inventory is to be done, additional ports for such measurements need to be accommodated.

2.2.2.2 Differences Between Getter Materials

The main classes of materials used as getters are heavy metals and their alloys, carbon-based materials, light metal alloys, MOFs, and zeolites. The differences between them are summarized in Table 2.4.

Heavy metal getters have been studied more than any other getter material for ^{3}T storage worldwide, especially transition metals and rare earths and typically in binary (AB, AB_2, and AB_5) or more complex alloys. The most widely used and studied getters, uranium and zirconium cobalt (ZrCo), are in this category and are considered reference materials. Other common materials include titanium, lanthanum nickel ($LaNi_5$), and binary compunds of zirconium (ZrFe, ZrNi). H uptake is generally spontaneous at ambient conditions, and release is within reasonable limits. However, they suffer from low gravimetric storage density (only 2–3% by weight) due to the mass of the metals used. Uranium powders are also pyrophoric, and can spontaneously ignite in air when specific surface area reaches 2 $\mathrm{cm^2\,g^{-1}}$, which occurs for spherical particle sizes below 1.59 mm (1/16 in) [40]. ZrCo has the closest performance to that of uranium, but is less difficult to handle. Uranium and ZrCo have an atomic H/getter ratio of about 3, while the same ratio for a Pd getter is about 0.7.

Hydrogen release temperatures range from a little over 100 to 850 °C. Metals (and nearly all getters) experience a hysteresis between hydriding and dehydriding, with the degree of hysteresis dependent on temperature and use history. They also exhibit the behavior where they can both capture and release H

Table 2.4: *Summary of the major advantages and disadvantages for using different getter materials for the capture and storage of H; table from [35]*

Material	Typical form	Advantages	Disadvantages
Metals	Uranium turnings/ powder	Fast kinetics, H uptake at ambient temperature and pressure possible with powder, favorable thermodynamic properties, widely studied and used for storage	Radioactive material, toxic, pyrophoric in powder form, susceptible to poisoning by O_2, N_2, large volumetric expansion on hydriding
	Titanium pellets/ sponge	No reaction with ambient air, much less pyrophoric compared to uranium, not radioactive	Relatively high regeneration temperature for H recovery, so suitable for long term storage, lower storage capacity compared to uranium
	Palladium powder	Not radioactive or pyrophoric even in powder form, relatively low regeneration temperature for H recovery	Low gravimetric storage density among metals, high cost
Metal alloys	Powder/Chips/ Pellets	Tunable H storage properties depending on metals present in alloy, wide variety of metal combinations can be used	Special synthesis techniques needed for each alloy
Carbon	Porous/Activated carbon, Nanotubes/Fibers	Opportunity of tuning storage properties by changing synthesis techniques and adding doping elements like palladium, recovery of H at ambient conditions possible	All usable forms have to be specially synthesized and treated, high pressure and cryogenic temperature of H needed to load appreciable amounts of H on carbon
Light elements	Chemical hydrides of nitrogen, lithium, aluminum, sodium, boron	High gravimetric density of H as compared to heavy metal based systems, property tuning possible and destabilization techniques can be applied to improve thermodynamic properties	Most compounds are thermodynamically too stable, very slow kinetics of hydriding and dehydriding, high temperature and pressure needed
Metal organic frameworks	Crystalline powder	High surface area and pore volume allow H to be physically adsorbed, recovery at ambient temperature possible, fast kinetics, durability over many cycles	High pressure and cryogenic temperature of H needed to load appreciable amounts of H, have to be synthesized specially, loss of surface area on exposure to air
Zeolites	Beads/Pellets	High surface area and pore volume allow H to be physically adsorbed, gas recovery at or above ambient temperature possible, much less expensive compared to any other material	High pressure and cryogenic temperature of H needed to load appreciable amounts of H

at a range of temperatures. Fig. 2.8 shows capture and release isotherms for ZrCo, demonstrating this effect. From that figure, it is also interesting to note that at and above 365 °C, the performance of the getter is severely compromised due to the thermal energy disrupting the hydride bonds.

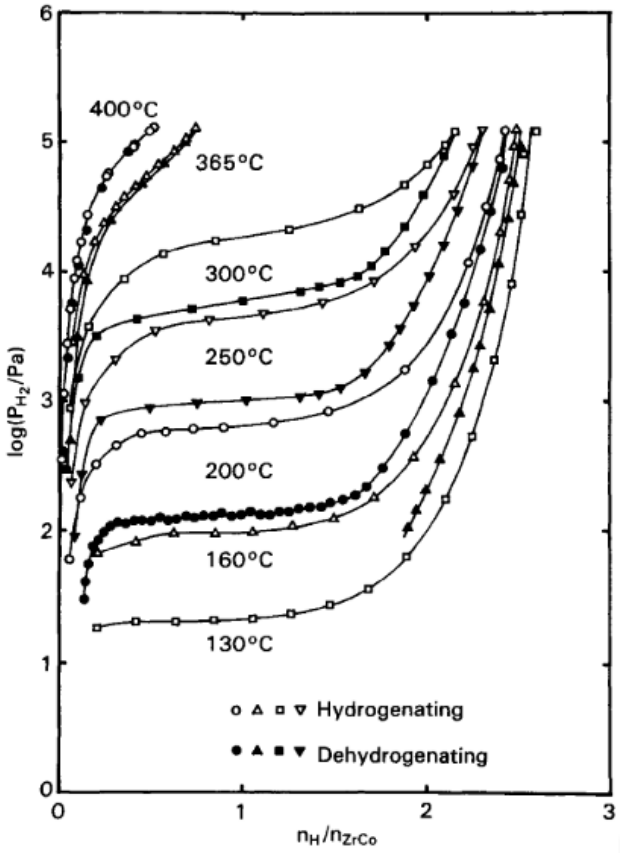

Figure 2.8: *The isotherms of the ZrCo-H system, including charge and release; chart from [41].*

Carbon-based getters include porous carbon, carbon nanotubes and fibers, and other structures. Nanotube banks are capable of condensing H to about 5–10% by weight; however, the results are difficult to reproduce. Variables affecting uptake include the structure (*i.e.*, single or multi-walled, fibers or ropes), the presence of other elements or doping agents (*e.g.*, lithium or potassium), and the manufacturing process used to make them. They can capture at room temperature, but require high pressures (1–10 bar) and exhibit higher storage capacities with higher filling pressures of H. Release temperatures range from 27–325 °C, depending on the nature of the nanotubes [35], perhaps limiting their use for H storage. Just as with carbon membranes, carbon-based getters also suffer from high manufacturing costs.

Activated carbon adsorbs H well, but performs best under high H pressures and temperatures around 77 K. It benefits from the fact that contaminant elements such as oxygen show only negligible effect on the getting efficiency. Activated carbon powder at 77 K is able to adsorb 1% H by weight at 1 bar of H, and 7% at 20 bar H.

Light element-based getters include nitrogen, boron, lithium, aluminum, and magnesium-based materials and are often referred to as chemical H storage materials or chemical hydrides. These getters

are most often investigated for use in onboard vehicle storage. While they have high H capacities, they form hydrides that are extremely stable, resulting in temperatures of 600–900 °C to dissociate them in the presence of a catalyst. They also store and release very slowly, limiting their practical use for a H recycling center.

MOF-based getters are capable of storing significant amounts of H by physically adsorbing them. They are porous compounds with metal ions coordinated with an organic molecule. They are tuned to have a large surface area because that area acts as the storage medium; however, an optimized surface area is 3100–4800 $m^2\,g^{-1}$. Values below this range reduce storage availability, and values above do not appreciably increase storage performance [35].

An example, $Zn_4O(BDC)_3$, where BDC is 1,4-benzenedicarboxylate, could adsorb up to 4.5 wt% of H at cryogenic temperatures and 1 bar pressure, and 1% under ambient temperature and 20 bar pressure. Their behavior can be further enhanced by adding metal ions (*e.g.*, Li^+, Cu^{2+}, Mg^{2+}), increasing the number of polarized links, and using smaller pore sizes. Because of these facts, the generally accepted mechanism for H uptake in MOF materials is the polarization of the H_2 molecule by the metals, followed by electrostatic stabilization [35]. A major problem with MOF getters is the cryogenic temperatures needed to maintain storage.

Zeolite-based getters are able to store H at high pressure (up to 900 bar) and high temperatures (up to 350 °C), which forces H into the zeolite's pores. Once inside, it remains confined even when cooled to room temperatures. This phenomenon, termed encapsulation, is highly dependent on the pressure, temperature, and nature of cations present in the zeolite framework [35]. Zeolites are also capable of physisorption at cryogenic temperatures (*e.g.*, 77 °C) when H pressures are low. Increased surface area corrilates well with increased storage capacity when physisorption is the dominant mechanism of H uptake [35].

2.2.3 Cryogenic Distillation

Cryogenic distillation separates the components of a gas mixture by exploiting differences in their boiling point. As an example, the process of cryogenic distillation for an air separation unit is illustrated below in Fig. 2.9. Feed air is pre-filtered to remove dust, then compressed, typically between 0.5–1 MPa, and passed through inter-stage coolers to remove water. This processed air is then passed through a molecular sieve to remove other impurity gases (*e.g.*, any remaining H_2O, CO_2, and hydrocarbons). The purified air is then passed to an integrated heat exchanger, causing some of the air to liquefy. The chilled, multi-phase fluid is fed into a cryogenic distillation column, which is further cooled by a separate device that either expands compressed air through a turbine or cools through other means.

Oxygen liquefies first, and is removed. As the temperature continues to drop, argon is liquefied, removed, and purified. The purification removes other liquefied gases in another distillation column until the desired purity is reached. Liquid nitrogen cools last of the three gases noted here, and is drawn off at the top of the column. High purity gases can be produced by boiling the liquids (*e.g.*, see the argon line shown in Fig. 2.9), or the remaining cold gases can be extracted and used to cool incoming air (*e.g.*, see the oxygen and nitrogen streams in Fig 2.9).

Table 2.5 outlines the temperatures that different gases liquefy and boil at standard temperature

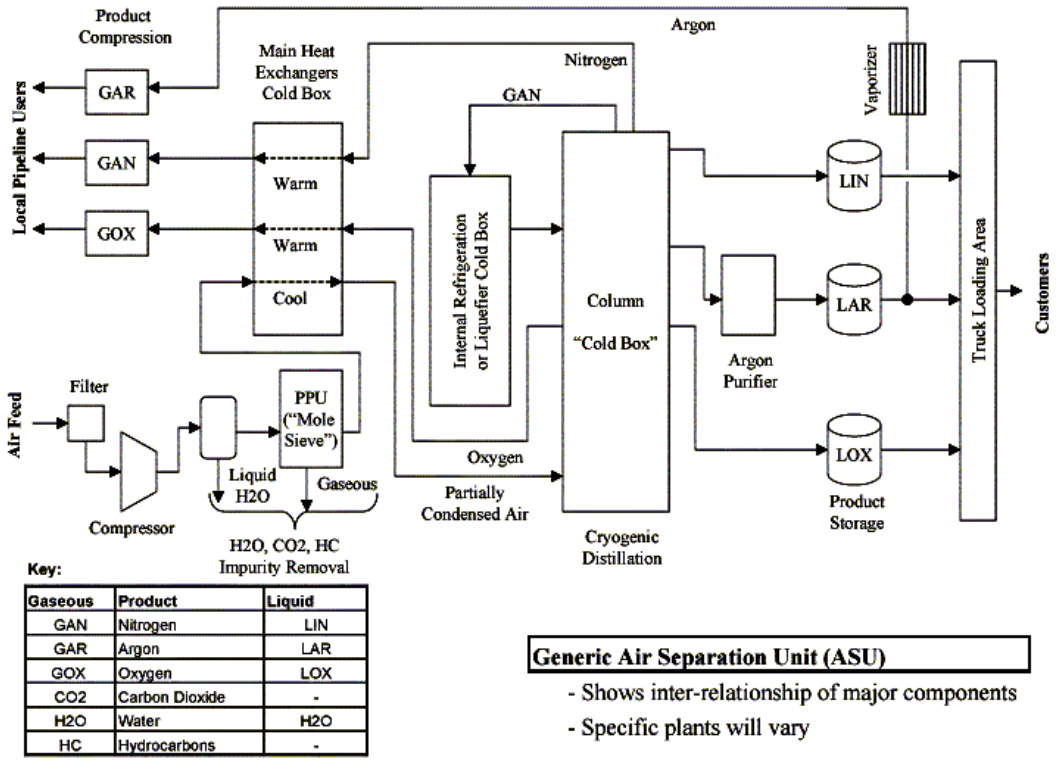

Figure 2.9: *Air is often separated by cryogenic distillation. The general process is depicted here for a typical gas distributor; drawing from [42].*

Table 2.5: *Summery of boiling points at standard pressure for different gases of potential interest sorted from lowest to highest; data from [43] (citation for page on ^3T; data for the other gases were obtained using the same service).*

	Boiling point	
Gas	(K)	(°C)
^3He	3.2	-269.95
^4He	4.23	-268.93
$^1P_2$	14.01	-259.16
$^2D_2$	23.67	-249.49
$^3T_2$	25.04	-248.12
N_2	77.36	-195.79
Ar	87.30	-185.85
O_2	90.19	-182.96

and pressure. The table is representative of a column in cryogenic distillation with feed coming in at the bottom. As previously stated, oxygen, with the highest boiling point, is removed first. Argon and nitrogen

are separated next as the mixture travels up the column. After they are removed, a mixture of H and He remains, which must be cooled significantly more before they can be separated. The differences between the isotopes of H can be a useful means for separating them. Note that pressure can be manipulated to shift the boiling point temperature of the components in the mixture, with the boiling point for different gases shifting by different amounts for the same pressure change. This can be utilized to increase the boiling point temperature gap between different gases, making separation easier.

2.3 Concluding Remarks on Separation

The material above outlines separation processes generally, as well as separation techniques specific to removing hydrogen. The purpose of the chapter was to provide the reader with an understanding of the options available for consideration in this project. As noted above, there are some other separations techniques that were not addressed here as they were not to be considered.

Chapter 3: Design of Separation System and Procedure

The original plan was to design a system that incorporates multiple separations processes that could separate a gas stream containing both hydrogen (H) and helium (He) to a high degree of purity. Over the course of two years, one separation method was spun off to a separate project with a slightly different focus, while the project covered in this thesis was eventually reduced in scope to include only a single separation method. This chapter discusses the design process for that system from method selection to final build, including necessary changes after assembly.

3.1 Determining Separation Methods to Use

The criteria used to select viable separation methods for this project included:

- Immediate deployability—evaluated by whether the necessary components are currently available for purchased from a vendor.
- Low cost as compared with other alternatives to keep the project within the established budget.
- High product purities—specifically, with H purities around 95%.
- Safety—the chosen methods needed to fit within the safety envelope set by the university.
- Small footprint—because the system would contain H, the entire system would need to fit in a laboratory chemical hood for the university-led experiments.
- Availability of comparable results—evaluated by how large the body of literature was for a method.

Of the three possible separations methods discussed in Sec. 2.2 for H and He mixed gases, cryogenic separation was immediately ruled out as an option. Even though the components can be readily sourced, such a separation system is large, complex, and beyond what could be supported by the available laboratory space.

Most of the membranes mentioned in Sec. 2.2.1 are still in the experimental phases, and, therefore, not available for immediate purchase. However, pure or alloyed palladium (Pd) and zeolite membranes can be ordered, and are eligible. After some investigation, it was concluded that, if possible, a Pd membrane would be preferred. This is because, unlike zeolite membranes, Pd has far fewer parameters that affect its performance, making its operation more predictable. As the standard to which all other membranes are compared, a large body of literature has accrued that would be useful for interpreting results and determining experimental procedures. When looking to source a membrane, we were informed that we would have access to a Pd membrane which was recently used in a different experiment that had ended, and so plans were made to use that membrane.

Most getters in Sec. 2.2.2 are likewise experimental, leaving a choice between heavy metal or light element getters. The heavy metal getters contain controlled and radioactive elements such as uranium, and the actinide metal powders are explosively pyrophoric under ambient conditions. However, similar to Pd for membranes, zirconium cobalt (ZrCo) is more predictable and has been selected as a standard to compare all other getters, providing the benefit of more literature than for the other getter materials besides uranium. It also has the benefit of not requiring temperatures that would be unreasonable for a

small bench-top system with limited heating capabilities, and can currently be ordered from two different companies.

3.2 Purpose and Overall System Design Goals

It was determined to investigate the use of a ZrCo getter powder and a Pd membrane for general H separation potential, emphasizing the recycling of a gas consisting of almost pure tritium (^{3}T) and helium-3 (^{3}He), such as what could be collected from spent exit signs. This system need to be able to rapidly test some parameters of ^{3}T/^{3}He separation, including temperature and gas flow rate. Key criteria guiding the design of the bench-top system included:

- The ability to rapidly evaluate parameters with minimal system changes—multiple experiment parameters would need to be varied without forcing significant changes in system components or layout. These parameters include the pressure of feed gas (which correlates to the amount of gas initially charged), the temperature of operation, and effects of flowing the gas versus a static system.
- Allowance for flexible gas input—the project sponsors specifically wanted to test the effects of the inclusion of an inert flow gas, which requires both a means of injecting the flow gas and a means of removing it from the mixture.
- Reduction of system volume—since the system would contain nearly pure H at some point during operation, it was desirable for safety to reduce the volume as much as possible. For the getter tank, a smaller volume allows operation without additional cooling in place. For both the getter tank and the membrane, a smaller volume also saves feed gas costs and allows rapid evaluation of operation parameters.
- Ease of manufacturing—designer was to work with the welding shop to design components that would be relatively easy to manufacture and required minimal customization.
- Ability to transition to pilot recycling—the system needed to be able to transition to use with actual ^{3}T/^{3}He mixed gas streams with minimal changes required to the system. The gas source selected for this criterion was exit signs which have been retired from service.

3.3 Evolution of the System and Its Components

As with any experiment, the design of the system and each component evolved over time. A discussion of overall system evolution will be followed by the major component changes, along with the rationale for those changes.

A piping and instrumentation diagram (P&ID) shows the configuration of system components, including vessels and instrumentation such as thermocouples (TCs), and is useful to show the evolution of the full system design. The major iterations for this system are shown in Fig.s 3.1—3.5. Each subsequent iteration describes the changes from the previous design under the P&ID.

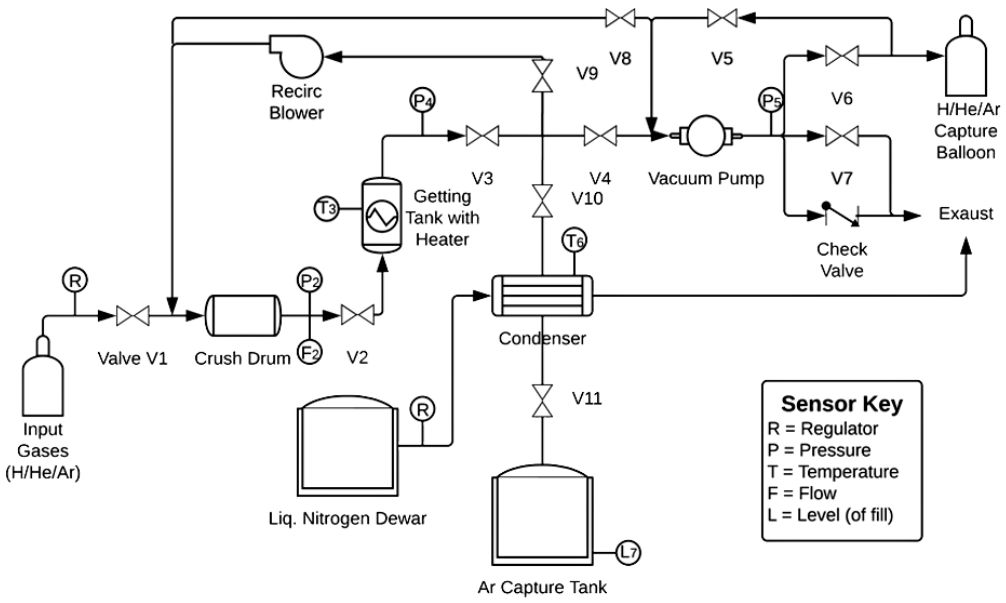

Figure 3.1: *First System P&ID. This is the base design used for discussions about making design decisions. For details, see Sec. 3.3.1*

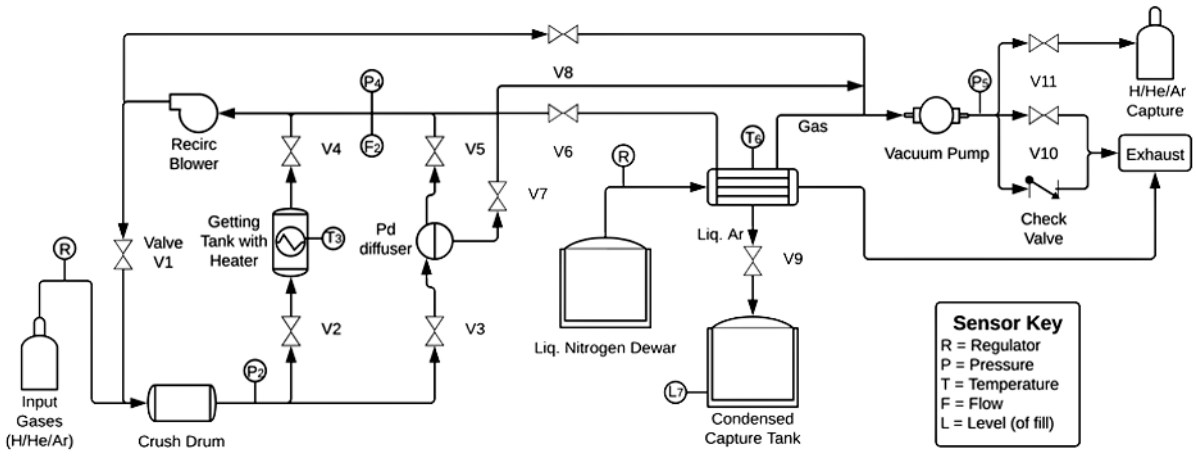

Figure 3.2: *First inclusion of membrane loop with direct connection to vacuum inlet.*

Flow through the condenser was clarified, flow meter F2 moved to be more effective, valve numbering changed to be more clear (getting loop had even-numbered valves, membrane had odd), and configuration modified to enhance flow. With this setup, operation through either separation loop flows counter-clockwise through V1 and either [V2, V4] or [V3, V5] and the blower. V6 and V8 would be closed to prevent flow elsewhere in the system. If flow gas was included, the forced flow could circulate counter-clockwise through either loop, V6, the condenser, V8, and V1, bypassing the blower. After H/He separations, the He/Ar mixture could be circulated clockwise through the Blower, V8, condenser, and V6, with V1, V4, and V5 closed. The loop allowing the gas capture tank to be vacuumed out was accidentally omitted.

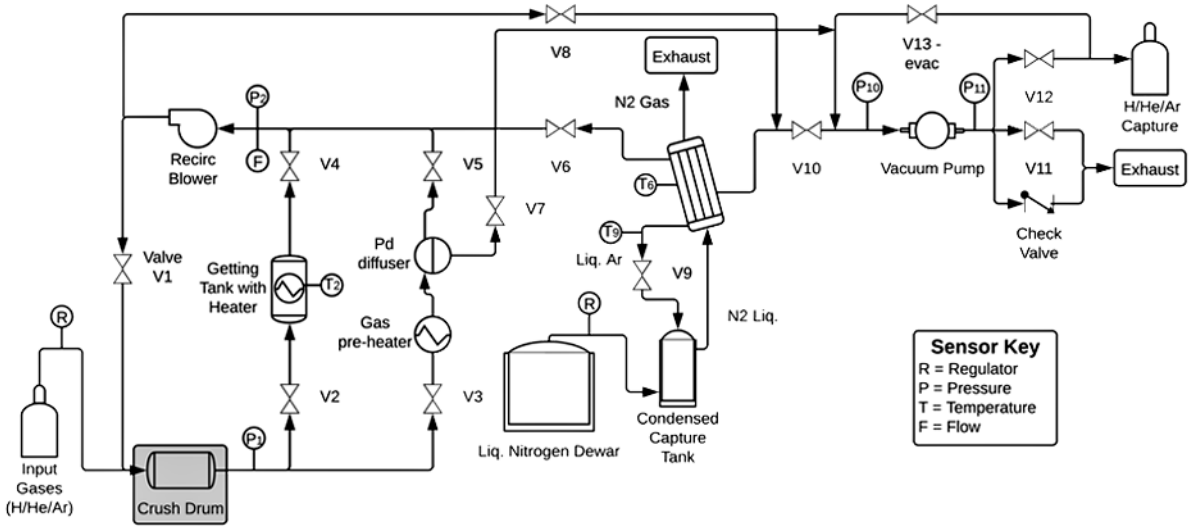

Figure 3.3: *Argon condenser clarification, heated membrane.*

Instrumentation and valves renumbered to simplify the operating procedure. P2 and F moved to other side of line 2-4 (getting line) so that flow could be reliably measured with either separation loop active. Level sensors removed. Crush drum distinctively marked to show it's a placeholder not to be included in the prototype system. A pre-heater was added to the membrane loop. The Ar condenser and liquid capture tank design was further developed, and expected orientation reflected in the diagram. The evacuation loop to vacuum out the gas capture tank was added back in.

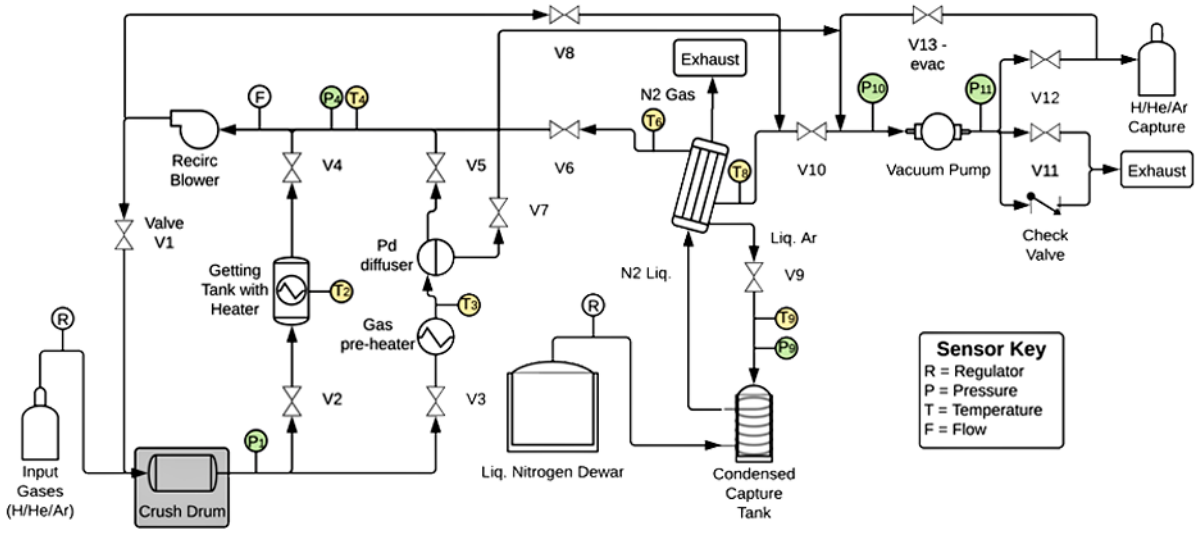

Figure 3.4: *Last draft iteration including all portions of the system that had been discussed.*

Instrumentation colored and renumbered to match numbering paradigms used elsewhere in the diagram. TC added to membrane loop. P4 moved away from blower inlet to reduce effects of turbulence at the inlet. TCs for condenser moved outside vessel to simplify manufacturing. Pressure gauge added to liquid capture tank to provide a means of measuring pressure buildup if the Ar was to boil off. LN flow path clarified, and condenser rotated to match new design configuration (see Sec. 3.3.3).

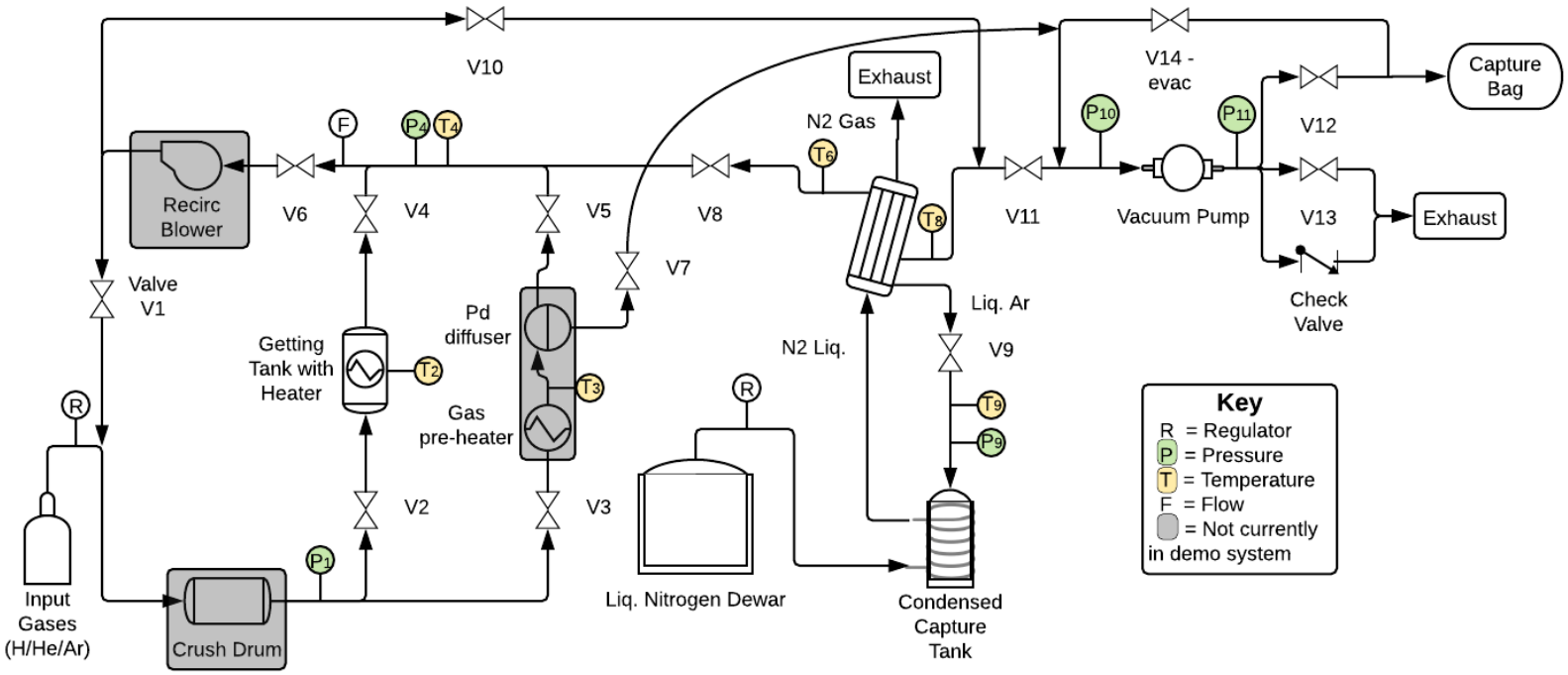

Figure 3.5: *Final system design for both separation methods.*

It was determined that the recirculation blower and membrane tank could not be included (see Sec. 3.3.1), so they were marked as such. Style of line from V7 to evacuation loop changed to make it clear that it was not teed into the lines between V6 and V8 or between V10 and V11, but into the evacuation loop by V14. It had been determined that fluorinated ethylene propylene gas sample bags would be used to capture the gas, not metal tanks, and was marked as such. V6 was added in front of the blower for two reasons: to close off the system as that blower would not be built in, and to allow for eventual operation with or without the blower. Valves were renumbered to allow for even-odd segments and loops, and to assign numbers higher than 10 to everything outside of the main separation loops to further help with segmentation for the written operating procedure.

3.3.1 Full System Design

The first iteration, shown in Fig. 3.1, provides the baseline for the other iterations, and so will be summarized here. It included a visual representation of where gas would be injected for exit sign processing (the crush drum), where the exit sign ampules would be crushed. The liberated gases would then flow to the getting tank, where H is captured. When only He remains, it is vacuumed out through valve 6 (V6) to a capture tank. As the project sponsors explicitly stated that they were interested in the inclusion of an inert flow gas to flush the gas mixture from the crush drum, the bottom portion of the diagram depicts a condenser to allow the removal of any added flow gas using liquid nitrogen (LN) as a coolant. The gas chosen was argon (Ar) because it liquefies below the temperature of liquid nitrogen. An additional loop to test the effects on getter performance of forcing the flow of the mixture through a recirculation blower was also included for discussion. The ability to flow the gases in the system could also be a means to provide cooling for the getter powder. Finally, a loop through V5 to evacuate the capture tank is included.

By the final iteration, the system design consisted of a membrane separation loop in parallel with the getting tank. Instrumentation had been more carefully considered, and specifics for the condenser and liquid Ar capture tanks had been worked out and reflected in the diagram. The membrane loop requires continuous vacuuming on the back side to maintain the maximum concentration differential (through V7), so it is directly connected to the inlet of the vacuum pump by a dedicated line.

The portions marked with gray in Fig. 3.5 are to be excluded from the build, but remain in the P&ID as placeholders to aid the sponsors with scale-up. The crush drum is excluded because the system is filled by compressed gas cylinders for our tests. The membrane loop was excluded because the Pd membrane could not be obtained. Because the membrane tank had to be designed around the membrane, the tank design could not be completed. The blower was excluded for budget reasons, and because no off-the-shelf blower or vacuum pump equipment could handle the expected -200 to +400 °C. It was explained by multiple equipment manufacturers that such devices were designed to operate either in elevated or cryogenic temperatures, but not both, due to the demanding tolerance required to maintain vacuum pressures. However, custom or parallel systems can handle this range, and it had been concluded that circulation would benefit the separation processes, so it remained as a placeholder on the P&ID.

3.3.2 Getter Tank

As the most important part of the system (since the membrane tank could not be included), the Getter Tank both was the first component designed, and had the most iterations of any component. The design generally followed the guidelines outlined by Bhattacharyya laid out in Sec. 2.2.2.1 [35]. Namely, it was designed to have an internal vessel holding the cartridge heater and the getter powder, with an outer vessel to allow gas flow and to act as a buffer for H diffusion. The getter is trapped in the inner vessel using micron-scale screens, which are made of 316L stainless steel. The getter bed was initially designed for a specific amount of H, but was later enlarged to make the getter tank easier to handle. Inlets and instrumentation ports penetrate through the outer vessel, and an outlet is positioned to force gas flow through the inner vessel.

Two main designs were initially considered, shown in Fig. 3.6. Both concepts used porous plates (metal barriers with pores on the micron scale) on the bottom and top of the getter tank to keep the getter powder inside the vessel while still allowing gases to flow through. The concept on the left of Fig. 3.6 flows gas from the bottom, through a diffuser, and out the top. The concept on the right injects the gas either on the side or top of the vessel, flows through the annulus, and then drifts up through the getter and out the top. The diffused injection would be a flanged connection, while the upper/side injection would either be screwed together at the top or bolted down with no flange.

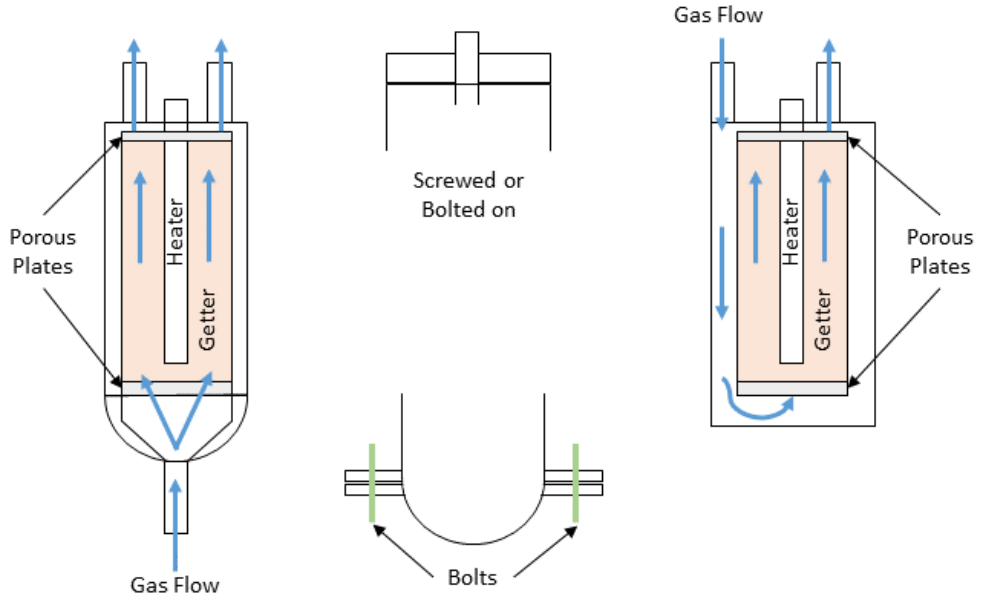

Figure 3.6: *Getter tank design concepts. Left: upward flow through a diffuser and out the top; Right: injection through top or side and flow through annulus; Middle: methods of securing the tanks.*

It was determined that manufacturing and mounting the upward flow tank would be significantly more difficult, and so the getter tank was designed with a side entry port and a lid secured with small screws. Trying to design for an expected amount of gas, the volume of the inner vessel was initially calculated to hold the volume of getter necessary to capture one sign's worth of H (0.224 mmol_{H_1} or 2.5 mL_{H_2}) to reduce activity during tests with ^{3}T, as one sign contains approximately 6.5 Ci of ^{3}T. This internal volume was found to be 0.018 cm^3, assuming a getting efficiency of 80% [41], or about 12.6 $\text{mmol}_{\text{H}_1}/\text{cm}^3_{\text{getter}}$. This volume resulted in a tank less than 1/2 in long, which was too small to be conveniently handled. The inner vessel was adjusted to 5 inches tall with an effective internal volume (excluding volume taken up by the cartridge heater) of 20.5 cm^3, enough to capture 1,154 signs (5.8 L or 1.56 g) of ^{3}T.

Other design principles guiding the initial concept included:

- Balance system compactness with manufacturability. Standard pipe is used for vessels, with schedules high enough to give needed thickness.
- The lid seals the outer vessel. Gas enters via a tube through the outer vessel, and most of the gas

must pass through the inner vessel to escape via a tube through the lid, allowing the inner vessel to remain without a tight seal against the lid.

- Heater has intimate contact with getter powder.
- Two TCs enter through the bottom for redundant measurements.

This design is detailed in Appendix A.

In discussions with machinists and welders, two major issues necessitated design changes. First, the groove for the seal for a compact lid design would leave dangerously thin walls, making for a brittle component. Additionally, o-ring and gasket materials generally cannot survive the temperatures expected for getter activation (up to 450 °C for ZrCo), and such a compact design puts the seal within millimeters of the heater, exposing it to high heat fluxes. Second, the system did not have allowances for thermal expansion which could result in high stresses. The inner vessel initially was designed with 1/8 in rigid legs welded to the bottom, and was designed to seat against the lid (see Appendix A). The manufacturing team suggested adding some space for thermal allowance, and switching from a compact lid to a flange that could be more easily cooled to preserve the o-ring.

To solve these problems, the next design iteration saw a flange with small bolts and the inclusion of a stacked wave disk spring under the getter tank. To prevent sideways motion, pegs were added on the bottom of the outer vessel floor to center the spring and inner vessel. The bottom of the outer vessel was broken out as a separate part that would be welded on, which was not explicitly addressed in the original drawings. This iteration is also included in Appendix A.

The final major iteration came from a design review, where methods of cooling the o-ring were discussed. It was decided to base the flange on ASME flange design principles and to include a copper cooling tube in the flange itself. ASME standards dictated a much larger flange with four large bolts instead of the three smaller ones [44]. Then, when ordering components, it was discovered that the porous plates, which were assumed to be 1/16 in thick, were actually sintered steel screens less than 0.01 in thick, necessitating design changes to the inner vessel. The screens would be sandwiched between two washers and inserted into rings cut out of the inner vessel walls. The final drawings are in Appendix B.

3.3.3 Condenser

Initially, the condenser was envisioned as a horizontal shell-in-tube heat exchanger with a H/He/Ar mixture flowing in from one side through the shell, and LN flowing counter-currently through the tubes. Liquefied Ar would drip off the tubes to the bottom, which would be sloped towards a drain, shown in Fig. 3.7. This design suffered from being difficult to manufacture (notably the slope on the bottom), and from the fact that small amounts of Ar were likely to be used in the small system, and it was unsure if the condensation beads formed on the tubes would collect into large enough drops to fall and flow through the drain. Additionally, even if the drops did fall, the slope was not cooled, and would boil off much of what fell.

Dr. Christensen, being an experienced heat exchanger designer, simplified the design to a vertical shell-in-tube, with LN flowing up through the tubes. The mixed gas would enter from the side approximately 1/3 from the bottom, and exit out the top. Condensed Ar will flow down the vertical tubes by gravity,

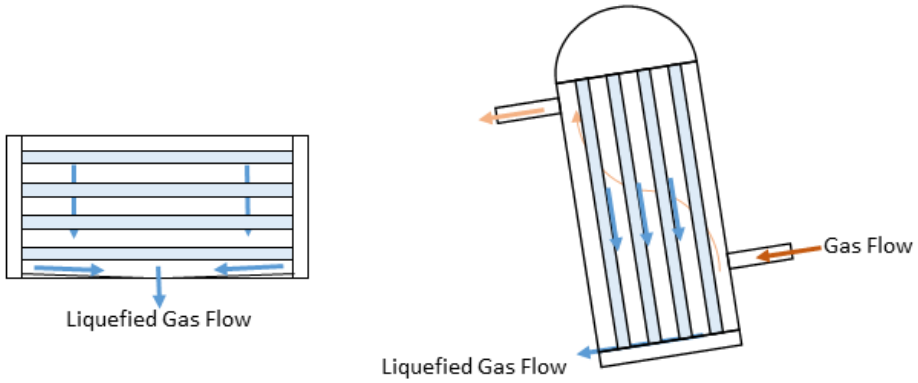

Figure 3.7: *Argon condenser design concepts. Left: initial horizontal design; Right: tilted vertical design.*

even in small quantities, and then flow out the side of the tilted cylinder. This design also kept the Ar pool in contact with a wall that was also in contact with LN, helping to keep it liquefied. After manufacture, the possibility of flooding the vessel with liquid nitrogen on the shell side and flowing the gas mixture up through the tubes from the bottom was discussed. In that configuration, heat transfer would be more efficient, and the liquefied argon could drip through a tee below the vessel to the holding tank.

Other design principles guiding the initial concept included:

- Balance system compactness with manufacturability. Standard pipe is used for vessels, with schedules high enough to give needed thickness.
- The end-caps are identical, with flared openings to allow LN to spread out and fill all tubes (or to allow liquefied argon to flow back through the gas inlet).
- Gases flow through, contacting the tubes, and any gases not liquefied escape through a tube near the top. In the design where the shell is flooded with LN, the non-liquefied gas would escape out the top of the heat exchanger, and boiled nitrogen would escape through the side tube.
- Instrumentation is included in the entrance and exit tubes, rather than in the condenser itself, to allow the system to be fully enclosed.

CAD work did not begin until after the change to a vertical design, with only minor changes. As it did not go through significant, rigorous design iterations, no drawing is included in Appendix A, and the only drawing included will be the final in Appendix B.

The liquid holding tank attached to the condenser was designed to be a small vacuum flask, such as a metal drinking bottle, wrapped in tubing through which LN would flow on its way to the condenser. The wrapped flask would be in a container filled with insulating material (see Fig. 3.8). Before rigorous CAD work began, some initial setbacks resulted in the option for Ar being cut from the system build (see Sec. 3.4). No formal engineering drawings were made of this component.

However, preliminary investigation into the feasibility of this design found that the vapor pressure of liquid Ar at the boiling point of LN (77.36 K) was 4.4 psi (0.3 atm) [45], which is significantly higher than

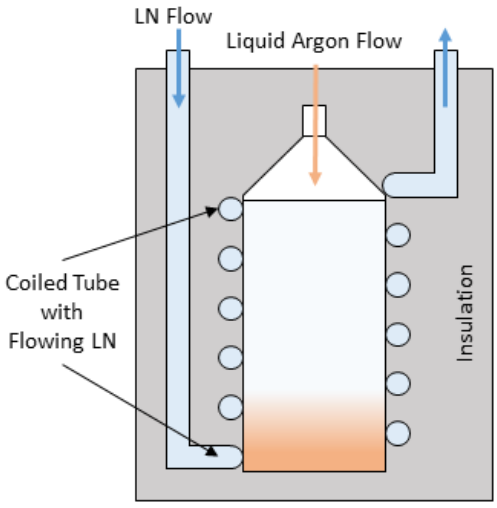

Figure 3.8: *Argon capture tank design concept.*

vacuum pressure. A pressure gauge and TC was added to the capture tank just below the isolation valve. The TC would help determine if liquid Ar was flowing, while the pressure gauge would help determine the rate of boil-off and confirm vapor pressure in the tank if this preliminary capture tank design is included at some future date. It is expected that at least one iteration on the liquid Ar tank design will be necessary before construction (*e.g.*, to include a pressure relief valve).

3.3.4 Membrane Vessel

A Pd membrane was included fairly early on in the system design, as it was thought that we'd be able to borrow one for the experiment. A rough, initial first draft of the vessel to hold the membrane was put together to facilitate discussion and act as a placeholder until the membrane was located, as its exact dimensions were unknown. The second iteration of the tank design was to build on the example in Fig. 2.2 with discussions determining the best way to fold concepts from that example system into the present design. However, this discussion led to an understanding that the membrane could not be obtained and further led to the decision to cut the membrane from the design. This initial design followed similar design principles to the other components:

- Balance system compactness with manufacturability. Standard pipe is used for vessels, with schedules high enough to give needed thickness.
- Heater must have intimate contact with membrane.
- Instrumentation is positioned outside the vessel to allow for integral design and greater sensitivity to control heaters.
- The membrane must remain undamaged, so seal and holder is designed around exact geometry.

This design be found in Appendix A.

Study of gas membrane systems and input from interviews recommended that the membrane loop

be capable of some form of gas flow, leading to the solidification of the blower in the full system design. Design of the vessel, however, did not continue past the initial draft, as it was cut from the system. It remained on the final P&ID to indicate where it would fit in the process, should the project sponsors choose to incorporate it later.

3.4 System Build and Simplification

The full system, as designed, could not be built because the membrane loop could not be completed and a blower could not be sourced. It was decided to reduce the system to focus on the getter, leading to the design in Fig. 3.9. While the system was being built, some features of the design could not be implemented, and the system was built as closely as possible to the original design. A few additional changes were made to ensure the system would still work as designed. This final design P&ID is included below as Fig. 3.10.

Differences between the original reduced design and the final as-built design include:

- Addition of a vessel referred to as the Fill Tank. This helped to standardize the amount of gas that was charged to the system (rather than relying on length of tubing from the cylinders) and charged more gas to the system because the vacuum pump volume was much larger than expected. For safety, it was determined that V0 must be closed when running to preclude any blow back into the H-containing tank.
- Addition of a TC (T1) by the fill tank. This was added because when H is released, it is hot enough to potentially cause damage to the capture bag or other equipment. So, it was planned to allow the H to occupy the fill tank where its temperature could be monitored by T1 until it had cooled sufficiently for removal.
- Elimination of the line between V0 and V10. This was done to allow the system to be more compact.
- Addition of a pressure transducer (PT) on the evacuation line. Because the vacuum pump's internal volume was so large, the changes in pressure after the getter tank were too small to be read by analogue pressure gauges, and an instrument with higher resolution was deemed beneficial.
- Addition of V15, V16 in front of the capture bag. Due to the accidental use of the wrong graphic in the original reduced system P&ID (a tank instead of a bag), those two valves are added so that one could be removed with each capture tank (containing He, then containing H).

While testing the system, it was found that the gap between the hole in the top screen and the heater rod was greater than 5 µm, and powder was escaping through the tank outlet. An in-line filter was purchased and inserted between the getting tank and V10. Additionally, minor adjustments were made to improve the usability of the system in the lab setting. After adding all the instrumentation, sensors, and wiring, the system was complete and ready to perform a validation run with nitrogen. Photos of the final system can be seen in Fig 3.11.

3.5 Data Capture

The Laboratory Virtual Instrument Engineering Workbench (LabVIEW) code, from National Instruments, was chosen for data collection because the team already had experience working with it, and

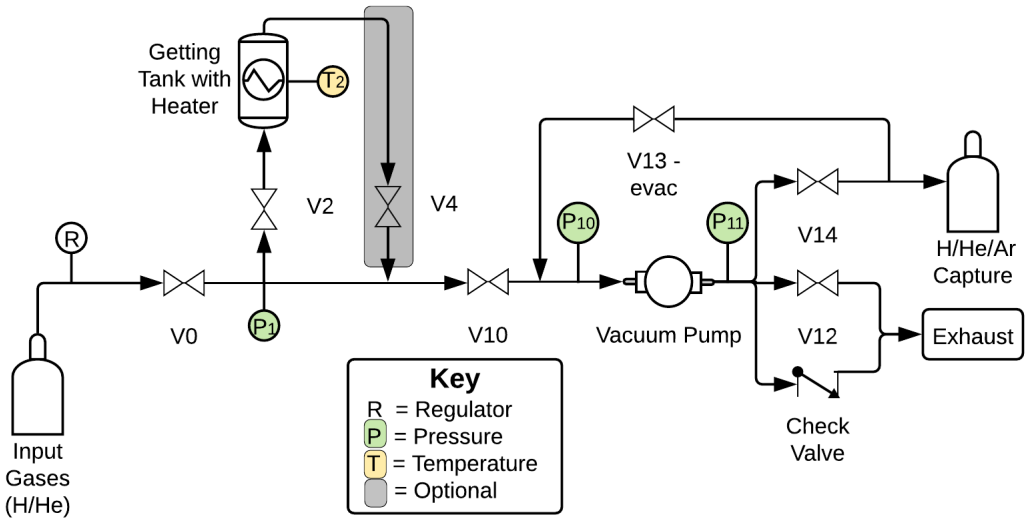

Figure 3.9: *P&ID for the simplified or reduced system, optionally including a valve on the outlet of the getter tank. The original numbering was unintentionally carried over.*

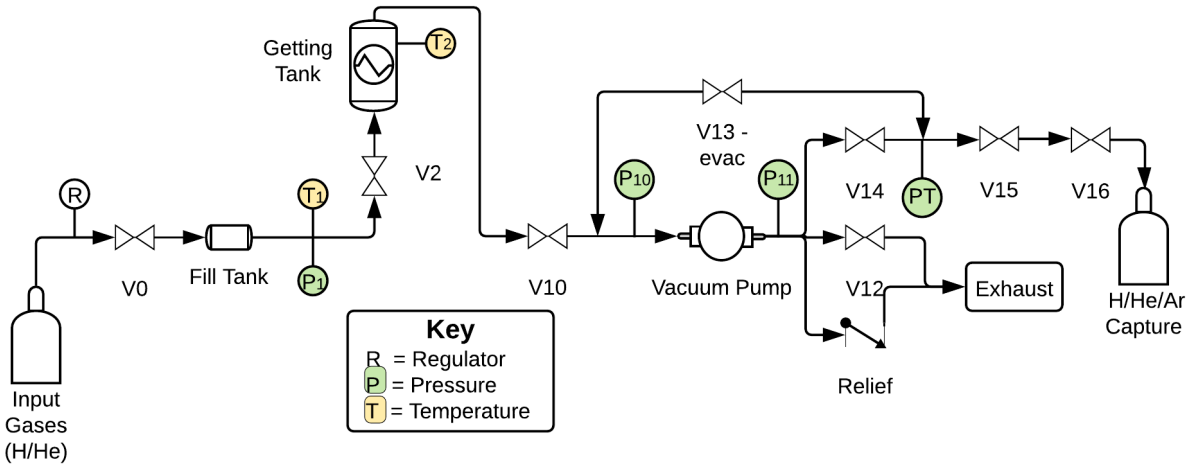

Figure 3.10: *P&ID for the reduced system as it was built.*

because much of the hardware was already owned by the department. The front panel shows the P&ID of the as-built system with readouts for the instrumentation positioned where it would sit on the P&ID. Below this is a grid of data to assist the experimenter, including expected pressures and gas purity which are computed when the program starts. After these are computed, the program reads in four TCs and the pressure transducer every two seconds, displays them on the P&ID, tracks them on a chart, and writes them to a file. The redundant TCs have their signals averaged, as well.

Screenshots of the code and front panel, a more detailed explanation of the code, and more details about the setup is included in Appendix D.

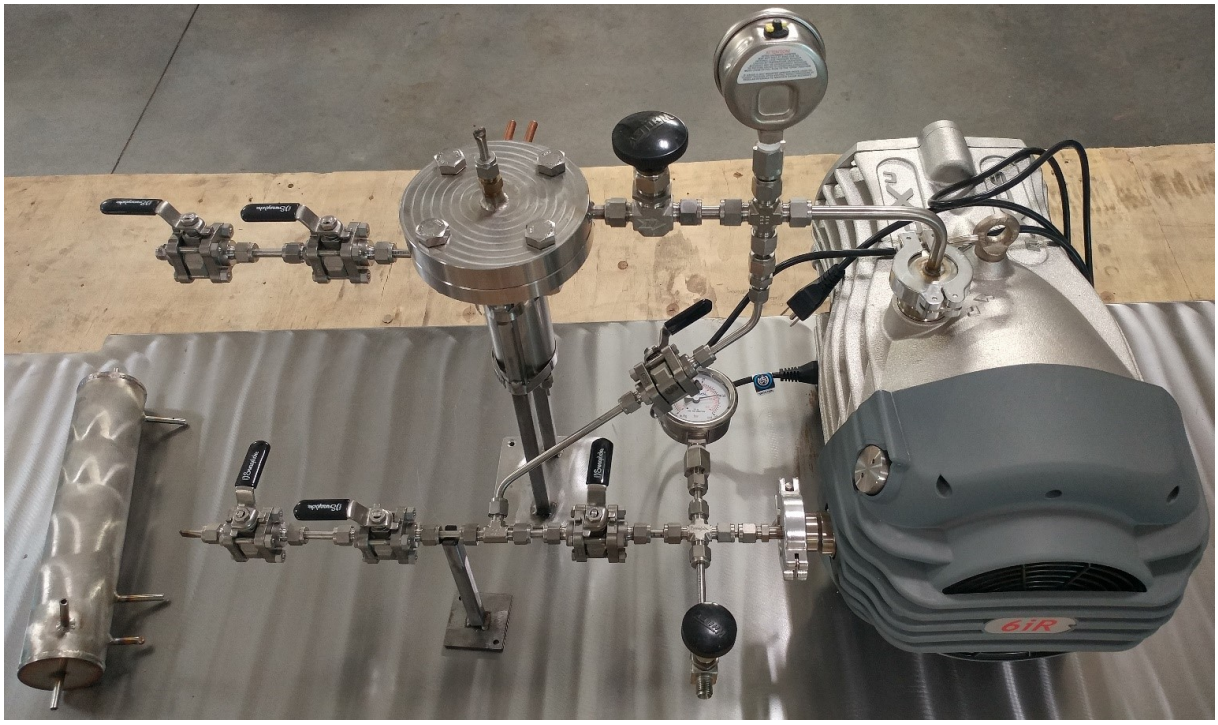

(a) *View of the system from the back side while still in the shop. The Ar condenser can be seen on the left, disconnected from the system.*

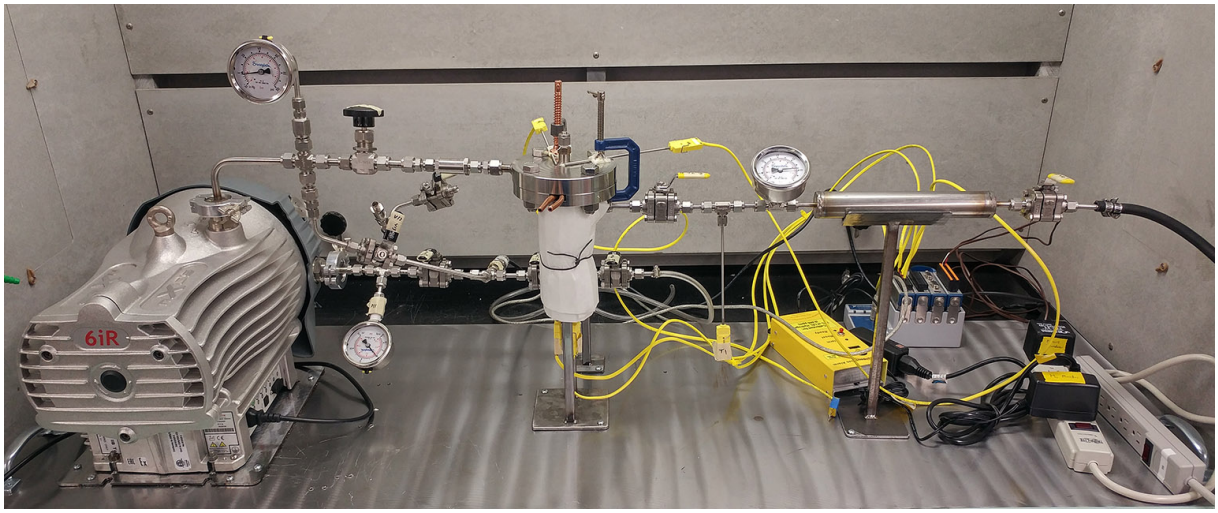

(b) *Front view of the completed system in the hood at the lab. Differences between this image and the image above include: (1) the inclusion of the Fill Tank a pressure gauge and a TC on right before the getter tank; (2) black-handled valves replaced with yellow-handled steam valves to survive the possible 400 °C gas that will be in it; (3) replaced pressure gauge on the left before the vacuum pump; (4) inclusion of pressure relief valves on vacuum pump outlet, (5) insulation on the getter tank; (6) pressure transducer in back visible just to the left of the getter tank; (7) inclusion of electronics.*

Figure 3.11: *Photos of the system, as built, including a back view in the shop, and a hood view in the lab*

Chapter 4: Validation and Lessons Learned

4.1 Development of Experimental Procedures

For the purposes of this thesis, the only experimentation performed will be simple validation tests to show that the system holds pressure and the getter removes hydrogen (H). However, some additional tests were planned for the full system design to collect useful information, which can be easily implemented by other students or the sponsors later. These will be discussed in Sec. 4.1.2.

4.1.1 Validation

After the system had been designed, a procedure was drafted to validate the system, and reduced the procedure to a step-by-step, written standard operating procedure (SOP). It was based on Fig. 3.5 under the assumption that a membrane would be provided. Each validation run consisted of charging the lead line of the system to inject less than 0.02 mol of H gas, and then stepping through the necessary actions to separate the mixed gas. Procedures for including an argon (Ar) flow gas were also drafted.

For the membrane, extraction of the H occurs during the run by continually vacuuming and collecting what flows through the membrane, leaving behind helium (He) and, if included, Ar. When all H has been extracted, the collection bag is replaced with an empty one, the Ar is condensed out, then the He collected by vacuuming it out. For the getter, the H is captured in the powder, leaving He and, if included, Ar. In this case, the Ar is condensed out, and the He vacuumed out first. After the He is fully collected, the H is released by heating the getter powder. When the powder has released most of the H adsorbed into it (monitored by pressure increase rate), the valves to the getter are closed and the isolated H is allowed to cool. When the H temperature drops to the point where the temperature will not harm the equipment, the gas is vacuumed out. Approximately half of the H will remain with the getter, so the heat-isolate-cool-capture procedure is repeated until a cutoff pressure is reached.

Because the original SOP was written to reference Fig. 3.5, the design changes outlined in Sec. 3.4 necessitated that the procedure be rewritten so that the Ar condensation and membrane sections were removed and references to system components matched Fig. 3.10. Otherwise, the separation procedure remained basically the same as previously described. Writing the SOP before the design had been completed proved to be extremely valuable for understanding where instrumentation was needed, and contributed major adjustments to the overall design.

4.1.2 Additional Planned Experiments

Most studies have investigated the effects of changing pressure (concentration gradient) on the behavior of these systems. For this system, the pressure is more or less set to contribute to a reduction of H in the name of safety, which limits charging the initial vessel to 100 psi (around 0.75 mmol of H_2) for work done in university labs. However, for the getter to simply adsorb the H out of the mixture, the only requirement is that the partial pressure of H be higher than the partial pressure above the zirconium cobalt (ZrCo) hydride. For the membrane, the concentration gradient, measured using pressures, is the

driving force leading to diffusion across the membrane, and is, therefore, significant to the rate of separation as the H concentration continuously drops during the experiment. The limit is reached when the partial pressure of H on the feed side is equal to the vacuum pressure on the product side, though the rate of diffusion will likely slow enough that the experiment could be considered at an endpoint before that threshold is reached. These experiments are discussed below.

4.1.2.1 Temperature Dependence

This test will explore the effect of temperature on the performance of the getter and the membrane. The independent variable, the one over which we have control, is the temperature of the separation systems. The dependent variable is the time that it takes to reach half of the expected total pressure (due to the near-complete removal of H from the 50-50 H/He mixed stream) or for instrumentation to hold a constant value (implying a different thermodynamic limit has been reached). System modifications include adding a heater around the fill tank, and possibly charging the system with more gas by adding more volume and/or filling to higher pressures.

The general procedure is to charge the fill volume at lab temperature, and then valve it off from the source gas. The fill tank will then be heated to temperature for the test. When the separation apparatus (*i.e.*, getter or membrane loop) and the gas in the fill tank are at the target temperature, valves leading to the separation apparatus of choice are opened to allow the heated gas to flow to it. Pressures will be periodically measured until the ending conditions outlined above are met. The heaters will then be turned off, the system will be allowed to cool, and gases extracted from the system to prepare for the next run. For the getter, it will also be important to measure the pressure as the H is released for each temperature run. For simplicity, the release temperature will be the same as the capture temperature unless the capture temperature is less than 250 °C, as lower release temperatures may not fully release the majority of the H captured. Because the getter volume is low, heating rates should be high enough to reach temperatures up to about 300 °C in less than 30 seconds, with a heater controller used to minimize temperature overruns.

Getter - Sources suggest that activated ZrCo captures effectively at temperatures above 100 °C and releases H above 150 °C [41], but hint that an optimum temperature for capturing and releasing H in the shortest amount of time is dependent on powder hydriding history. There are also optimum temperatures for maximizing the service life of the getter which are not likely to be the same as the temperature optimizing getting speed. This test will help in identifying the temperature that captures and releases in the least amount of time. The data from this test can later be used to determine performance changes over time.

Other studies have looked at H solubility in ZrCo from 130–500 °C [41, 46] using 5–10 runs at different pressures. These experiments show marked difference in behavior below 200 °C, and above 350 °C (see Fig. 2.8). The getting portion of the system was designed to survive temperatures up to 350 °C, though temperatures as high as 500 °C can be achieved using the built-in flange cooling. For the temperature dependence tests, a span from 50–400 °C will be investigated, with a release at 250 °C to "clear" the getter after runs below 250 °C. The order that the temperature tests will be held is randomized to avoid bias, though it is noted that getter performance degrades over time. To account for this, two runs at

each temperature will be independently randomized. Table 4.1 details the proposed 20 temperature runs to relate temperature to adsorption/desorption rates.

Palladium Membrane - Pure palladium (Pd) membranes transport best above 350 °C [33], with the rate of H transport increasing with increasing temperature. However, as He is also small (the kinetic diameter of H_2 is 289 pm [47], and the kinetic diameter for He is 260 pm [48]), there will likely be a temperature at which He permeation sharply begins to increase. Other H isotopes have diameters even closer to He, with deuterium (^{2}D) having a kinetic diameter of 269 pm and tritium (^{3}T) being even smaller [49]. The Pd benefits from the ability to catalyze the dissociation of H at its surface and dissolve it, but Pd does not appear to feature mechanisms to inhibit the diffusion of He, typically along grain boundaries. This diffusion rate is expected to increase with increasing temperatures.

Pd membrane studies found in literature have typically spanned from room temperature to over 1300 °C, finding very little change in solubility after 400 °C but demonstrating increasing transport rates as temperature increased (see Fig. 2.4. The membrane tank would have been designed to survive up to 600 °C by separating an inner vessel from the outer vessel and providing active cooling for the outer vessel, similar to the getter tank. Pd also undergoes phase transition (combined $\alpha + \beta$) below 300 °C, which increases the crystal lattice parameter and leads to defect formation and recrystallization from hydride formation and release [33]. It is, therefore, desirable to perform fewer runs at those lower temperatures. A modified order was conceived that randomized temperatures above 300 °C, then randomized those below, and then repeated the randomization for temperatures above 300 °C to determine changes due to damage from previous runs, if any. Table 4.1 details the proposed membrane runs.

Table 4.1: *Suggested test matrix to test the dependence of transport rates with temperature.*

Getter			**Membrane**		
T (°C)	**Order 1**	**Order 2**	**T (°C)**	**Order 1**	**Order 2**
50	1	4	150	9	–
75	8	7	200	8	–
100	2	5	250	10	–
125	9	1	300	3	6
150	3	6	350	5	3
175	5	9	400	1	4
200	7	8	450	6	5
250	6	10	500	4	1
300	4	3	550	7	7
350	10	2	600	2	2

4.1.2.2 Saturation

This test, exclusively for the getter since the Pd membrane will not store meaningful quantities of H, will measure how much H can be held in the getter. Theoretical calculations using 12.6 $\text{mmol}_\text{H}/\text{cm}^3_\text{getter}$ [41] put the amount of H that could be captured in the system at 0.258 mol. With around 0.02 mol inserted per run, this would take an expected 13 runs. There are three ways to reduce this number. The first is to charge both the fill tank and the getter tank to 100 psi, which approximately doubles the H load. The second would be a switch to higher purity H. The maximum H per charge, for pure H at 100 psi in both the fill and getter tanks, is about 0.08 moles, which would take just over four runs to theoretically saturate the getter powder. The third way is simply to tee in a large reservoir that can hold a significant gas volumes. This latter method is preferred, as it also allows careful heating control over the gas charged into the system, and the extra reservoir could be made large enough increase the amount of H in the system enough to only require one run. However, non-negligible amounts of heating will be generated as the getter adsorbs all the H at once, and the increase in total H within the system could lead to an increased explosion risk.

The procedure would be to charge the system to the chosen pressure, valve off the system from the source gas, let the gas into the getting tank, and heat the getter to a target collection temperature. By observing the pressure trend over time, it can be seen when the H has been captured. If it was all captured, more H is injected by first allowing the system to cool, pumping out any non-H gas, then recharging the system as described above to continue the run. This capture process is repeated as many times as necessary until the pressure no longer drops sufficiently far to signify a full H capture from the most recent system charge. It is expected that longer dwell times will be necessary the more saturated the getter becomes. If the pressure change is less than 10% of the expected reduction from adsorbing all the H charged in the system after an arbitrarily set threshold dwell time (*e.g.*, two hours), the getter is assumed to be saturated. The system is then vacuumed out, and all the captured H is released, and the resulting pressure measured. The released H is then collected in a capture tank or bag, and the amount of collected H is again measured.

Since literature already addresses the theoretical maximum loading for activated ZrCo powder (*e.g.*, [41, 39]), this test would be to confirm properties for the current getter sample, and to measure degradation over time.

4.2 Final System Adjustments and Results of Validation Runs

After the system redesign was implemented, the system was leak checked in the shop to around 50 psi. After it had demonstrated that it held pressure, it was bolted to a steel plate and transported to the lab. There, the getter tank was filled with powder, and while rolling it to fully insert the heater rod, a significant amount of powder leaked out. Three possibilities were considered for why this happened. First, because the funnel used to fill the inner vessel could not fit down inside the fitting, some of the powder used to fill the tank may have settled on the top of the screen, easily spilling out the side port when disturbed. Second, perhaps the screen was not positioned correctly, had been damaged, or left a large enough gap around the heater rod to allow powder to escape. However, because the internal getter

vessel had been welded to the top flange, the status of the screen could not be investigated. Third, even though literature suggests that a screen mesh of 5 µm was sufficient, perhaps the screen was not holding back the getter powder. Further tests in the system clarified that the screen system was allowing getter powder to pass into the system, prompting the purchase of an inline filter with a 2 µm mesh, which is the typical lower limit mentioned in literature for experiments with getters [35].

While waiting for the filter to be delivered, the electrical connections, instrumentation, and other minor adjustments were made in preparation for the validation run. During a pressure check after an instrumentation adjustment, it was noticed that the system had suddenly started to leak. A systematic check revealed that some of the weld-on fittings were leaking from the body threads (*i.e.*, the threads on the welded-on connector rather than from the nut threads or ferrules that are more common leak points). This was likely caused by over-tightening the 1/8 in nuts securing the thermocouples (TCs) into these connectors, though it is possible that the threads experienced thermal warping during welding. The outer vessel was removed from the lab, taken to the shop, and those fittings were ground off and replaced with new ones that were welded in quarter turns and cooled with compressed air between each turn to minimize risk of heat warping. After re-assembly, it was noted that the leak rate was nearly the same, though no gas was leaking through the welded fittings.

Testing again with soapy water, it was discovered that the heater rod was leaking through the wiring. When removed, it was discovered that the inconel jacket around the heater had failed through what looked like corrosion and was now allowing gas to escape. Previously, while making final preparations for the validation runs, the heat controller had accidentally been turned on, and since the TC guiding its control logic had been disconnected from the system, the cartridge heater had overheated, burning out in the process. The damage is shown in Fig. 4.1. Simulations suggested that the temperatures exceeded 700 °C, possibly catalyzing or accelerating the chemical interactions between the heater jacket and the getter powder. The heater was replaced, and it was noticed that a significant amount of getter powder was trapped in front of the filter, again confirming that the screen around the heater rod was failing to keep powder in the inner vessel. The heater controller was reset and programmed for a slow ramp rate on the heater.

After the system passed a vacuum pressure test, the mock experimental run was started. The fill tank was charged to 80 psi, and after it was verified to hold, it was let into the getter tank, which was also verified to hold the pressure for 10 minutes. The heater was turned on, and set to 30 °C (from a lab temperature of 20.3 °C). The TC was attached to the top flange using a C-clamp, and the delay caused by the poor thermal conductivity of the stainless steel resulted in a temperature overshoot. By the time the TC stopped climbing 10 minutes later, it peak at 40.2 °C. It was allowed to cool to 36 °C to rule out the possibility of a fused relay in the controller, and then set for 50 °C. The fuse on the controller blew shortly afterwords. The controller was a simple proportional-integral-derivative (PID) controller that adjusted the current as necessary to maintain the current setpoint. The fuse was replaced so the controller could be used to watch the temperature, but the heater was unplugged from the controller and plugged into a 120V variable autotransformer (variac) to allow for easy, manual control over current draw to investigate the cause of the fuse melting.

Over the next 20 minutes, output was adjusted from 10% to 100% of full output on the variac. The

measured temperature did not increase during that period. Unsure if the variac was working properly, the heater was directly connected to the power strip, and 5 minutes later, the temperature measured by the TC in the controller was still dropping. The systems were powered down, and before leaving the lab, the system was pressurized again, revealing that the system had begun to leak at about the same rate it had leaked when the last heater rod had failed.

The second heater was taken out and examined. While not visibly corroded through, it also showed signs of corrosion beginning and similar scorch marks as the first one (see Fig. 4.1). Interestingly, when plugged into the power strip while outside the system, it did heat, though it drew enough power that it tripped the breaker in the power strip. It is postulated that due to the loss of a significant amount of getter powder, that much of the heated portion of the rod was not in contact with anything but the fill gas, generating extremely high temperatures. This is supported by the scorching on the rod jacket, and distinct lines between the scorching and more metal-colored portions of the rod. It is also notable that the corrosion only appears below this line. The rod jacket was made of incoloy 800, which oxidizes around 980 °C [50], though it is not thought to have reached these high temperatures in the test run

Figure 4.1: *Heater rod damage. Both heater rods pictured: Set [A, B] are the first heater rod; set [C, D] are the second. Corrosion and particularly visible damage is circled in red. Additional comments in the text.*

because the incoloy itself would have conducted more of the 900 °C temperature difference within the time that the TC registered 40 °C. Instead, it is postulated that skin oils from handling the rods or something originating from the getter powder flashed or burned, scorching the surface.

Looking again at Fig. 4.1, a few observations can be made. In (A), two full penetrations on the rod, circled in red, appear to have corroded through the incoloy 800 sheath, which is less than 0.4 mm thick. On the other side (B), another apparent corrosion spot, circled in red, is visible but has not obviously penetrated the sheath. Both (A) and (B) show pronounced discoloration on the upper portion, and a distinct color change just above the blemish spots where is it thought to have entered the powder. This sharp delineation supports the theory that the heater rod was not fully submerged in the powder. The second heater stayed on significantly longer before the controller fuse blew, and the overall scorched area on the rod was larger with more pronounced discoloration. In (C), a crack in the sheath weld is clearly visible, with a particularly sharp line circled. In (D), what appears to be the beginnings of apparent corrosion is circled, with other questionable spots visible. This second rod was operated under known nitrogen cover to at a pressure of about 50 psi. After the fuse on the controller popped, leak rate grew to about 5 psi min^{-1} at 80 psi, measured after a full cool down the next day. The dramatic increase in discoloration on the rods and of the powder leads us to believe that the powder currently in the getter tank has been rendered unusable and will need to be replaced.

Since it is possible that at least one of the heater rods reached temperatures above 700 °C, it should be noted that ZrCo undergoes a sustained self-accelerating reactions with oxygen around 227 °C and with nitrogen around 727 °C [51]. The system was filled with nitrogen during the validation run, but non-negligible amounts of oxygen likely remained. It is unknown what gases were in the system when the heater was accidentally turned on; it is possible that the system was filled with atmospheric air. In any case, it is thought that either these reactions or a direct reaction with the incoloy jacket likely caused the corrosion effects on both heaters, and the scorching was caused either by oxidation of the incoloy directly, residues on the rod burning, or something in the powder burning or flashing. Further analysis, including a chemical and crystallographic analysis, would be required to determine the true cause of damage in the heater rods.

4.3 Lessons Learned and Suggestions

The experience gained working on the project associated with this thesis has led to some lessons and suggestions for any group looking to continue this work or another group looking to perform similar work. Those suggestions and lessons will be presented below.

1. The getter powder should have had a thermal conductivity around 2 $\text{W m}^{-1}\,\text{K}^{-1}$ [35]. Simulations of the getter tank that inserted a full 400 W of heat into such a material resulted in heater temperatures exceeding 500 °C within 60 seconds. It was assumed that the controller would not allow the full 400 W to be inserted because the TC would respond more quickly—which turned out to be a poor assumption (see #3). A weaker heater or slower ramp rate (the final run was around 10 $^{\circ}\text{C}\,\text{min}^{-1}$) would be required to use the current design, though a better approach would be to consider using an alternative heating method such as heating ropes around the outside of the inner vessel.

2. There appears to have been some sort of interaction between hot inconel and ZrCo getter powder, which also precludes the direct contact of an inconel-sheathed heater with the powder. Use of a different sheathing material is necessary, or, as previously recommended, use a different method of heating, preferably one that doesn't directly contact the getter powder.
3. Our choice of TC placement was ineffective for controlling powder temperature. TCs on the top flange required heat to conduct up the unheated upper portion of the heating rod and through any stainless steel between that rod and the TC, leading to delays that, with the high heating rates, led to component damage. The TCs in the vessel relied on the gas conducting the heat, which could be in motion or have lower conductivity than the powder. It is strongly recommended to place TCs either in direct contact with the getter, or in a location that will measure higher temperatures than the powder will experience (*e.g.*, in the conduction path). With the current design, by heating the outside of the inner vessel (as in suggestion 1 above), a steel-clad TC could be inserted into the tank to measure "centerline" temperature in the powder.
4. Order extra components of anything that might fail. For the current design, not only were parts ordered for the full system design (the smaller system actually built being about 1/3 the size), but extra components were ordered, including an extra cartridge heater, extra pressure gauges, extra thermocouples, etc. No matter how well thought-out the design might be, when it comes time to build and operate apparatus, unforeseen problems will arise, and having spare parts allows these problems to be more quickly resolved.

The suggestions above indicate that a different approach (*i.e.*, design) for the getting system would be appropriate and beneficial.

4.4 Improved Design

A new design was analyzed for the getter system that both resolves the issues encountered with the current design and adapts the designs found in literature for commercial recycling. Literature depicts getting systems arranged in grids, with copper either in the grids or distributed throughout the getter [35, 39, 52]. Screens with a mesh size of 2–5 µm or porous materials with similar sized pores were sufficient to hold in the powder. The new system adapts and innovates on these principles to achieve a system that is inexpensive to build and provides for the flexible operation of the system for ^{3}T recycling.

The new system is comprised of a box with screens over the top and back with a screened door in front that is heated by two 200–400 W rod heaters and optionally cooled by fluid flowing in a cooling channel in the baseplate. The channels both cool the powder down between activation runs and can remove the heat generated during H capture. A removable tray with 77 wells drilled into it to hold getter powder fits inside the box, held down by leaf springs. The wells are covered by a screen with a mesh size of <5 µm. Holes are drilled through the sides of the wells to provide an additional path for the mixed gas to flow through, which are likewise covered on both sides by the same sized screen. TC holes are drilled into the sides of the tray between central wells, and can be inserted after the tray is locked in the screened box. Drawings can be found in Appendix C.

The heater plate is meant to be mounted in a horizontal vessel. The holding box frame is then bolted

onto it. The leaf springs are attached to the lid of the box, which is then bolted to the frame. Cartridge heaters and cooling lines are attached to the heater plate through gas-tight penetrations in the vessel. The getting tray is inserted into the box, and the door is bolted into place through the heated plate to secure the tray in place. Sheathed TCs are then inserted into the getter tray through holes in the holding box, and the insulated wires pass through gas-tight penetrations in the vessel. It is recommended that gas flow be directed at the back of the holding box so as to encourage gas flow through the holes near the bottom of the wells. This external vessel should be designed to the constraints of the facility where it will be run; as such the author does not provide a design for the external vessel explicitly in this work.

The system was sized so that the tray would hold enough getter for 1,000 signs' worth of H (0.68 g), assuming the same getting efficiency of 12.6 $\mathrm{mmol_H/cm^3_{getter}}$ used in Chap. 3. 1,000 signs started with 20,000 Ci of activity, and after 20 years would still have some 6,500 Ci, requiring access in a hot cell if the loaded powder is to be removed, analyzed, or relocated (*e.g.*, for storage to be used as a helium-3 (^{3}He) incubator). For this reason, the getting tray utilizes raised screen covers to facilitate operation using mechanical manipulators in a hot cell. The system can be made of aluminum or copper, but if made from aluminum then the wells on the tray should be electroplated in copper, as other designs have used copper and not suffered adverse interactions with the powder [39].

The system was designed to operate between lab temperature and 500 °C to facilitate the activation of the getter. To activate ZrCo powder, a procedure of de-gassing at 400–450 °C followed by hydriding at a lower temperature is repeated several times [41], usually at high H pressure [46], after which it is chemically active to multiple gases [53], including H. After it is active, it will capture at room temperature when H pressures are relatively high, and at slightly elevated temperatures when H pressure is lower. From a review of literature, the current author recommends capturing H at temperatures between 100–200 °C. Because the powder reacts readily with components of atmospheric air, an airtight box is recommended for transferring the getter from the vessel to any releasing or storage portions of the system.

The new design was analyzed with the **An**alysis **Sys**tem (ANSYS) code package, with the heater plate, frame, and tray made of aluminum 6061 and the wells filled with getter powder (see Fig. 4.2) [54]. Thermophysical values for aluminum were provided by ANSYS, while the values for ZrCo were obtained by Sei-Hun *et al.* [55]. This analysis found that, with 800 W of heat input, the getter system would heat to the activation temperatures of 450 °C within 7 minutes in a vacuum, and would require nearly 25 minutes with convective flow of a purge gas. After the powder was activated, the recommended getting temperature could be obtained in less than two minutes for 100 °C, assuming constant H/He flow, and less than five minutes for 200 °C. Additionally, cool-down to an average system temperature of 40 °C (considered a safe temperature for removal) under convection and radiation alone required 42 minutes, confirming the benefit of the cooling channels for more rapidly running the powder through activation temperature cycles. More details about the analysis can be found in Appendix E.

The simulation covered two hours, with 800 W of heat applied only in the first hour, and constant convective and radiative cooling over the full two hours. Because of the position of the heaters, the temperature distribution in the getter powder is not uniform (see Fig. 4.3). Fig. 4.4 shows the heating profile for nine different wells for the entire two-hour run, which demonstrates how similar the temperatures are during the full simulation. While the distribution is not uniform, the standard deviation was less than

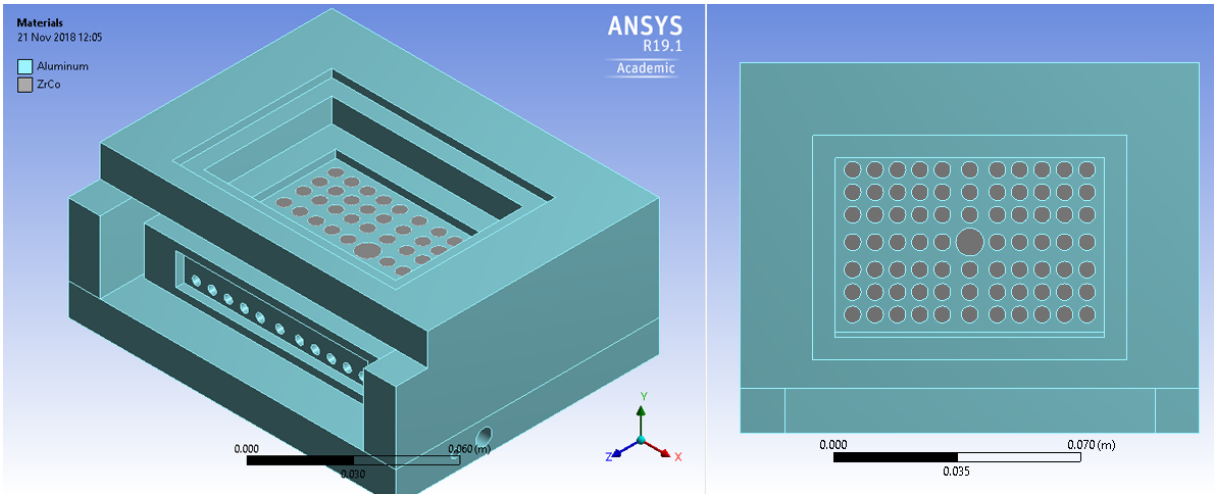

Figure 4.2: *Material arrangement for the analysis of the new design, where green is aluminum and grey is ZrCo powder; Left: Orthographic view, Right: View from directly overhead. Screens removed for clarity.*

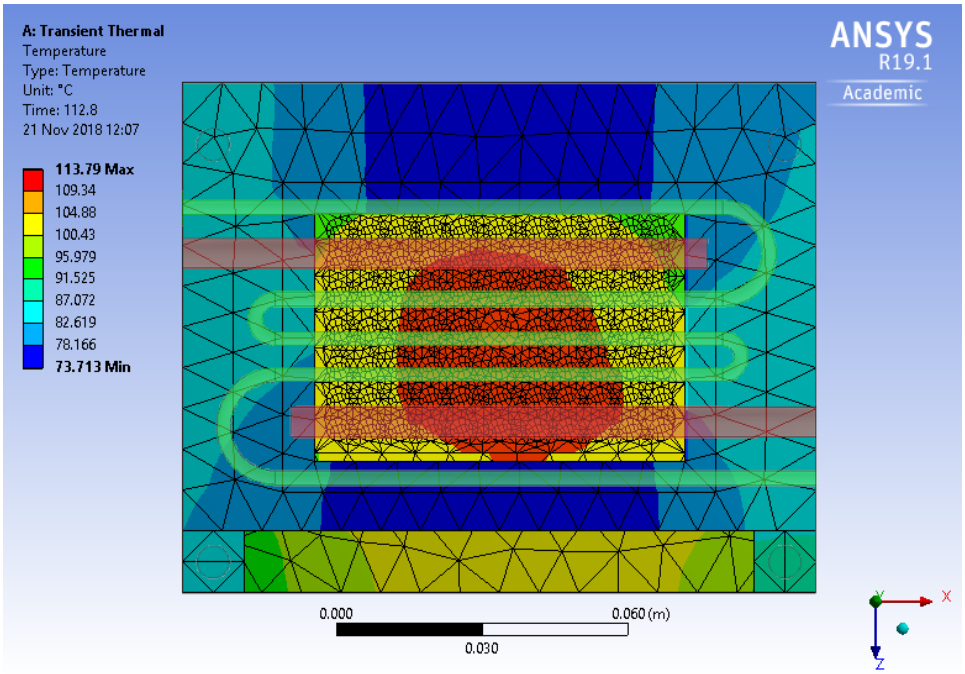

Figure 4.3: *Temperature distribution in getter tray around the time that the getter powder in all wells reaches 100* °C*, with location of heaters (light red) and the cooling channel (light green) superimposed. The heating and cooling both are supplied below the getter tray. Colors for the getter bed (center) exaggerated for clarity. The red region was orange, the yellow region remained the same, and the vivid green in the corners was the pale green under yellow in the key.*

3 °C during heating. The standard deviation would be smaller (*i.e.*, well temperatures more uniform) if (1) the temperature was held constant, *i.e.*, controlled, as it would be during an experimental run; (2) the tray was made of a more conductive material, *e.g.*, copper; or (3) copper or aluminum beads were

mixed into the powder to increase its thermal conductivity.

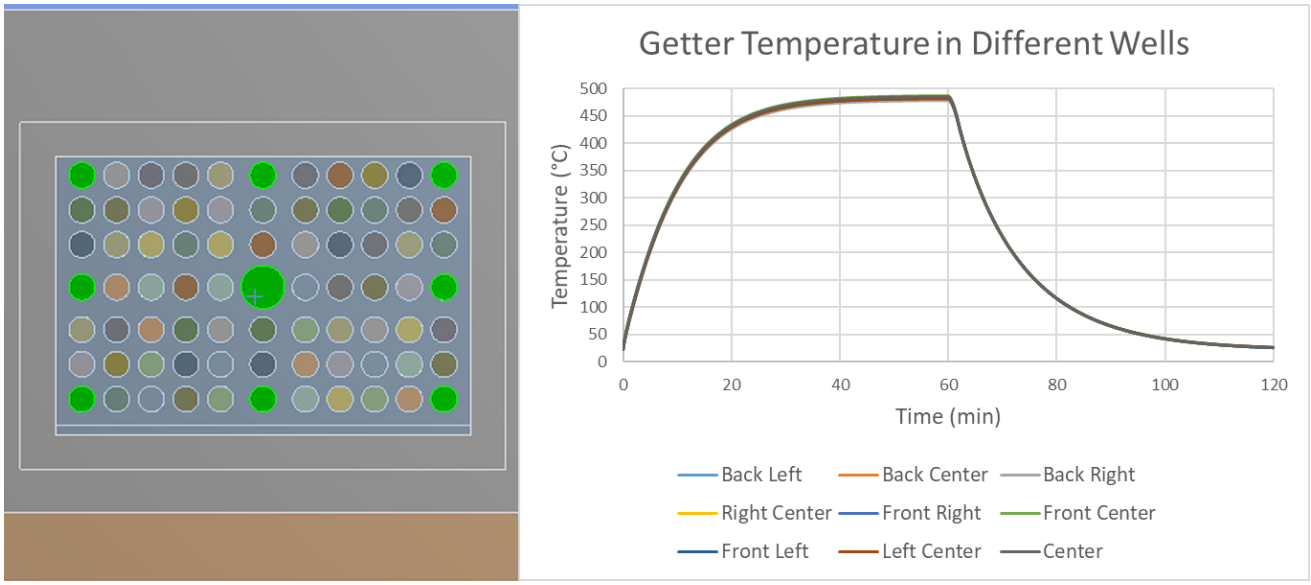

Figure 4.4: *Temperature profile of the tracked wells over the full two-hour simulation; Left: The nine wells where average volume temperature was tracked, marked in green; Right: Temperature profiles of the nine wells over the full two-hour run*

After using the getter, the tray can be quickly extracted from the box by removing the right front bolt to swing the front door open. This tray can then be quickly placed in a sealed box or vessel and transported elsewhere for further processing (*e.g.*, releasing the captured H for storage) or stored (*e.g.*, as a ^{3}He incubator). This quick removal is necessary because activated getter powder is extremely reactive with multiple gases in typical atmospheric air, and needs to be protected. This reactivity is reduced the more saturated the getter becomes. To resume operations, a new tray is inserted. Alternatively, initial capture and post-capture processing can be conducted in-place by setting up parallel batch systems using a bypass (*e.g.*, see Fig. 4.5).

The bypass is beneficial because it allows the side not in use to be flooded with an inert gas or vacuumed out before the tray is removed, preventing unwanted reactions with components of air. It will likely be necessary to remove the tray robotically, both because of chemical activity of the powder and because the tray could have up to 6,500 Ci of ^{3}T in it.

This redesign offers a simple, compact system that both corrects the problems encountered with the previous design (items 1–4 below) and provides several additional benefits. These features include:

1. Full heater contact with conductive material, preventing the burnout seen in the vertical tank design.
2. Heater separate from the getter powder, preventing any chemical interaction between the powder and the heater materials.
3. TCs positioned in immediate vicinity of powder and in the path of conduction, providing better response to and control over the temperature. Over the entire simulated run, the TCs showed

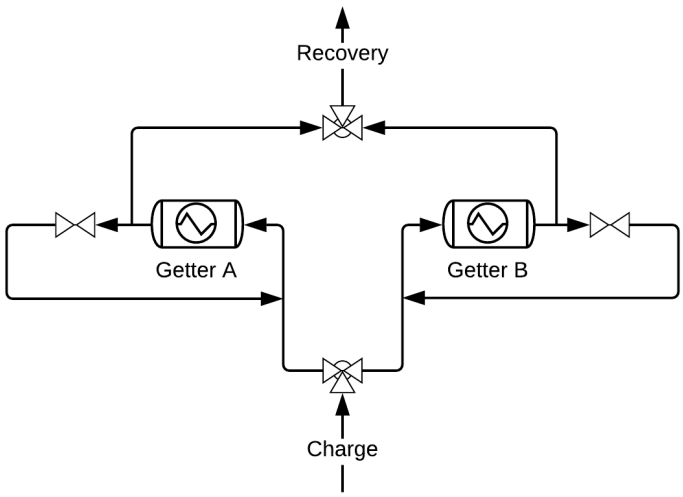

Figure 4.5: *Example parallel arrangement for getter system including bypass valves to allow for semi-continuous operation of the system. This arrangement allows for collection and recovery in the same system, precluding the need to handle the chemically active, highly radioactive tray.*

the powder mean temperature +0.57/-1.34 °C when furthest off, and averaged +0.21/-0.047 from overall system mean throughout the run.

4. Getter contained in separate package that is fully sealed at all times. The vertical tank, both as designed and as built, had gaps around screen where the heater was inserted, preventing it from completely sealing, and would be open when removed from the system.
5. Both heating and cooling provided from a relatively uniform source below the powder, keeping all powder within a few degrees of the same temperature.
6. Easier access to the getter allows for quick replacement and easy removal of all the getter powder, providing a more flexible system. The design of the tray facilitates access in a hot cell by using raised covers. It may be necessary to make the system larger to use larger screws for hot cell access.
7. Larger screen area on the top, combined with the channels through the bottoms of each well, provides space for the getter powder to expand, preventing damage to system components or powder leakage over time.

The author recommends the getter tray design to continue this work.

Chapter 5: Summary and Conclusions

5.1 Significance

This work investigated methods for the separation of hydrogen (H) from a mixture also containing helium (He) to extract both to a purity of 95% or better. The work focused on investigating the economical recycling of tritium (^{3}T) and its decay product, helium-3 (^{3}He). These valuable gases are often wasted in long-term repositories even while significant efforts are undertaken at high cost to produce the gases. This work has found that two separations methods stand out from the dozens of available methods as particularly well suited for recycling high-purity ^{3}T and ^{3}He, namely metal membrane and metallic getter methods. Further, membranes made of palladium (Pd) alloys offer predictable behavior and known operation methods due to the large body of research conducted on such membranes; while zirconium cobalt (ZrCo) as a getting material offers excellent performance, a higher gravimetric storage capacity, and improved safety over other metal getters while also benefiting from a large body of research.

Three systems were designed for testing various parameters of such a separations system:

1. A conceptual system that contained both the getter and the membrane sub-systems. This system was detailed in Sec. 3.3 and Fig. 3.5. While the design of the sub-systems continued to evolve, the overall system design remains sound except for modifications in the specifics of the separation loops. Specifically, the new getter system would reside in a larger, horizontal vessel with penetrations for gas and cooling inlets and outlets, as well as instrumentation lines, and the membrane system would likely be a similar double-vesseled setup.
2. A reduced system containing only a vertical getter tank (excluding the membrane subsystem). This reduced system and associated vertical tank design, described in Sec. 3.4 and 3.3.2, was built and tested. It was found that the vertical design and hole for the heater rod through the screen on the internal vessel resulted in a system that did not reliably cover the heater rods to supply heat transfer or provide rapid enough thermal detection. It was also discovered that the getter powder chemically interacted with the heater sheath materials at these higher temperatures. This system design provided many valuable insights that were leveraged in the third system design.
3. A new, improved getter system that designed out the problems encountered in the initial getter tank design, incorporated the best of other designs in literature, and provided additional innovations that eased system operation and use for a recycling system. This system, described in Sec. 4.4, is useful both as a test system and as a production system, providing easy scale-up. Analysis was carried out to predict time-to-temperature and temperature distributions to provide operational insight.

This work provided a foundation for the project sponsors to investigate the separation of ^{3}T from its decay product, ^{3}He, allowing for the economical separation of these two gases. Further, the ^{3}T can be stored at typical laboratory temperatures using a getter power, which can act as a ^{3}He incubator because, after ^{3}T decays, the ^{3}He cannot maintain the hydride bond and is released from the getter. This work provided a system design that incorporates the experience of literature and experimentation which will provide valuable insights on key system design parameters. Suggested experiments were provided for

testing the temperature dependence of the mass transport into the getter and through the membrane, as well as a saturation test for the getter to determine performance compared to those published in literature (see Sec. 4.1.2).

5.2 Future Implications

The University or the sponsors can continue this work, building the improved getter tank to follow the suggested design and performing the work outlined in Sec. 4.4. Upon successful operation of the getter tray design using typical H and He, the system could be used for temperature sensitivity and saturation experiments, such as those outlined in Sec. 4.1.2. After all scoping experiments are complete, the system can then be switched over to ^{3}T and ^{3}He and Geiger-Müller counters or spectrographs can be used to provide additional insight about the adsorption behavior of the getter. The differences caused by the much larger ^{3}T compared to natural H could be easily compared by repeating previous experiments.

This system is easily scaled up for production by either placing two vessels in parallel with at least four trays to allow the saturation of one vessel, then a switch to the other while the tray is replaced in the first vessel. The saturated tray can then release its ^{3}T in a separate system optimized for ^{3}T handling, then that tray used to replace a saturated tray in the capture system. Alternatively, the trays can be enlarged to hold more ^{3}T, though this is not recommended due to the high radioactivity (up to 6,500 Ci) in a fully saturated tray as currently designed. It is likely that the getter trays would either need to be further reduced in size, not fully filled with getter, or not fully saturated to allow for safe operation or to comply with licensing constraints.

References

[1] Eric Miller. Hydrogen Supply / Demand; IEA North American Roadmap Workshop. Technical report, US Department of Energy, 2014.
http://www.iea.org/media/workshops/2014/hydrogenroadmap/7doeericmiller.pdf.

[2] Dolf Gielen and Giorgio Simbolotti. Prospects for Hydrogen and Fuel Cells. Technical report, International Energy Agency, 2005. https://inis.iaea.org/search/search.aspx?orig{_}q=RN:38115309.

[3] Henry H. Mantsch, Hazime Saitô, and Ian C.P. Smith. Deuterium Magnetic Resonance, Applications in Chemistry, Physics and Biology. *Progress in Nuclear Magnetic Resonance Spectroscopy*, 11(4):211–272, Jan 1977.

[4] Birgit Vennesland. Some Applications of Deuterium to the Study of Enzyme Mechanisms. *Discussions of the Faraday Society*, 20:240, Jan 1955.

[5] McCoy, Michael. Heavy Problems for Heavy Water. *Chemical and Engineering News*, 90(22), 2012.
https://cen.acs.org/articles/90/i22/Heavy-Problems-Heavy-Water.html.

[6] Luis W. Alvarez and Robert Cornog. Helium and Hydrogen of Mass 3. *Physical Review*, 56(6):613–613, Sep 1939.

[7] P. Gierszewski. Tritium Supply for Near-term Fusion Devices. *Fusion Engineering and Design*, 10:399–403, Jan 1989.

[8] Mitsuru Kikuchi, Karl. Lackner, and M. Q. Tran. *Fusion Physics*. International Atomic Energy Agency, 2012.

[9] Stefano Atzeni and Jürgen Meyer-ter Vehn. *The Physics of Inertial Fusion*. Oxford University Press, 2004.

[10] Richard J. Pearson, Armando B. Antoniazzi, and William J. Nuttall. Tritium Supply and Use: A Key Issue for the Development of Nuclear Fusion Energy. *Fusion Engineering and Design*, May 2018.

[11] Rolland P Johnson, Robert Abrams, Mary Anne, Clare Cummings, and Thomas J Roberts. Production and Collection of He-3 and other Valuable Isotopes Using Mu*STAR. *9th International Particle Accelerator Conference: Vancouver, BC, Canada*, pages 7–9, 2018.

[12] US Department of Energy. SRS Tritium Facilities Factsheets, 2011.
https://www.srs.gov/general/news/facts.htm.

[13] Dana A. Shea and Daniel Morgan. The Helium-3 Shortage: Supply, Demand, and Options for Congress. Technical report, Congressional Research Service, 2010.

[14] Matthew Gunther. Scientists Unearth One of World's Largest Helium Gas Deposits, 2016.
https://www.chemistryworld.com/news/scientists-unearth-one-of-worlds-largest-helium-gas-deposits/1010122.article.

[15] J. D. Seader, Ernest J. Henley, and D. Keith Roper. *Separation Process Principles*. John Wiley & Sons, Inc., Hoboken, New Jersey, 3 edition, 1988.

[16] Phillip C Wankat. *Separation Process Engineering*. Pearson Education, Inc., Upper Saddle River, New Jersey, 3 edition, 2012.

[17] Walter J Moore. *Physical Chemistry*. Prentice-Hall Inc, London, UK, 4 edition, 1962.

[18] W. J. Koros, Y. H. Ma, and T. Shimidzu. Terminology for Membranes and Membrane Processes (IUPAC Recommendations 1996). *Pure and Applied Chemistry*, 68(7):1479–1489, Jan 1996.

[19] Walter F. Boron and Emile L. Boulpaep. *Medical Physiology: A Cellular and Molecular Approach*. W.B. Saunders, 2003.

[20] William J Koros and Rajiv Mahajan. Pushing the Limits on Possibilities for Large Scale Gas Separation: Which Strategies? *Journal of Membrane Science*, 175(2):181–196, Aug 2000.

[21] Yoshihiro Makide, Satoru Hagiwara, Osamu Kurihara, Kazuo Takeuchi, Yo-ichi Ishikawa, Shigeyoshi Arai, Takeshi Tominaga, Ichiro Inoue, and Ryohei Nakane. Tritium Separation by CO_2 Laser Multiphoton Dissociation of Trifluoromethane. *Journal of Nuclear Science and Technology*, 17(8):645–647, 1980.

[22] Nathan W. Ockwig and Tina M. Nenoff. Membranes for Hydrogen Separation. *Chemical Reviews*, 107(10):4078–4110, 2007.

[23] Kourosh Malek and Marc-Olivier Coppens. Knudsen Self- and Fickian Diffusion in Rough Nanoporous Media. *The Journal of Chemical Physics*, 119(5):2801–2811, 2003.

[24] K. Oura, M. Katayama, V.G. Lifshits, A.A. Saranin, and A.V. Zotov. *Surface Science: An Introduction*. Springer Science & Business Media, 2003.

[25] Fèlix Casanova, Casey E Chiang, Chang-Peng Li, Igor V Roshchin, Anne M Ruminski, Michael J Sailor, and Ivan K Schuller. Gas Adsorption and Capillary Condensation in Nanoporous Alumina Films. *Nanotechnology*, 19:315709–315714, 2008.

[26] K. Kotoh, S. Takashima, and Y. Nakamura. Molecular-Sieving Effect of Zeolite 3A on Adsorption of H_2, HD and D_2. *Fusion Engineering and Design*, 84(7-11):1108–1112, Jun 2009.

[27] Sushil Adhikari and Sandun Fernando. Hydrogen Membrane Separation Techniques. *Industrial & Engineering Chemistry Research*, 45(3):875–881, 2006.

[28] U Balachandran, T Lee, L ChenN, S Song, J Picciolo, and S Dorris. Hydrogen Separation by Dense Cermet Membranes. *Fuel*, 85(2):150–155, 2006.

[29] S. A. Steward. Review of Hydrogen Isotope Permeability Through Materials. Technical report, Lawrence Livermore National Laboratory, 1983.

[30] Fernando Roa and J. Douglas Way. Influence of Alloy Composition and Membrane Fabrication on the Pressure Dependence of the Hydrogen Flux of Palladium-Copper Membranes. *Industrial & Engineering Chemistry Research*, 42:5827–5835, 2003.

[31] Alibaba Corperation. Alibaba, 2018. https://www.alibaba.com/?spm=a2700.7724857.scGlobalHomeHeader.6.580c36c3pqMPKG.

[32] APMEX. Palladium Spot Price, 2018. https://www.apmex.com/spotprices/palladium-price.

[33] Samhun Yun and S. Ted Oyama. Correlations in Palladium Membranes for Hydrogen Separation: A Review. *Journal of Membrane Science*, 375(1-2):28–45, Jun 2011.

[34] Ievgeniia Savchenko, Andreas Mavrandonakis, Thomas Heine, Hyunchul Oh, Julia Teufel, and Michael Hirscher. Hydrogen Isotope Separation in Metal-Organic Frameworks: Kinetic or Chemical Affinity Quantum-Sieving? *Microporous and Mesoporous Materials*, 216:133–137, Nov 2015.

[35] Rupsha Bhattacharyya and Sadhana Mohan. Solid State Storage of Hydrogen and Its Isotopes: An Engineering Overview. *Renewable and Sustainable Energy Reviews*, 41:872–883, Jan 2015.

[36] S Suda, N Kobayashi, and K Yoshida. Reaction Kinetics of Metal Hydrides and Their Mixtures. *Journal of the Less Common Metals*, 73(1):119–126, Sep 1980.

[37] Morten B. Ley, Lars H. Jepsen, Young-Su Lee, Young Whan Cho, José M. Bellosta von Colbe, Martin Dornheim, Masoud Rokni, Jens Oluf Jensen, Mikael Sloth, Yaroslav Filinchuk, Jens Erik Jørgensen, Flemming Besenbacher, and Torben R. Jensen. Complex Hydrides for Hydrogen Storage New Perspectives. *Materials Today*, 17(3):122–128, Apr 2014.

[38] D.E. Dedrick. Solid-State Hydrogen Storage System Design. *Solid-State Hydrogen Storage*, pages 82–103, 2008.

[39] Satoshi Konishi, Takanori Nagasaki, Nobuhisa Yokokawa, and Yuji Naruse. Development of Zirconium-Cobalt Beds for Recovery, Storage and Supply of Tritium. *Fusion Engineering and Design*, 10:355–358, 1989.

[40] H.B. Peacock and H.B. Pyrophoricity of Uranium. Technical report, Savannah River Site (SRS), Aiken, SC, Mar 1992. http://www.osti.gov/servlets/purl/10155050-udliOK.

[41] Takanori Nagasaki, Satoshi Konishi, Hiroji Katsuta, and Yuji Naruse. A Zirconium-Cobalt Compound as the Material for a Reversible Tritium Getter. *Fusion Technology*, 9(3):506–509, 1986.

[42] Inc Universal Industrial Gases. Overview of Cryogenic Air Separation and Liquefier Systems, 2003. http://www.uigi.com/cryodist.html#General.

[43] Various. Tritium Properties, 2018. https://pubchem.ncbi.nlm.nih.gov/compound/24824#section=Experimental-Properties.

[44] Pipe Flanges and Flanged Fittings, ASME/ANSI B16.5, 1996.

[45] D. H. Bowman, Ronald A. Aziz, and C. C. Lim. Vapor Pressure of Liquid Argon, Krypton, and Xenon. *Canadian Journal of Physics*, 47(3):267–273, Feb 1969.

[46] M. Devillers, M. Sirch, and R.-D. Penzhorn. Solubility of Hydrogen and Deuterium in ZrCo. *Journal of Nuclear Materials*, 207:53–61, 1993.

[47] Ahmad Fauzi Ismail, Kailash Chandra Khulbe, and Takeshi Matsuura. *Gas separation membranes: Polymeric and inorganic*. Springer International Publishing, 2015.

[48] Benny Freeman, Yuri Yampolskii, and Ingo Pinnau. *Materials Science of Membranes for Gas and Vapor Separation*. John Wiley & Sons, 2006.

[49] J.M. Salazar, S. Lectez, C. Gauvin, M. Macaud, J.P. Bellat, G. Weber, I. Bezverkhyy, and J.M. Simon. Adsorption of Hydrogen Isotopes in the Zeolite NaX: Experiments and Simulations. *International Journal of Hydrogen Energy*, 42(18):13099–13110, May 2017.

[50] Special Metals. Incoloy alloy 800H & 800HT Spec Sheet, 2004. `www.specialmetals.com/assets/smc/documents/alloys/incoloy/incoloy-alloys-800h-800ht.pdf`.

[51] P J Nigrey. Art Issue Paper on the Use of Hydrogen Getters in Transportation Packaging Sandia National Laboratories. Technical report, Sandia National Laboratories, Feb 2000.

[52] Kurt A. Terrani, G.W. Chinthaka Silva, Charles B. Yeamans, Mehdi Balooch, and Donald R. Olander. Fabrication and Characterization of Uranium-Thorium-Zirconium Hydrides. *Journal of Nuclear Materials*, 392(2):151–157, Jul 2009.

[53] R. D. Penzhorn, M. Devillers, and M. Sirch. Storage of Tritium in ZrCo Alloy: Effect of Pre-Exposure to Impurities Relevant to the Fusion Fuel Cycle. *Journal of Nuclear Materials*, 179-181(PART 2):863–866, 1991.

[54] Clinton Aluminum. Best Aluminum Alloys for Heat Transfer, 2017. `https://www.clintonaluminum.com/best-aluminum-alloys-for-heat-transfer`.

[55] Yun Sei-Hun, Cho Seungyon, Chang Min Ho, Kang Hyun-Goo, Lee Min Kyu, Jung Ki Jung, Park Ka Young, Chung Hongsuk, Koo Dae Seo, and Song Kyu-Min. Experimental Determination of Selected Thermo Physical Properties of ZrCo and $ZrCoH_x$. *Fusion Science and Technology*, 60(1):373–378, Jul 2011.

[56] ANSYS. ANSYS User Guide. `https://ansyshelp.ansys.com/account/secured?returnurl=/Views/Secured/corp/v191/wb_msh/msh_sizing_options.html`.

[57] Theodore L. Bergman, Adrienne S. Lavine, Frank P. Incropera, and David P. Dewitt. *Fundamentals of Heat and Mass Transfer*. Wiley, 2001.

Appendix A: Early-stage Drawings

This appendix contains early-stage drawings of various components, with the goal of showing the progression in component design. The different drawings in this appendix are noted on the list below.

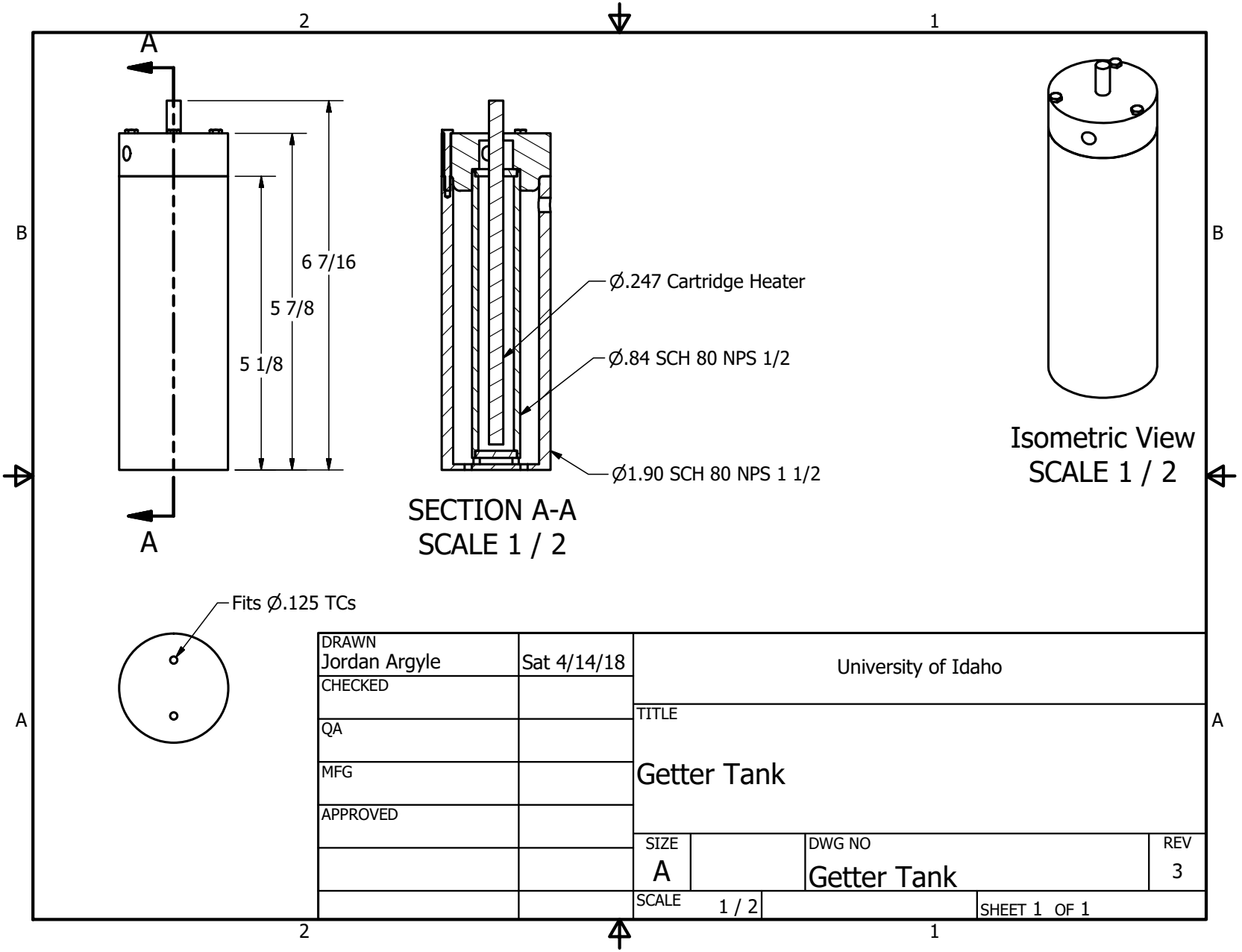
2
1
A
B
A
6 7/16
5 7/8
5 1/8
Ø.247 Cartridge Heater
Ø.84 SCH 80 NPS 1/2
Ø1.90 SCH 80 NPS 1 1/2
SECTION A-A
SCALE 1 / 2
Isometric View
SCALE 1 / 2
Fits Ø.125 TCs
DRAWN
Jordan Argyle
Sat 4/14/18
CHECKED
QA
MFG
APPROVED
University of Idaho
TITLE
Getter Tank
SIZE
A
DWG NO
Getter Tank
REV
3
SCALE
1 / 2
SHEET 1 OF 1

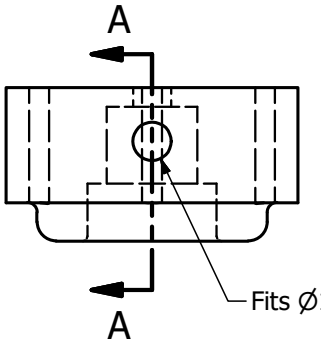

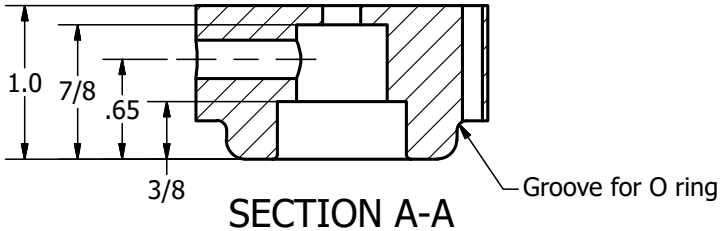

SECTION A-A
SCALE 1 : 1

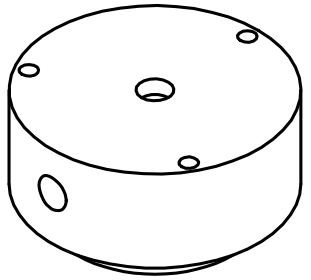

Isometric View
SCALE 1 : 1

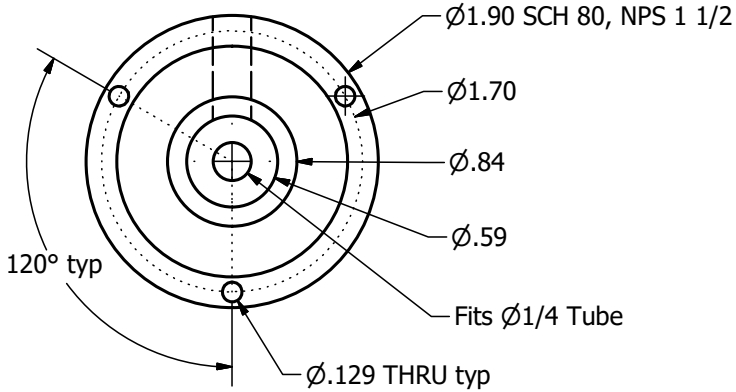

DRAWN Jordan Argyle	Sat 4/14/18	University of Idaho	
CHECKED			
QA		TITLE	
MFG		Vessel Lid	
APPROVED			
		SIZE A	DWG NO Getter Lid / REV 3
		SCALE 1 : 1	SHEET 1 OF 1

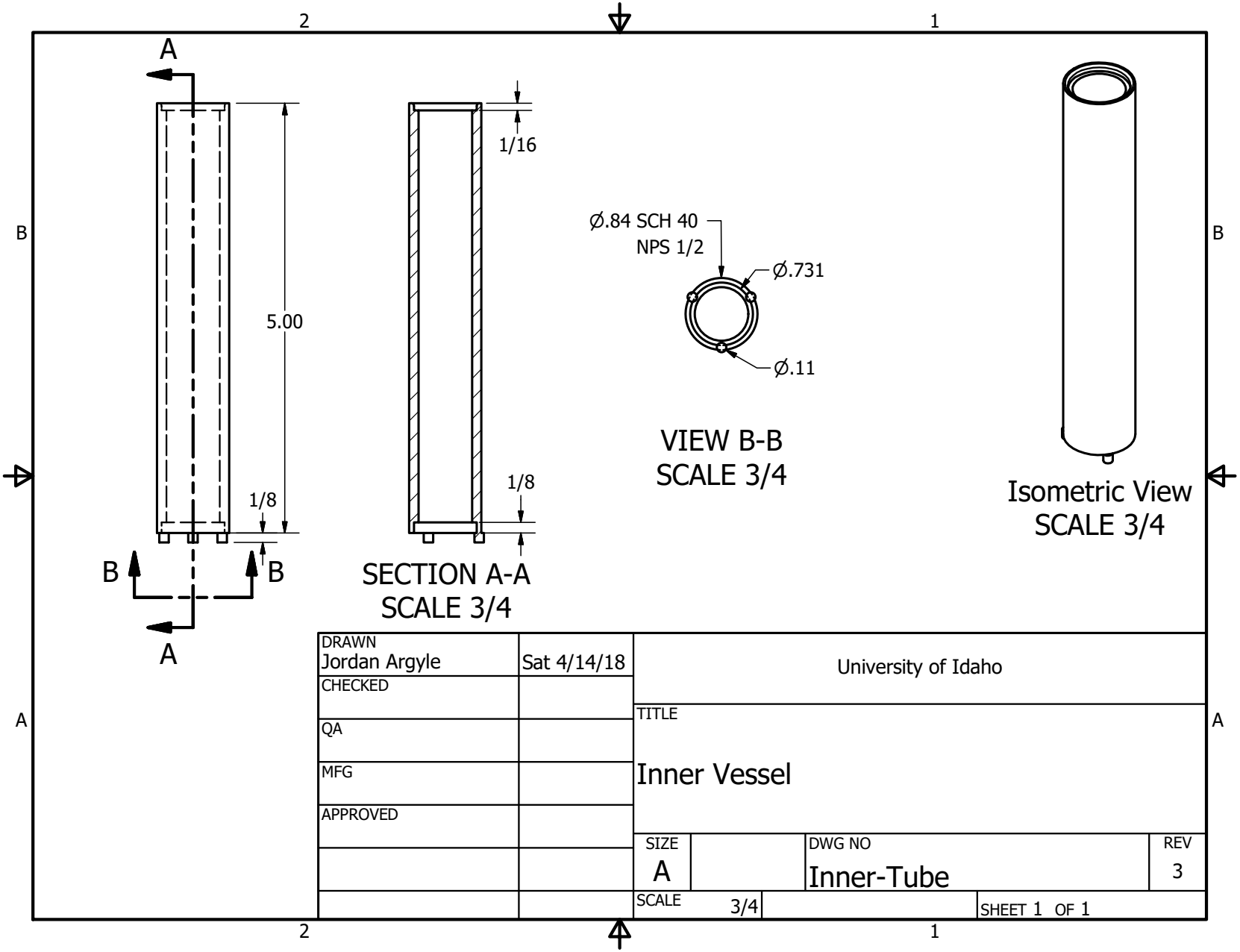
2
1
A
5.00
1/8
B
B
A
1/16
1/8
SECTION A-A
SCALE 3/4
Ø.84 SCH 40
NPS 1/2
Ø.731
Ø.11
VIEW B-B
SCALE 3/4
Isometric View
SCALE 3/4
B
A
DRAWN
Jordan Argyle
Sat 4/14/18
CHECKED
QA
MFG
APPROVED
University of Idaho
TITLE
Inner Vessel
SIZE
A
DWG NO
Inner-Tube
REV
3
SCALE
3/4
SHEET 1 OF 1

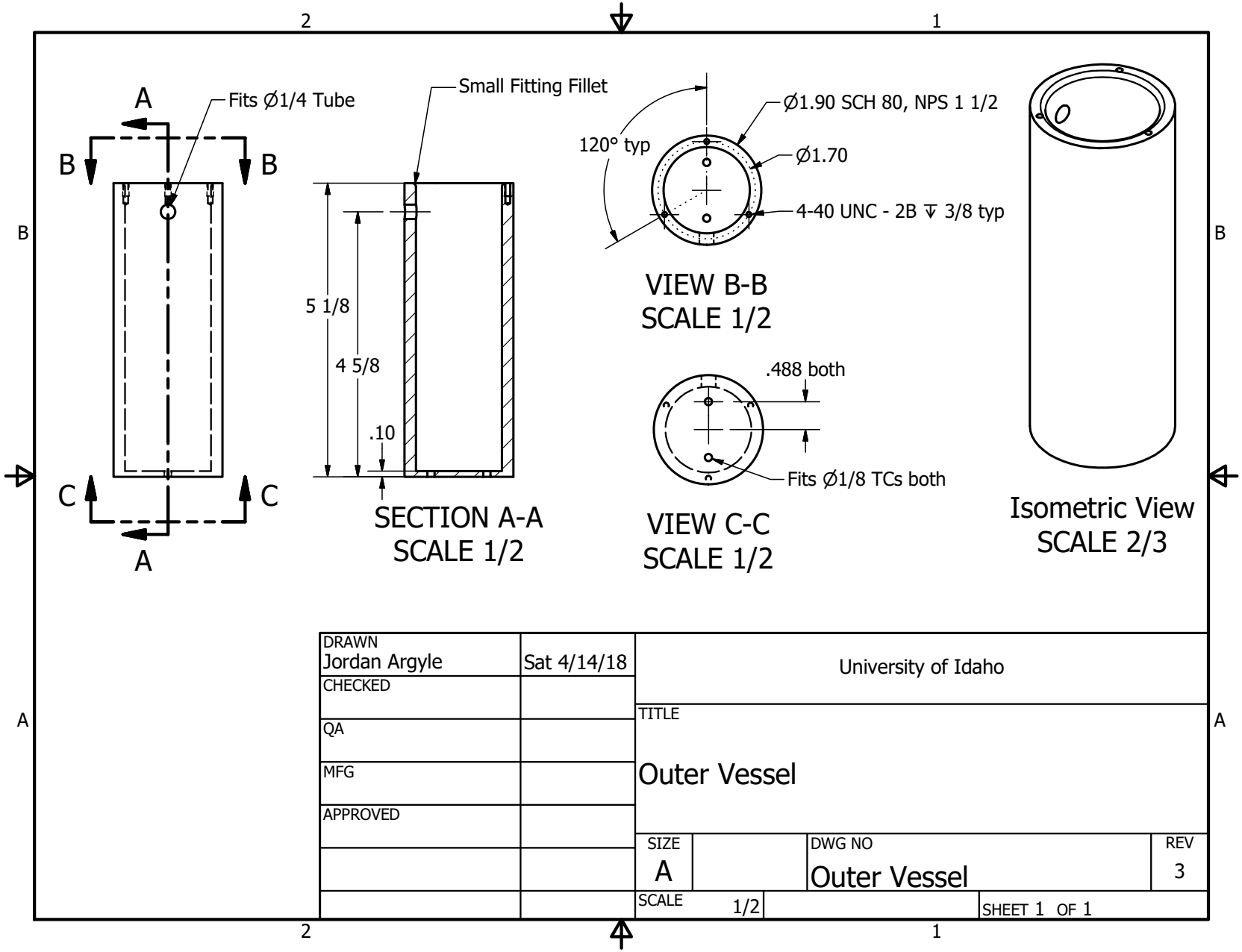
2
1
A
B
B
C
C
A
Fits Ø1/4 Tube
Small Fitting Fillet
5 1/8
4 5/8
.10
SECTION A-A
SCALE 1/2
120° typ
Ø1.90 SCH 80, NPS 1 1/2
Ø1.70
4-40 UNC - 2B ↧ 3/8 typ
VIEW B-B
SCALE 1/2
.488 both
Fits Ø1/8 TCs both
VIEW C-C
SCALE 1/2
Isometric View
SCALE 2/3
DRAWN
Jordan Argyle
Sat 4/14/18
CHECKED
QA
MFG
APPROVED
University of Idaho
TITLE
Outer Vessel
SIZE
A
DWG NO
Outer Vessel
REV
3
SCALE
1/2
SHEET 1 OF 1

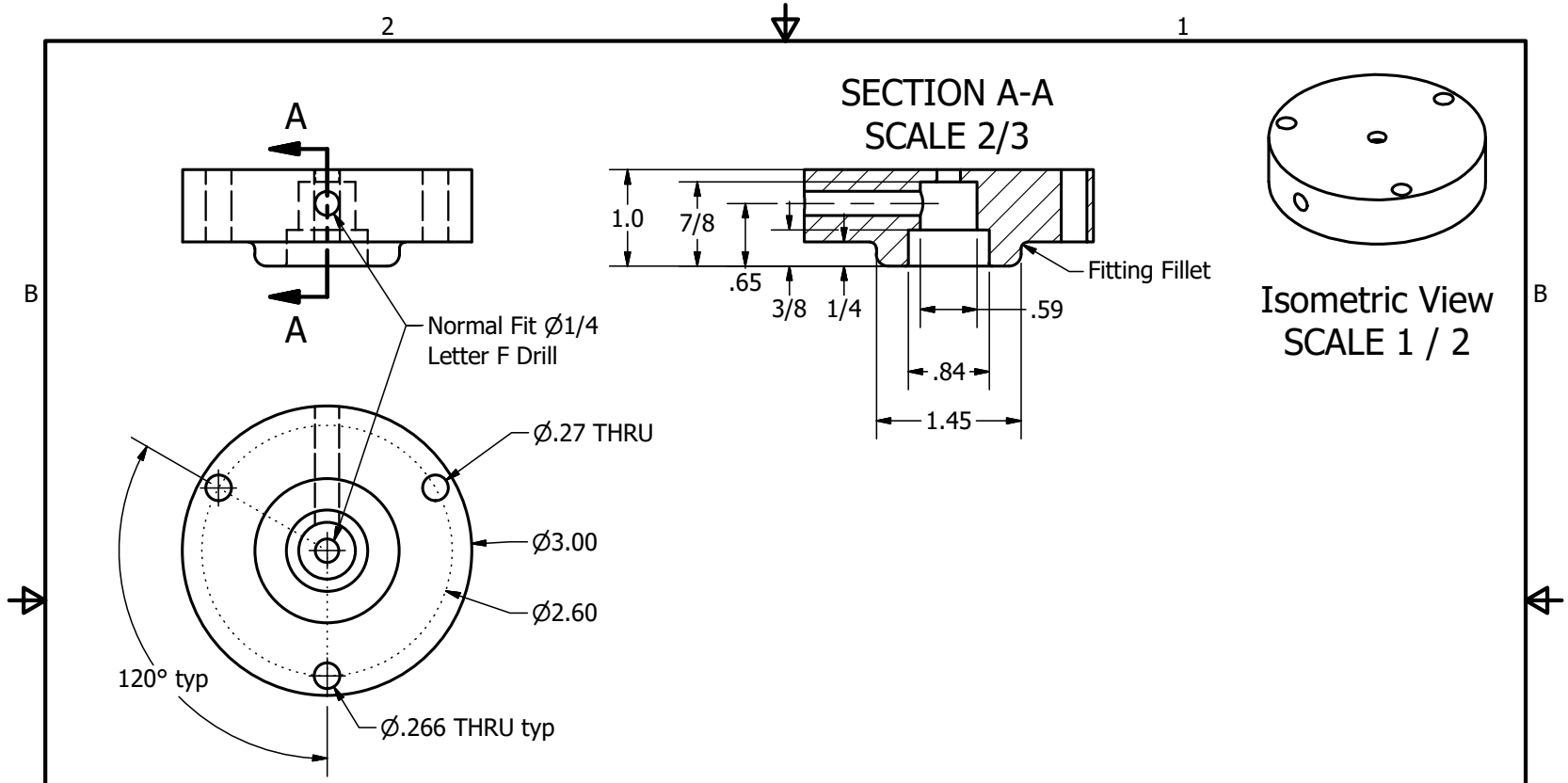

DRAWN Jordan Argyle	Sat 4/14/18	University of Idaho
CHECKED		
QA		TITLE
MFG		Vessel Lid
APPROVED		
		SIZE A | DWG NO Getter Lid | REV 4
		SCALE 2/3 | SHEET 1 OF 1

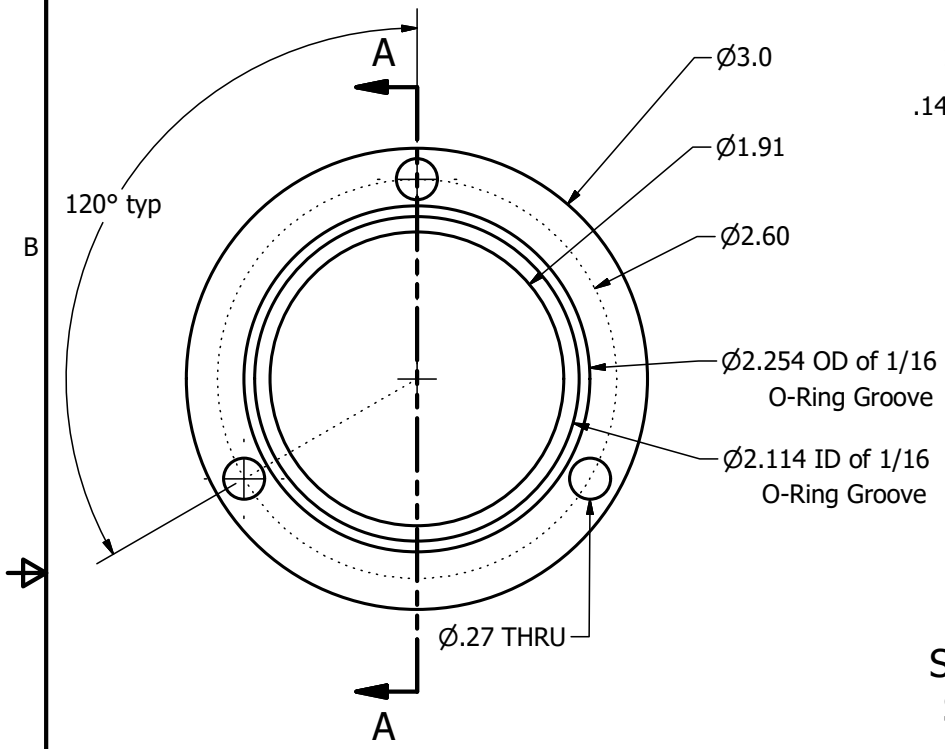

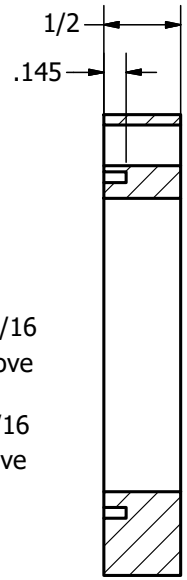

SECTION A-A
SCALE 1 : 1

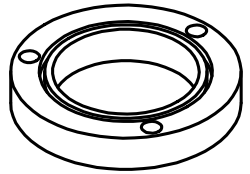

Isometric View
SCALE 1 / 2

DRAWN Jordan Argyle	Fri 4/20/18	University of Idaho	
CHECKED		TITLE Outer Vessel Ring	
QA			
MFG			
APPROVED			
		SIZE A	DWG NO Outer Vessel Ring / REV 4
		SCALE 1 : 1	SHEET 1 OF 1

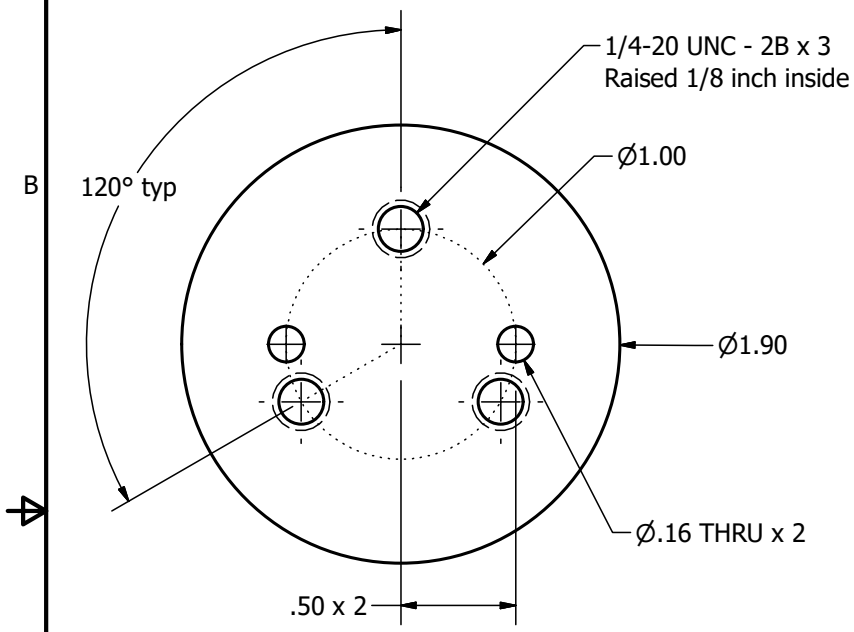

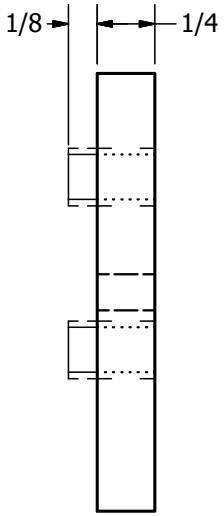

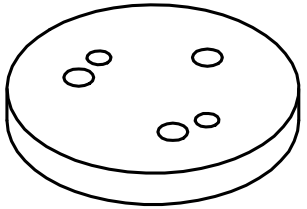

Isometric View
SCALE 1 : 1

DRAWN Jordan Argyle	Fri 4/20/18	University of Idaho	
CHECKED		TITLE Outer Vessel Bottom Plate	
QA			
MFG			
APPROVED			
		SIZE A	DWG NO Outer Vessel Bottom Plate / REV 4
		SCALE 1.5:1	SHEET 1 OF 1

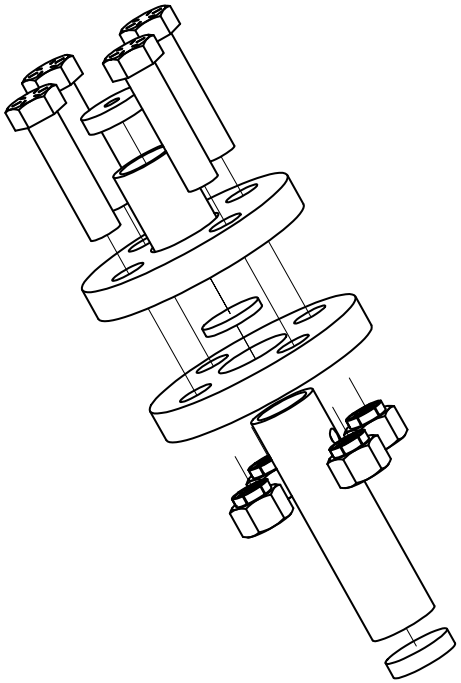

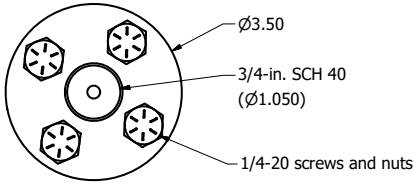

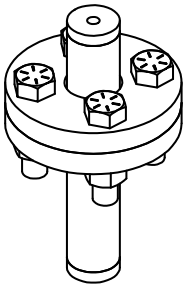

Isometric View
SCALE 1 / 2

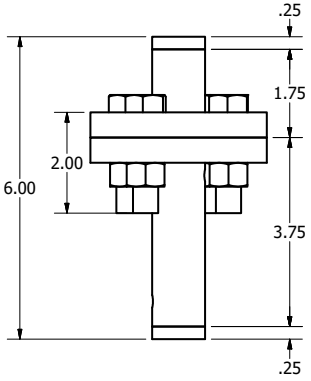

DRAWN Jordan Argyle	Fri 4/27/18	University of Idaho	
CHECKED		TITLE	
QA		Diffusion Tank	
MFG			
APPROVED		SIZE B	DWG NO Diffusion Tank / REV 1
		SCALE 1 / 2	SHEET 1 OF 1

Appendix B: Final Component Design Drawings

This appendix contains the final drawings of various components, which were sent to the shop for construction. The different drawings in this appendix are noted on the list below.

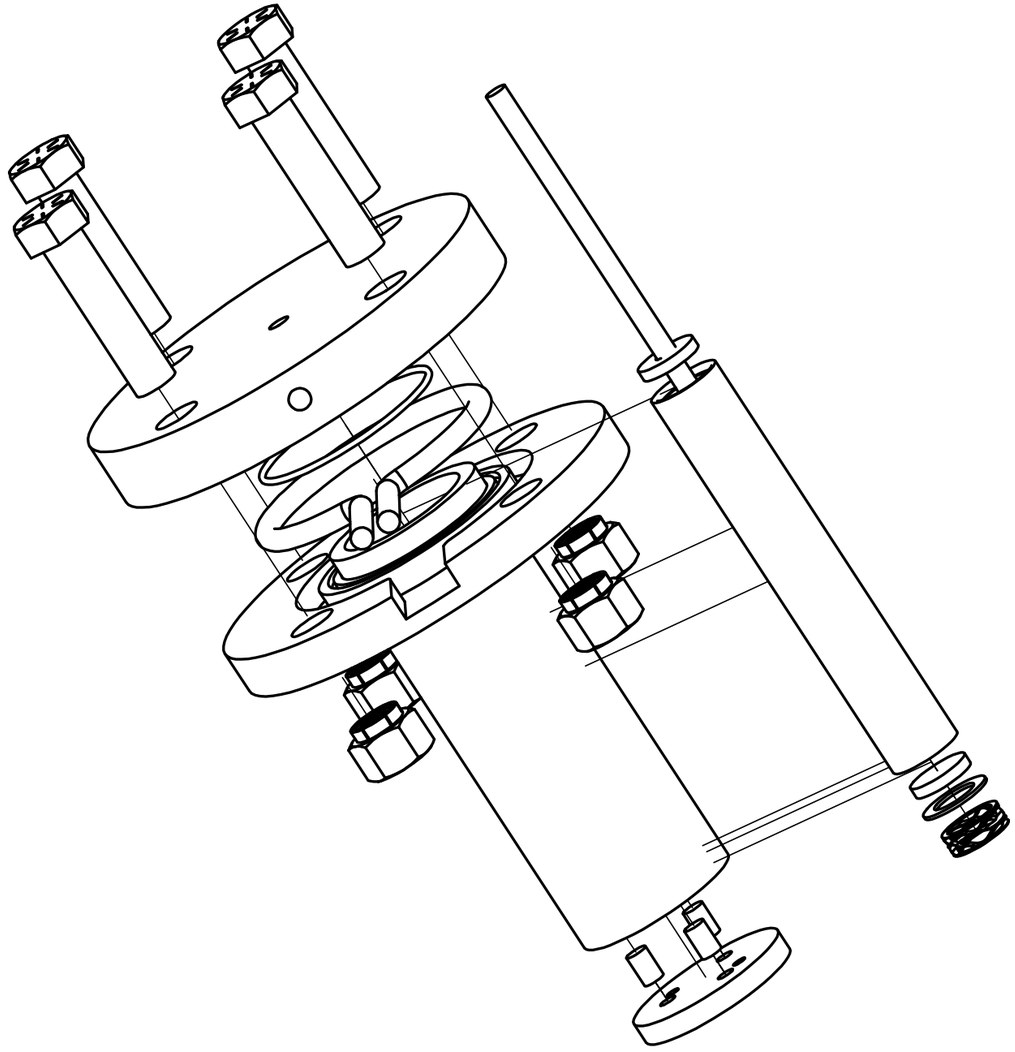

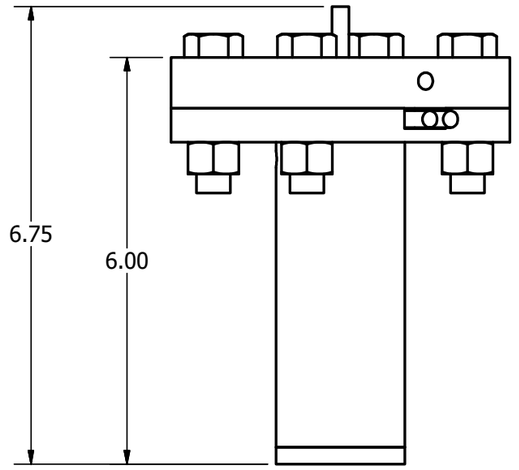

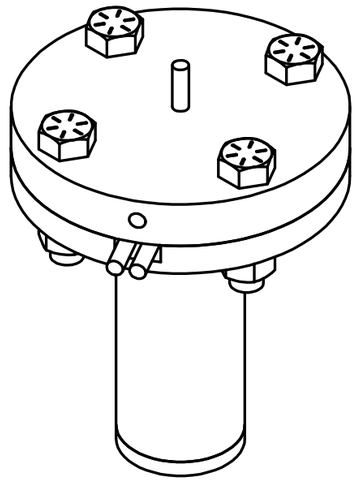

Isometric View
SCALE 1 / 2

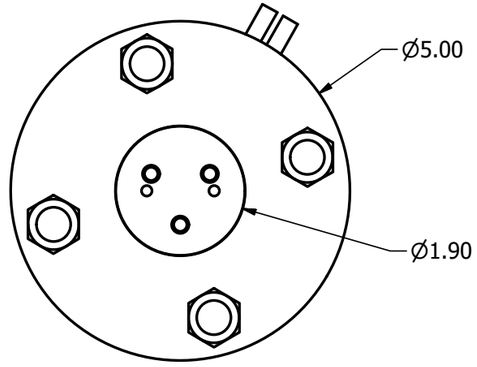

DRAWN Jordan Argyle	Mon 4/23/18	University of Idaho	
CHECKED		TITLE Getter Tank	
QA			
MFG			
APPROVED		SIZE B	DWG NO Getter Tank / REV 5
		SCALE 1 / 2	SHEET 1 OF 1

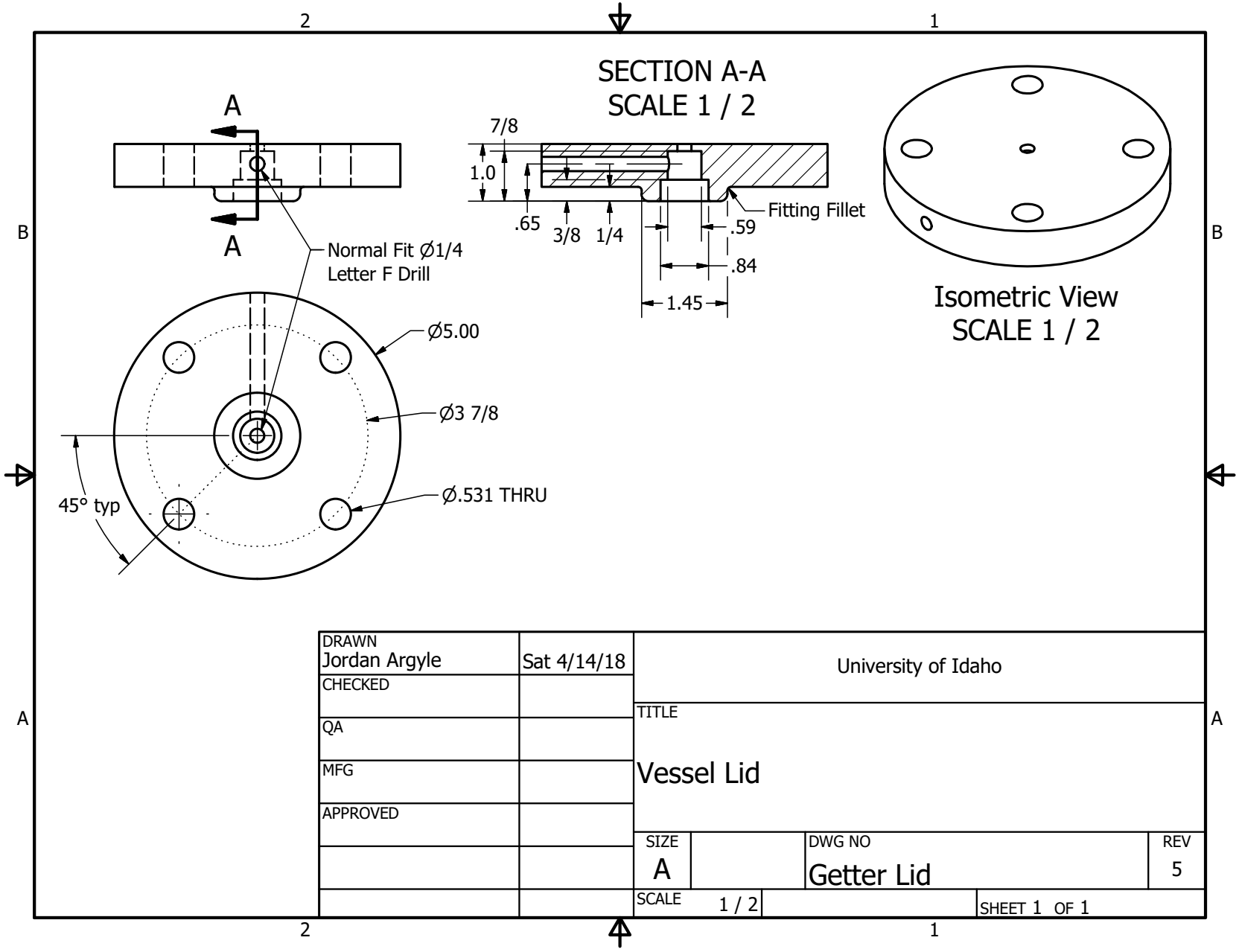
SECTION A-A
SCALE 1 / 2
A
A
7/8
1.0
.65
3/8
1/4
.59
.84
1.45
Fitting Fillet
Normal Fit Ø1/4
Letter F Drill
Ø5.00
Ø3 7/8
Ø.531 THRU
45° typ
Isometric View
SCALE 1 / 2
DRAWN
Jordan Argyle
Sat 4/14/18
CHECKED
QA
MFG
APPROVED
University of Idaho
TITLE
Vessel Lid
SIZE
A
DWG NO
Getter Lid
REV
5
SCALE
1 / 2
SHEET 1 OF 1

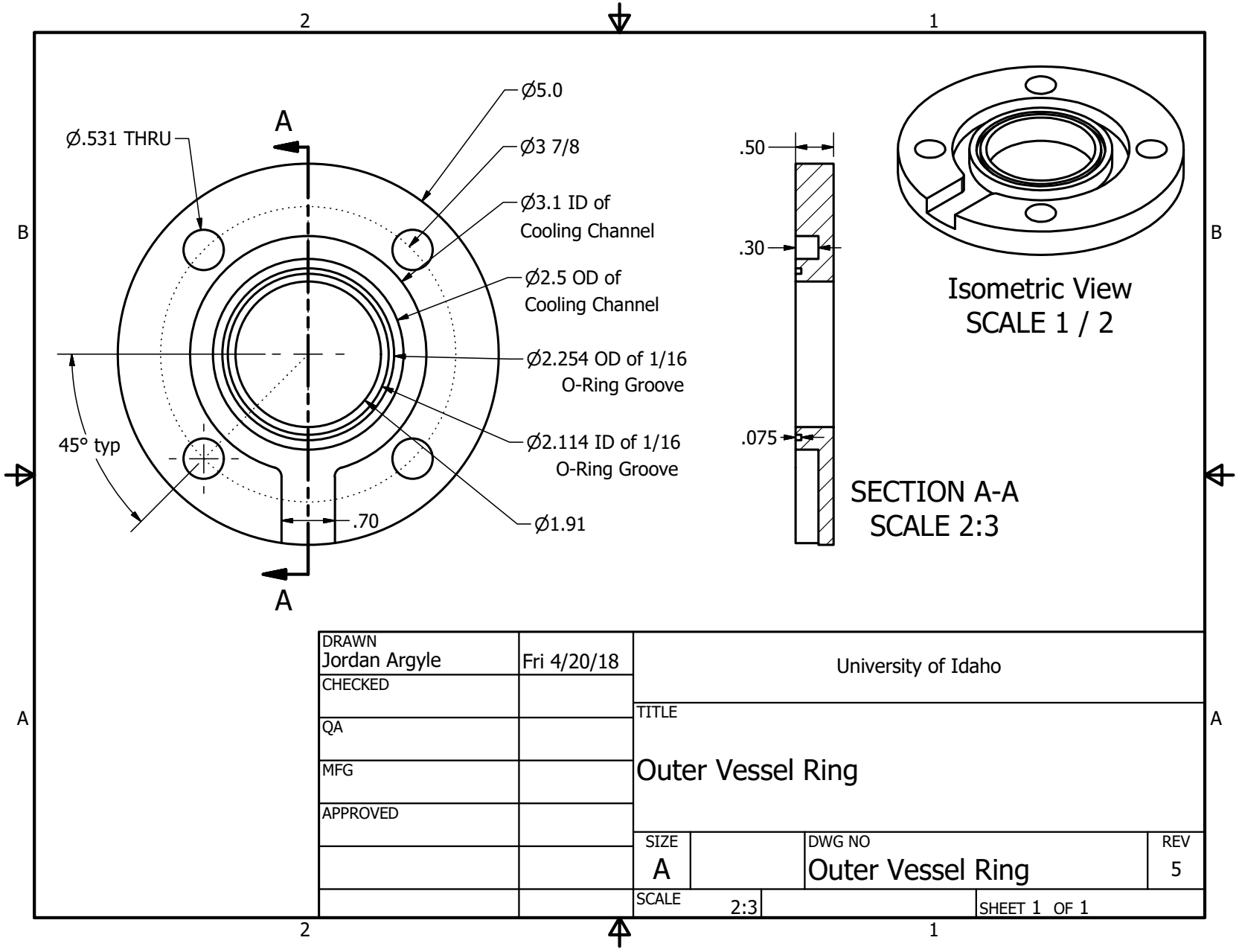
2
1
B
A
Ø.531 THRU
A
Ø5.0
Ø3 7/8
Ø3.1 ID of
Cooling Channel
Ø2.5 OD of
Cooling Channel
Ø2.254 OD of 1/16
O-Ring Groove
Ø2.114 ID of 1/16
O-Ring Groove
Ø1.91
45° typ
.70
A
.50
.30
.075
SECTION A-A
SCALE 2:3
Isometric View
SCALE 1 / 2
DRAWN
Jordan Argyle
Fri 4/20/18
CHECKED
QA
MFG
APPROVED
University of Idaho
TITLE
Outer Vessel Ring
SIZE
A
DWG NO
Outer Vessel Ring
REV
5
SCALE
2:3
SHEET 1 OF 1

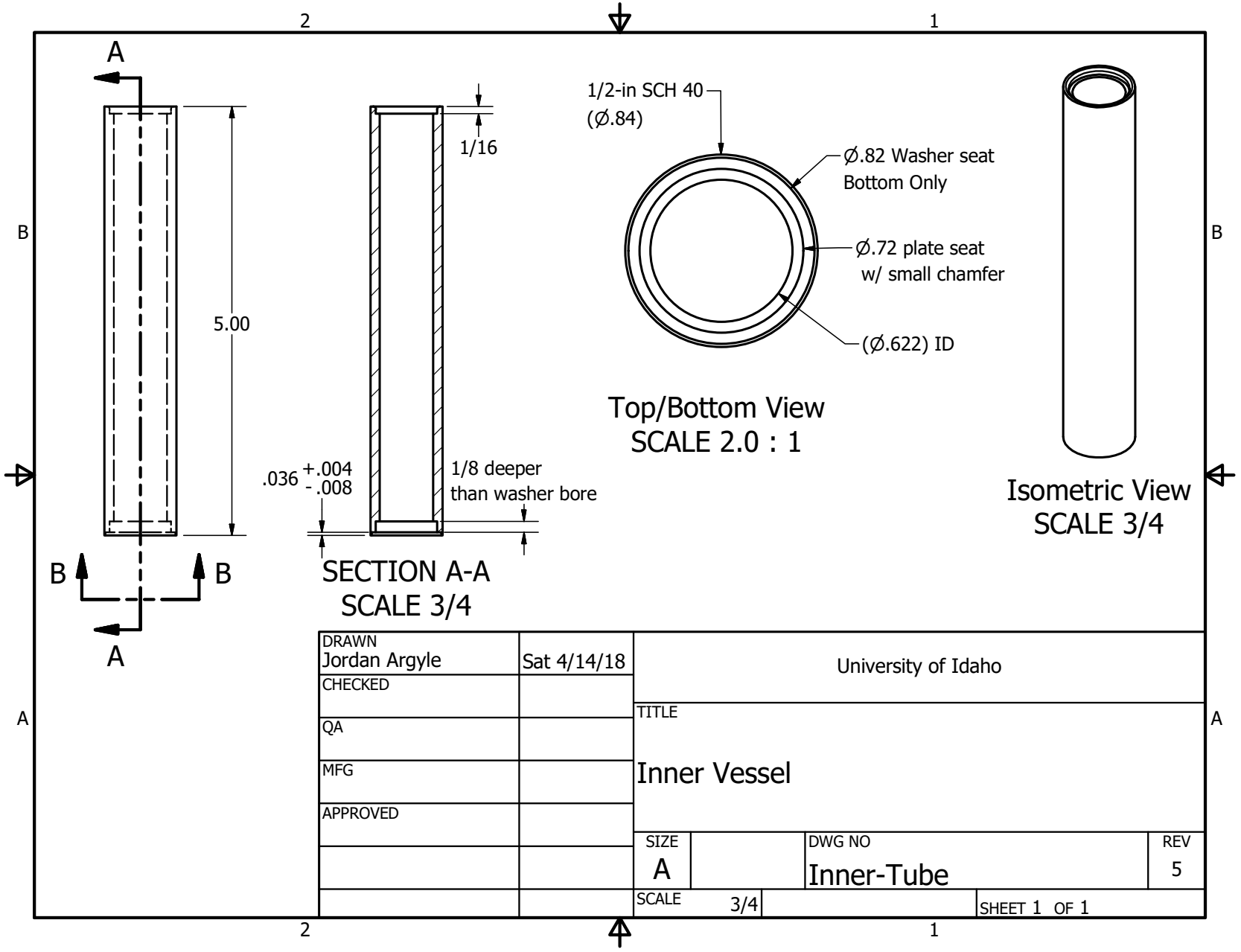
2
1
A
B
5.00
1/16
.036 +.004 -.008
1/8 deeper
than washer bore
SECTION A-A
SCALE 3/4
1/2-in SCH 40
(Ø.84)
Ø.82 Washer seat
Bottom Only
Ø.72 plate seat
w/ small chamfer
(Ø.622) ID
Top/Bottom View
SCALE 2.0 : 1
Isometric View
SCALE 3/4
DRAWN
Jordan Argyle
Sat 4/14/18
CHECKED
QA
MFG
APPROVED
University of Idaho
TITLE
Inner Vessel
SIZE
A
DWG NO
Inner-Tube
REV
5
SCALE
3/4
SHEET 1 OF 1

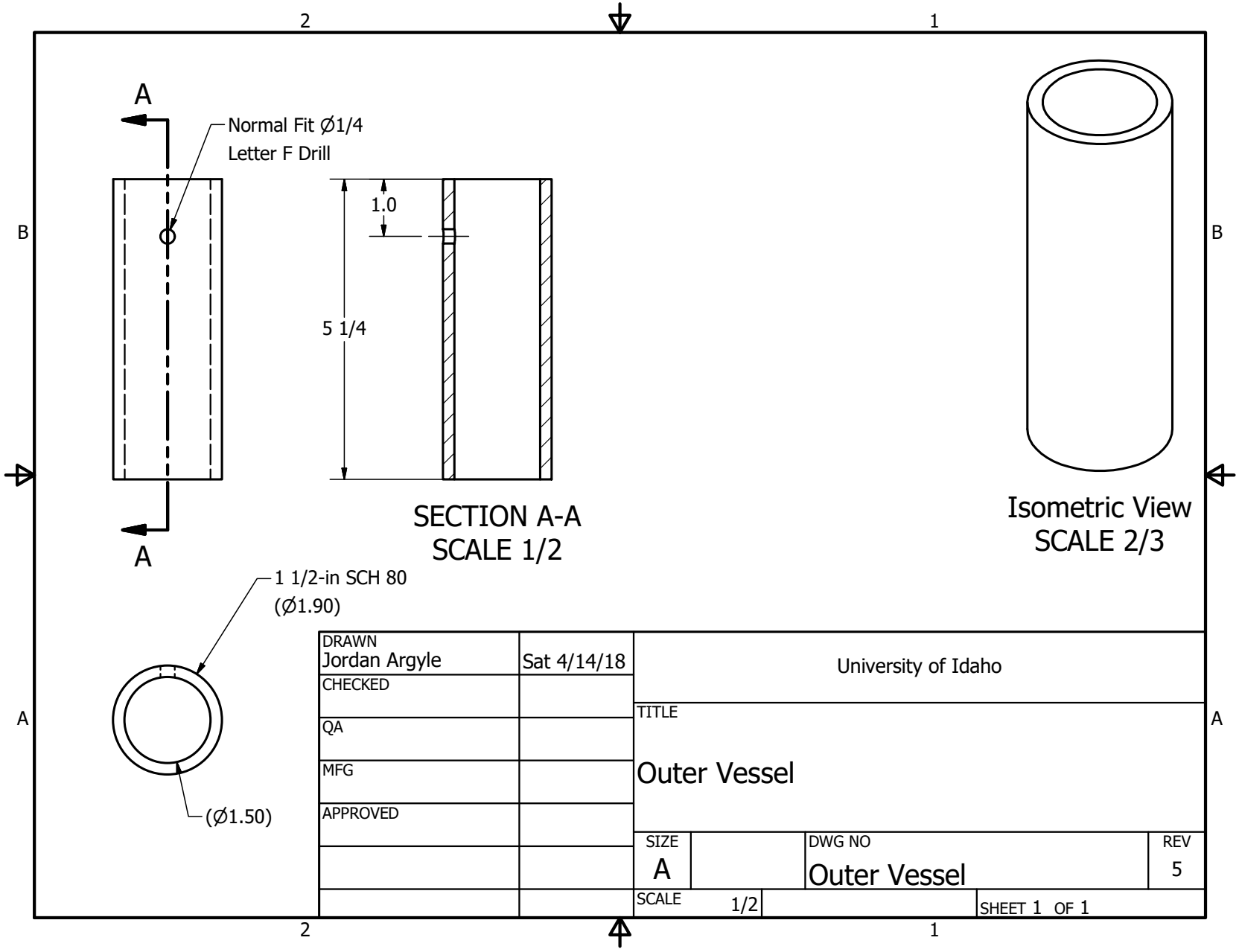
A
Normal Fit Ø1/4
Letter F Drill
1.0
5 1/4
A
SECTION A-A
SCALE 1/2
Isometric View
SCALE 2/3
1 1/2-in SCH 80
(Ø1.90)
(Ø1.50)
DRAWN
Jordan Argyle
Sat 4/14/18
CHECKED
QA
MFG
APPROVED
University of Idaho
TITLE
Outer Vessel
SIZE
A
DWG NO
Outer Vessel
REV
5
SCALE
1/2
SHEET 1 OF 1

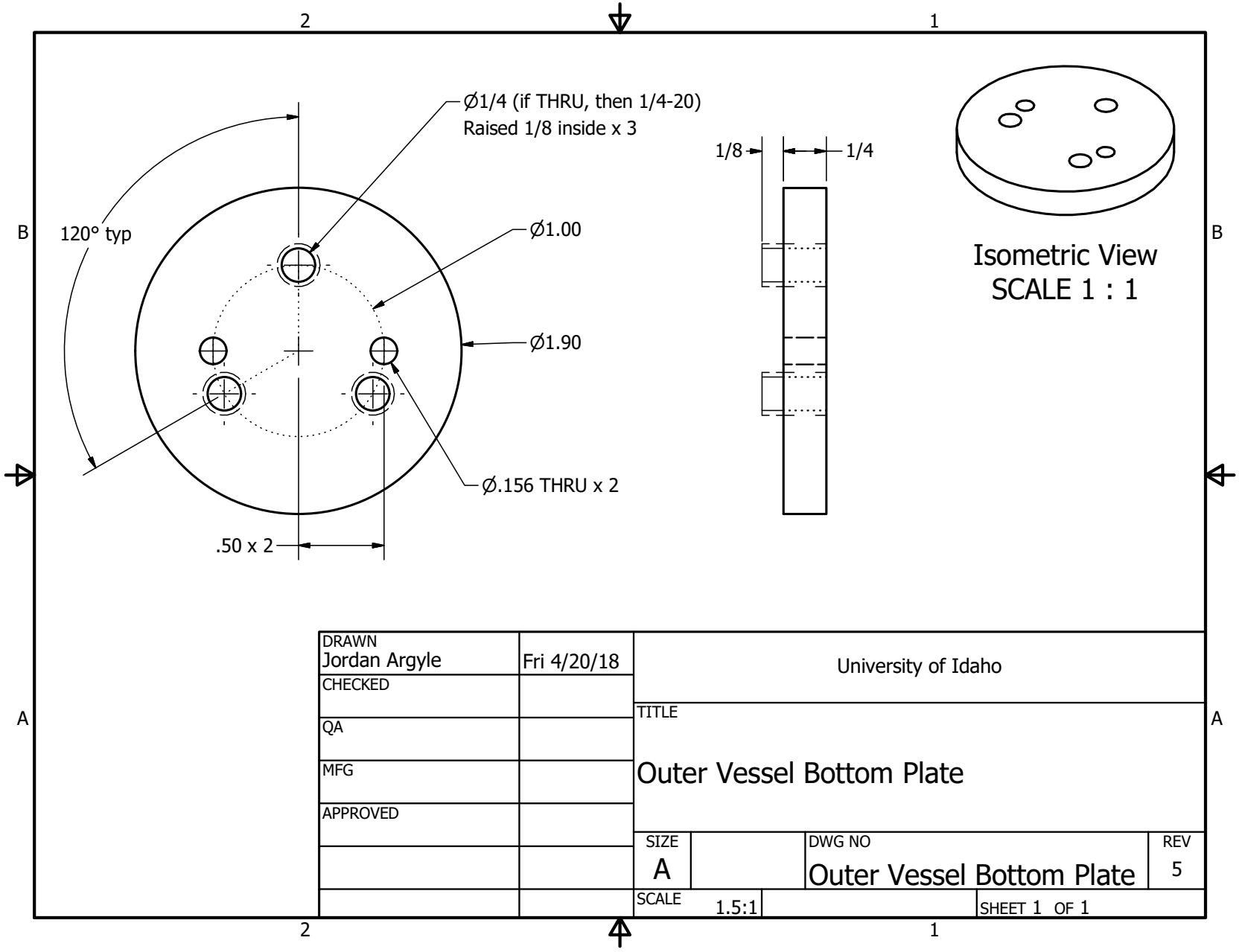
2
1
B
A
Ø1/4 (if THRU, then 1/4-20)
Raised 1/8 inside x 3
120° typ
Ø1.00
Ø1.90
Ø.156 THRU x 2
.50 x 2
1/8
1/4
Isometric View
SCALE 1 : 1
DRAWN
Jordan Argyle
Fri 4/20/18
CHECKED
QA
MFG
APPROVED
University of Idaho
TITLE
Outer Vessel Bottom Plate
SIZE
A
DWG NO
Outer Vessel Bottom Plate
REV
5
SCALE
1.5:1
SHEET 1 OF 1

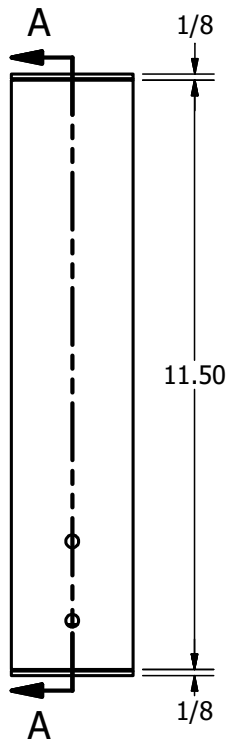

SECTION A-A
SCALE 1/3

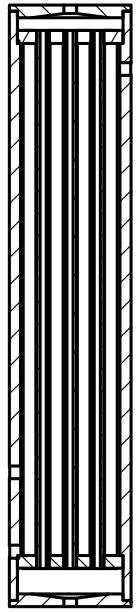

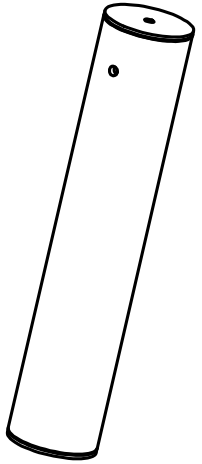

Isometric View
SCALE 1 / 4

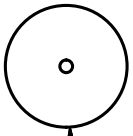

DRAWN Jordan Argyle	Fri 4/13/18	University of Idaho
CHECKED		TITLE: Argon Condenser
QA		
MFG		
APPROVED		
		SIZE A | DWG NO Assembly | REV 5
		SCALE 1/3 | SHEET 1 OF 6

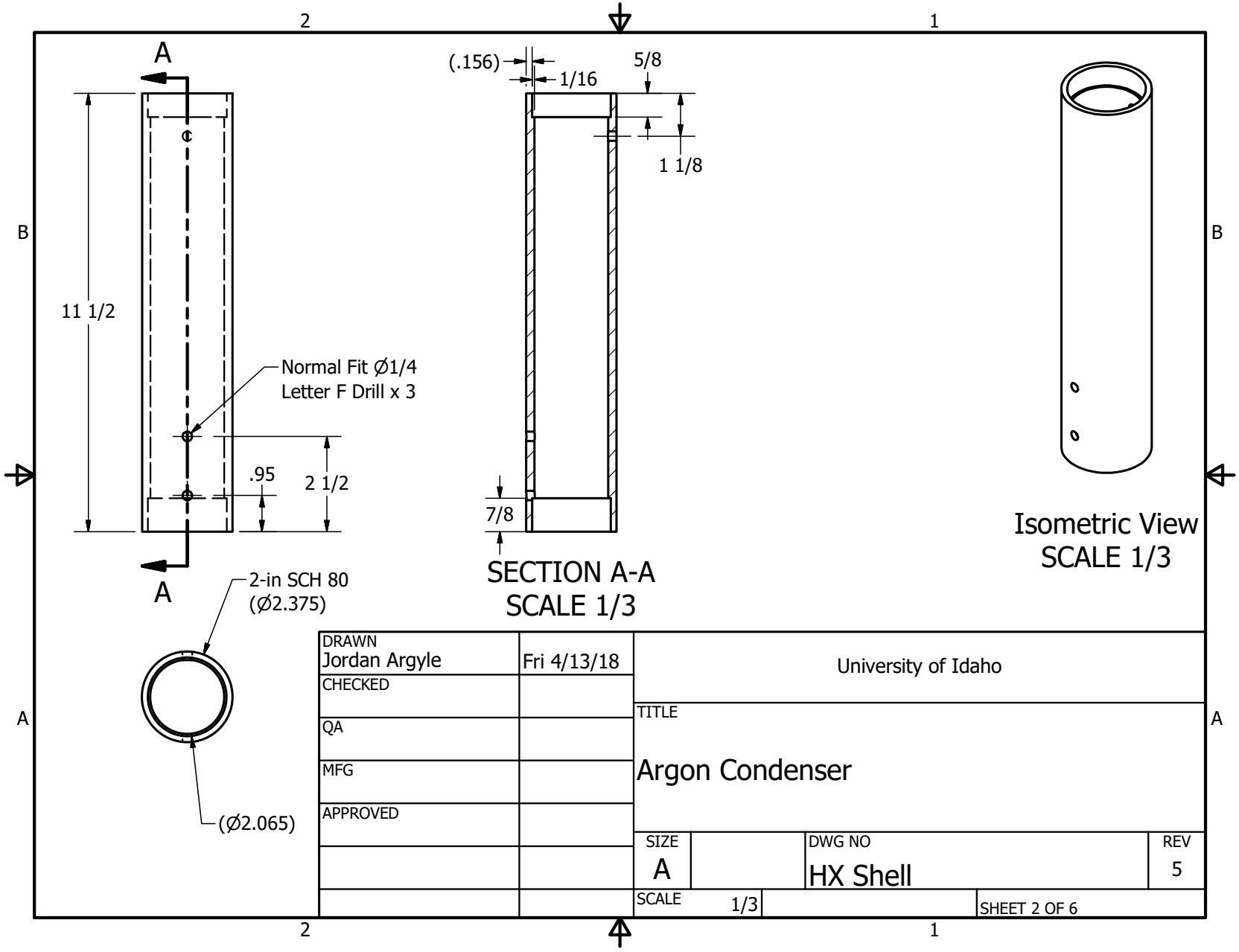
A
A
11 1/2
Normal Fit Ø1/4
Letter F Drill x 3
.95
2 1/2
2-in SCH 80
(Ø2.375)
(Ø2.065)
(.156)
1/16
5/8
1 1/8
7/8
SECTION A-A
SCALE 1/3
Isometric View
SCALE 1/3
DRAWN
Jordan Argyle
Fri 4/13/18
CHECKED
QA
MFG
APPROVED
University of Idaho
TITLE
Argon Condenser
SIZE
A
DWG NO
HX Shell
REV
5
SCALE
1/3
SHEET 2 OF 6

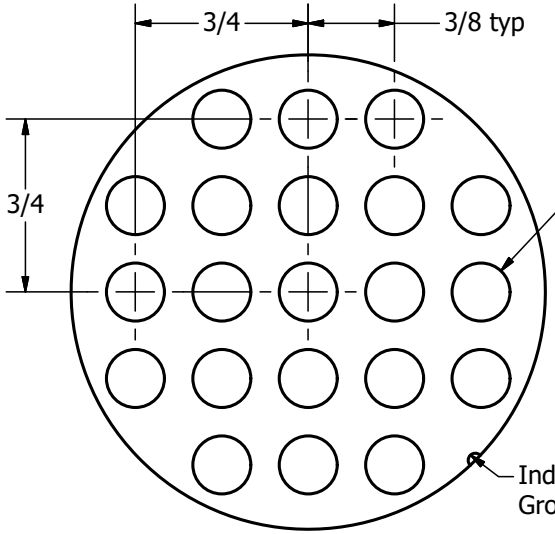

Top View
SCALE 3/2

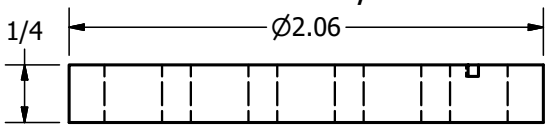

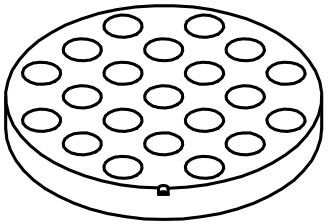

Isometric View
SCALE 1 : 1

DRAWN Jordan Argyle	Fri 4/13/18	University of Idaho	
CHECKED			
QA		TITLE Argon Condenser	
MFG			
APPROVED			
		SIZE A	DWG NO Tube Sheet / REV 5
		SCALE 3/2	SHEET 4 OF 6

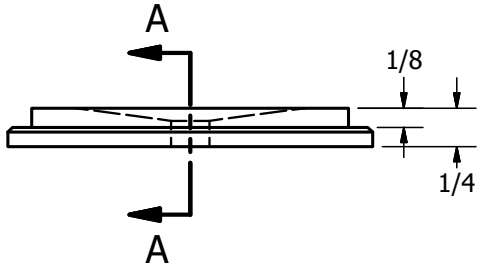

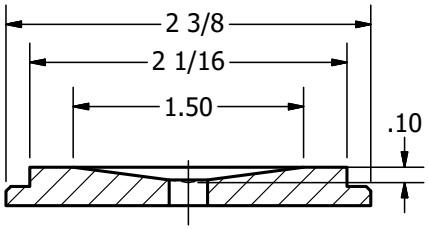

SECTION A-A
SCALE 1 : 1

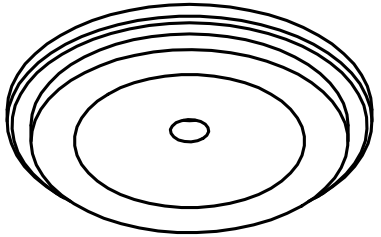

Isometric View
SCALE 1 : 1

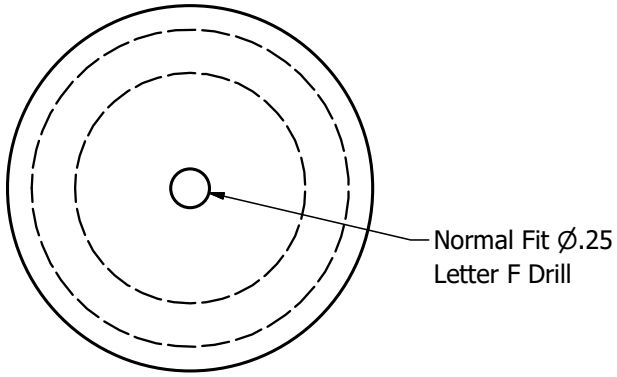

Top View
SCALE 1 : 1

DRAWN Jordan Argyle	Fri 4/13/18	University of Idaho	
CHECKED			
QA		TITLE	
MFG		Argon Condenser	
APPROVED			
		SIZE A	DWG NO Endcaps / REV 5
		SCALE 1 : 1	SHEET 3 OF 6

Appendix C: Getter System Redesign

This appendix contains the drawings for the full getter system redesign, necessitated by the problems encountered validating the vertical getter tank from Appendix B. This design was verified using ANSYS (see Appendix E), but not built or validated due to time constraints. The different drawings in this appendix are noted on the list below.

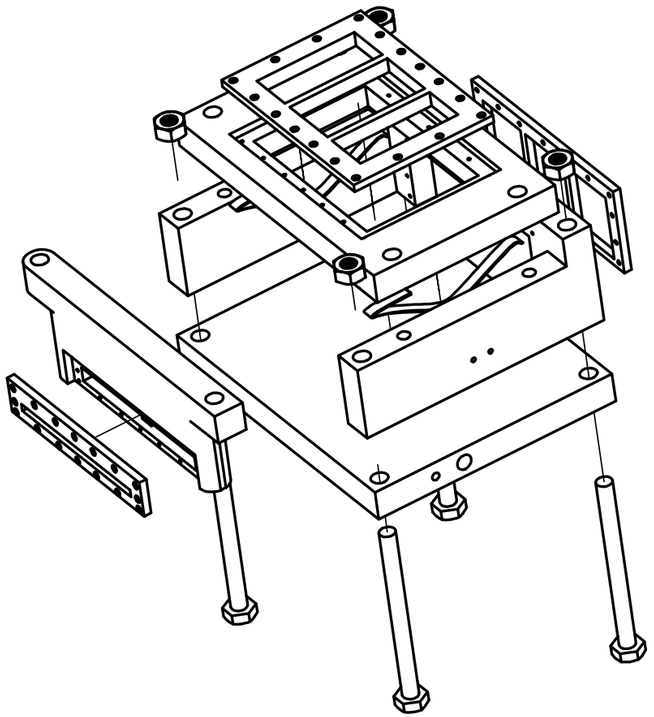

Holding Box

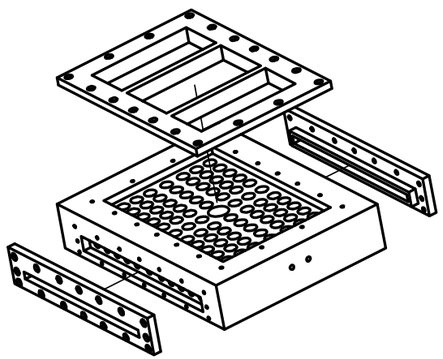

Getter Tray

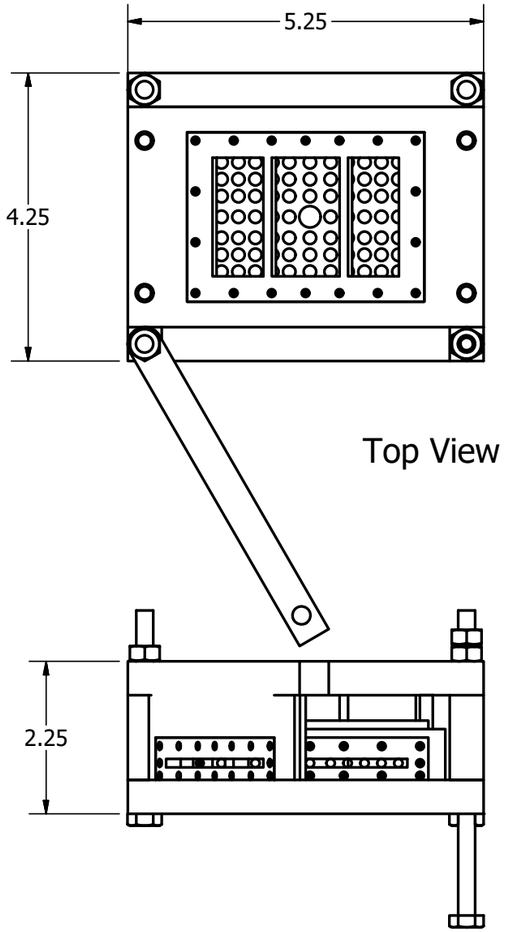

Top View

Front View

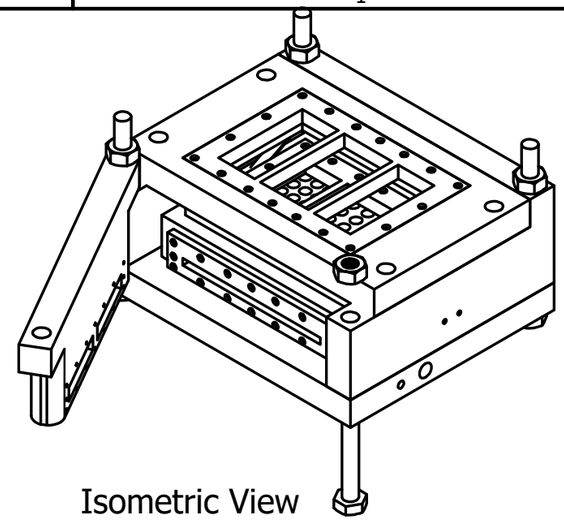

Isometric View
SCALE 1 : 2

Notes:
All units inches.

For all parts, unless otherwise specified, tolerances are:

.x ± .1 .xx ± .01

.xxx ± .003 y/x ± 1/(2x)

DRAWN Jordan Argyle	11/27/18	University of Idaho
CHECKED		TITLE: Getter Tray Assembly
QA		
MFG		
APPROVED		
		SIZE B · DWG NO Getter Tray Assembly · REV 2
		SCALE 1 : 2 · SHEET 1 of 10

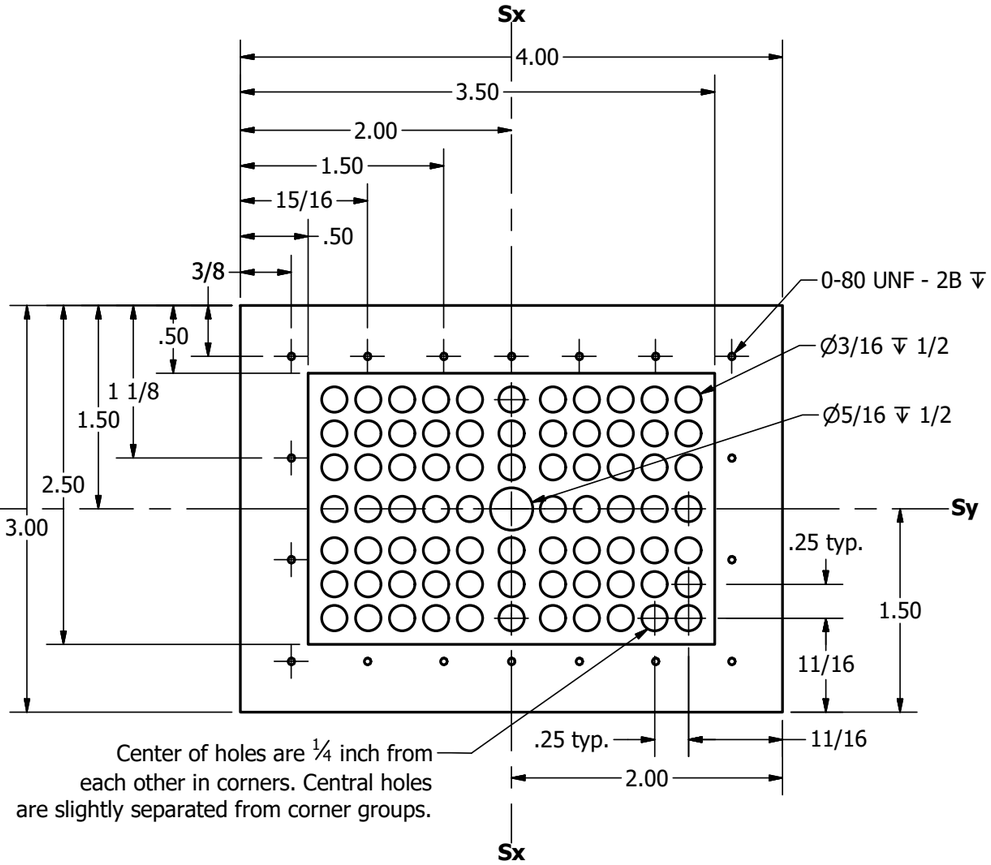

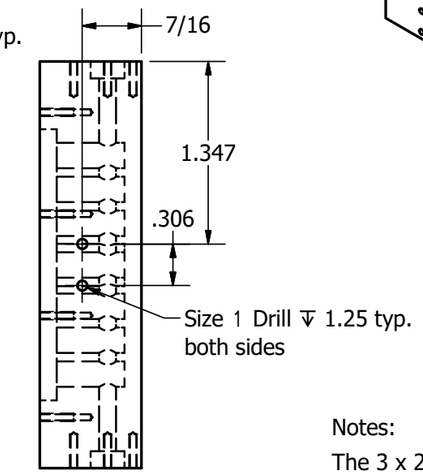

Not a section view

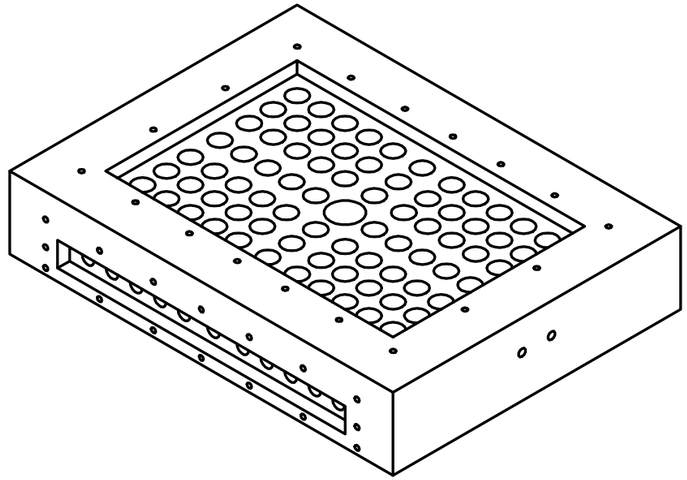

Isometric View
SCALE 1 : 1

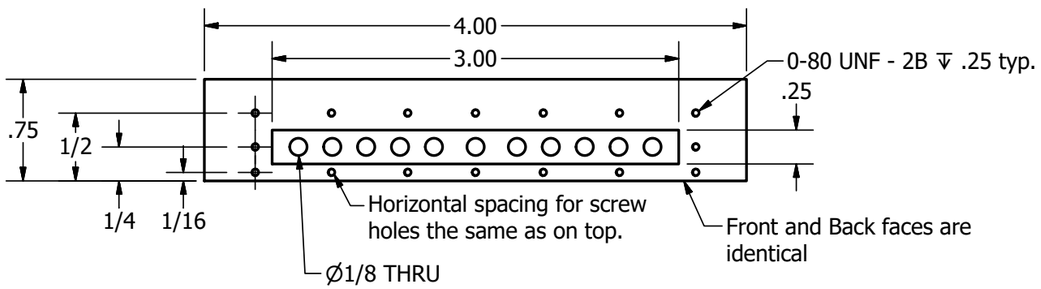

Notes:

The 3 x 2 inch cutout on top and the 3 x ¼ inch cutouts over the holes on the front and back is ⅛ deep.

Screw holes to be drilled throgh cover, screen, and tray at same time.

Getter tray is symmetric across **Sx** and **Sy**, forming 4 identical quandrants on top, identical front and back faces, and identical side faces.

All units inches.

DRAWN Jordan Argyle	11/27/18	University of Idaho
CHECKED		TITLE: Getter Tray
QA		
MFG		
APPROVED		
SIZE B	DWG NO Getter Tray	REV 2
SCALE 1 : 1		2 of 10

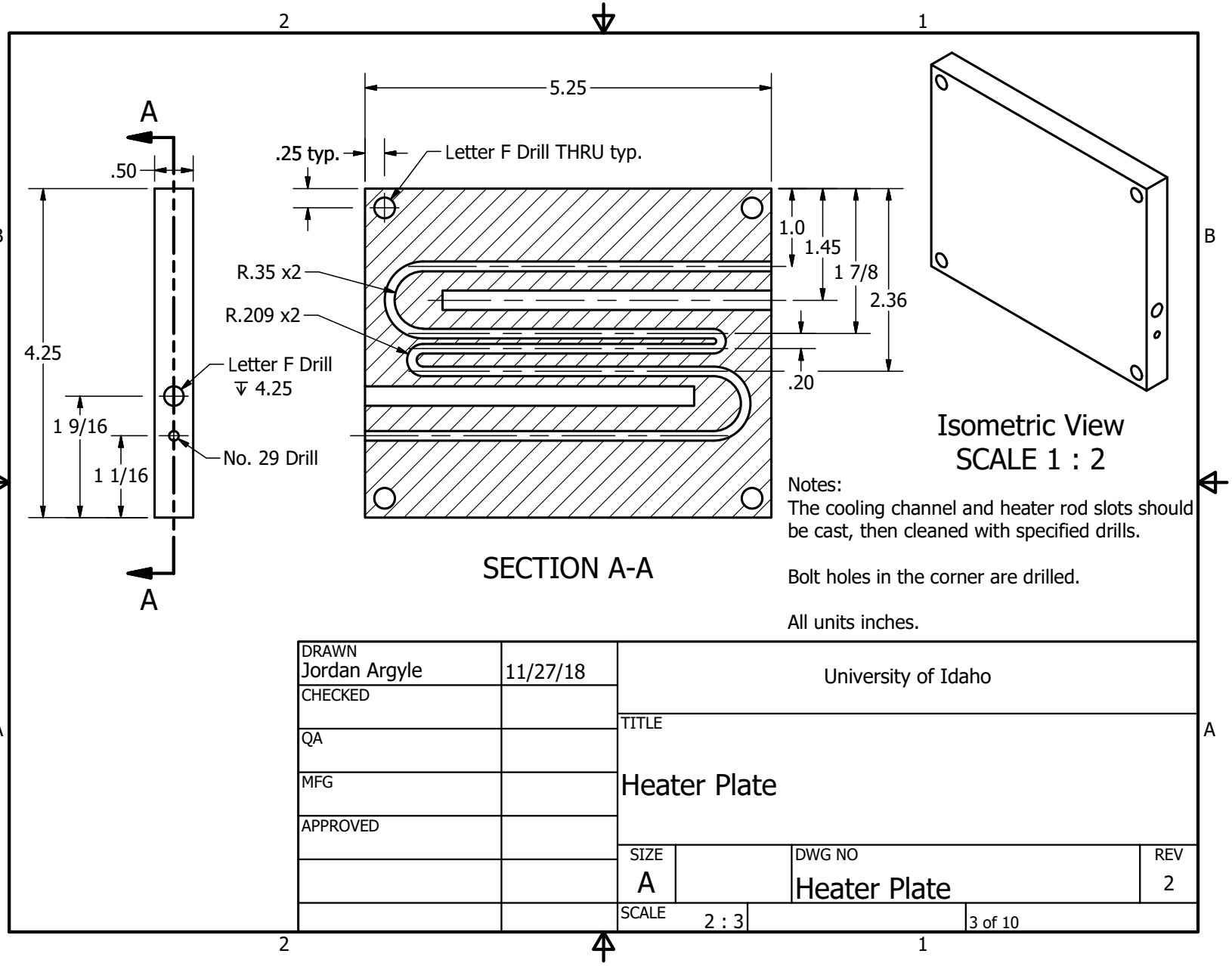
2
1
B
A
5.25
.25 typ.
Letter F Drill THRU typ.
.50
4.25
1 9/16
1 1/16
Letter F Drill
4.25
No. 29 Drill
R.35 x2
R.209 x2
1.0
1.45
1 7/8
2.36
.20
A
A
SECTION A-A
Isometric View
SCALE 1 : 2
Notes:
The cooling channel and heater rod slots should be cast, then cleaned with specified drills.
Bolt holes in the corner are drilled.
All units inches.
DRAWN
Jordan Argyle
11/27/18
CHECKED
QA
MFG
APPROVED
University of Idaho
TITLE
Heater Plate
SIZE
A
DWG NO
Heater Plate
REV
2
SCALE
2 : 3
3 of 10

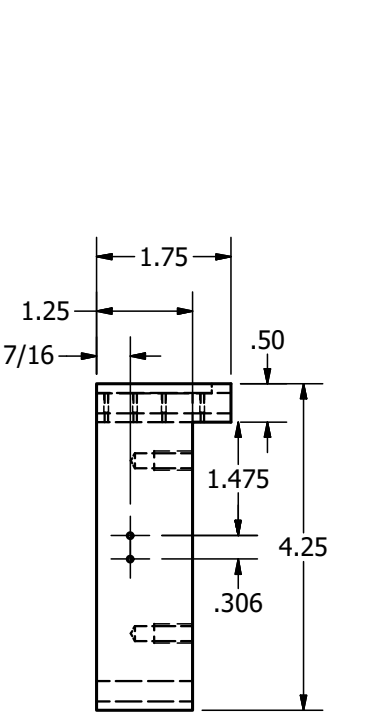

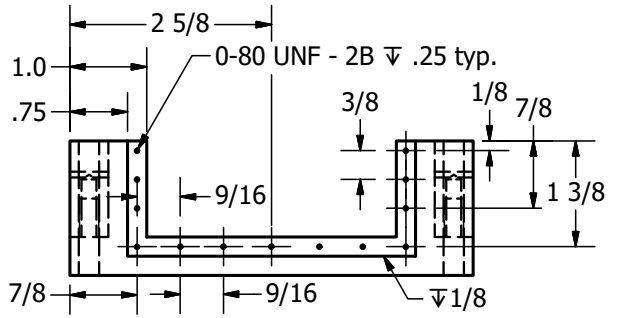

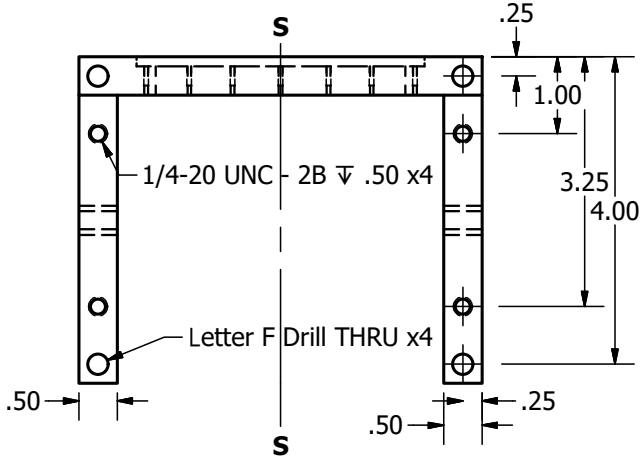

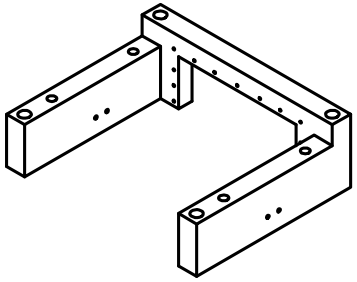

Isometric View
SCALE 1 : 3

Notes:
Frame is symmetric across **SS.**

Screw holes to be drilled throgh cover, screen, and tray at same time.

All units inches.

DRAWN Jordan Argyle	11/27/18	University of Idaho
CHECKED		TITLE: Holding Box Frame
QA		
MFG		
APPROVED		

SIZE		DWG NO	REV
A		Holding Box - Frame	2
SCALE 1 : 2			4 of 10

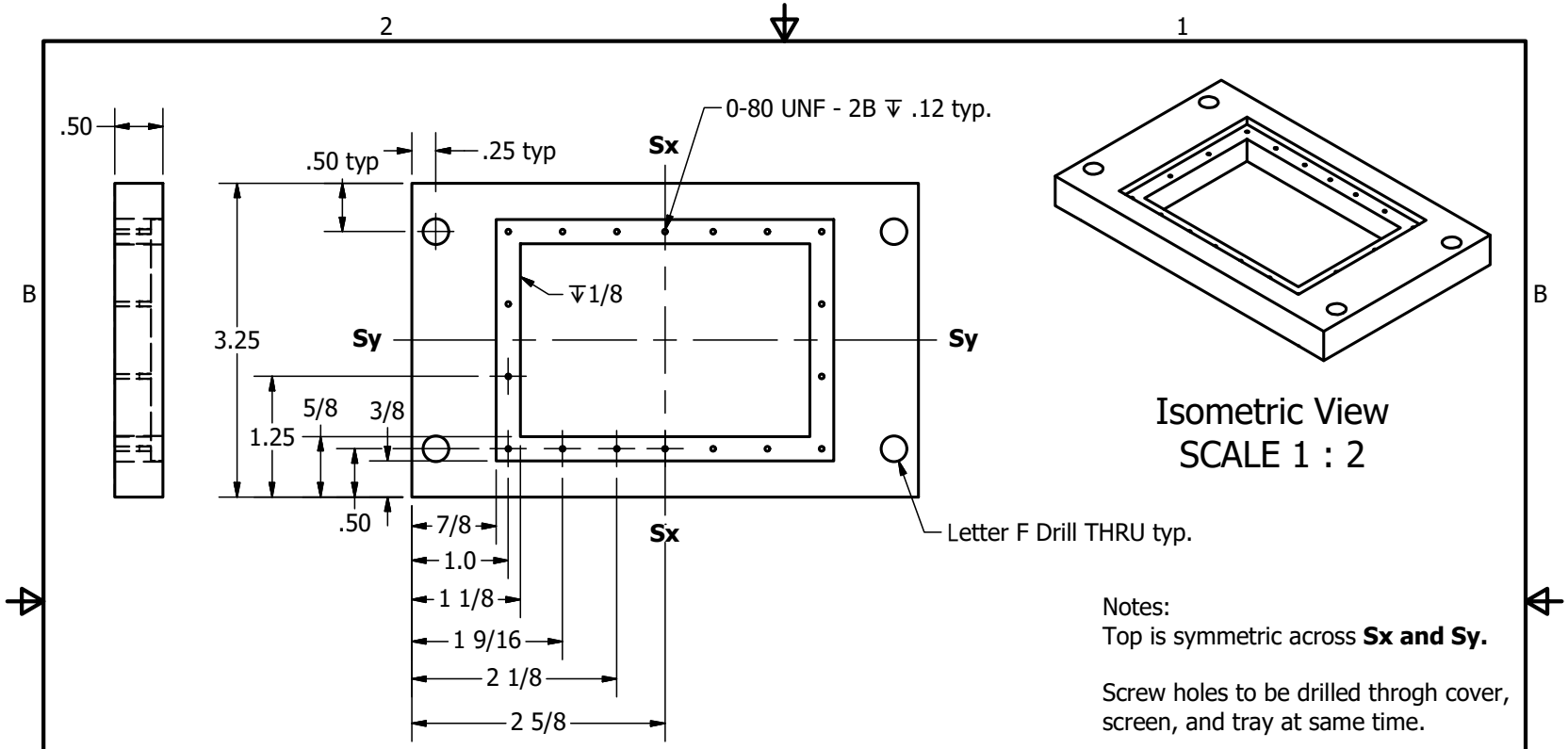

Isometric View
SCALE 1 : 2

Notes:
Top is symmetric across **Sx and Sy.**

Screw holes to be drilled throgh cover, screen, and tray at same time.

All units inches.

DRAWN Jordan Argyle	11/28/18	University of Idaho
CHECKED		TITLE: Holding Box Top
QA		
MFG		
APPROVED		

SIZE		DWG NO	REV
A		Holding Box - Top	2

SCALE 2 : 3 | 5 of 10

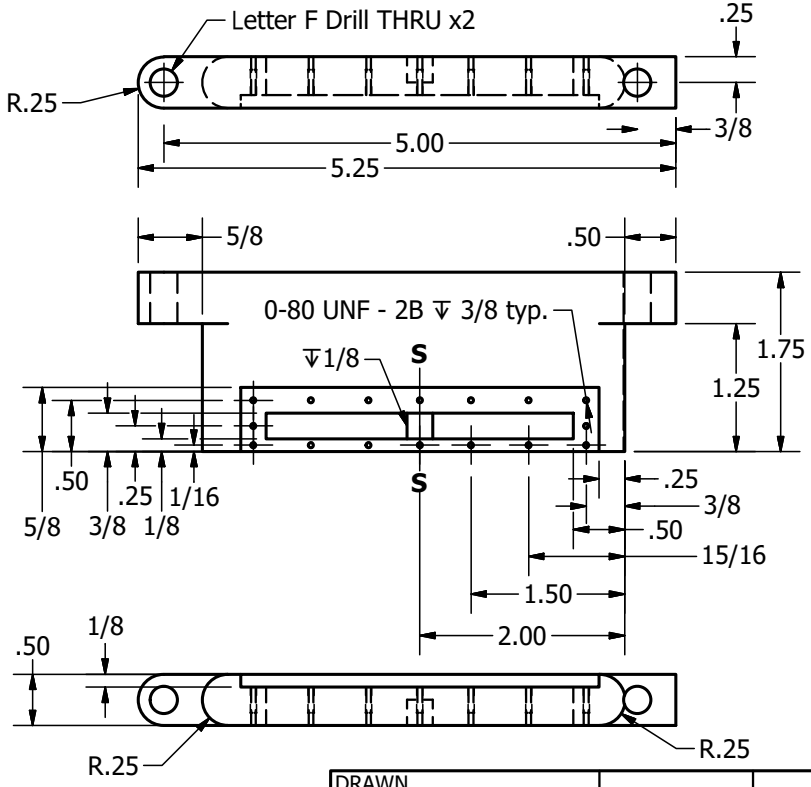

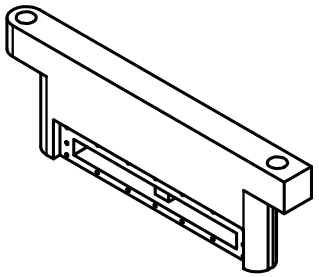

Isometric View
SCALE 1 : 2

Notes:
Screen slot on door is symmetric across **SS.**

Screw holes to be drilled throgh cover, screen, and tray at same time.

All units inches.

DRAWN Jordan Argyle	11/27/18	University of Idaho
CHECKED		TITLE: Holding Box Door
QA		
MFG		
APPROVED		

SIZE		DWG NO	REV
A		Holding Box - Door	2
SCALE 2 : 3			6 of 10

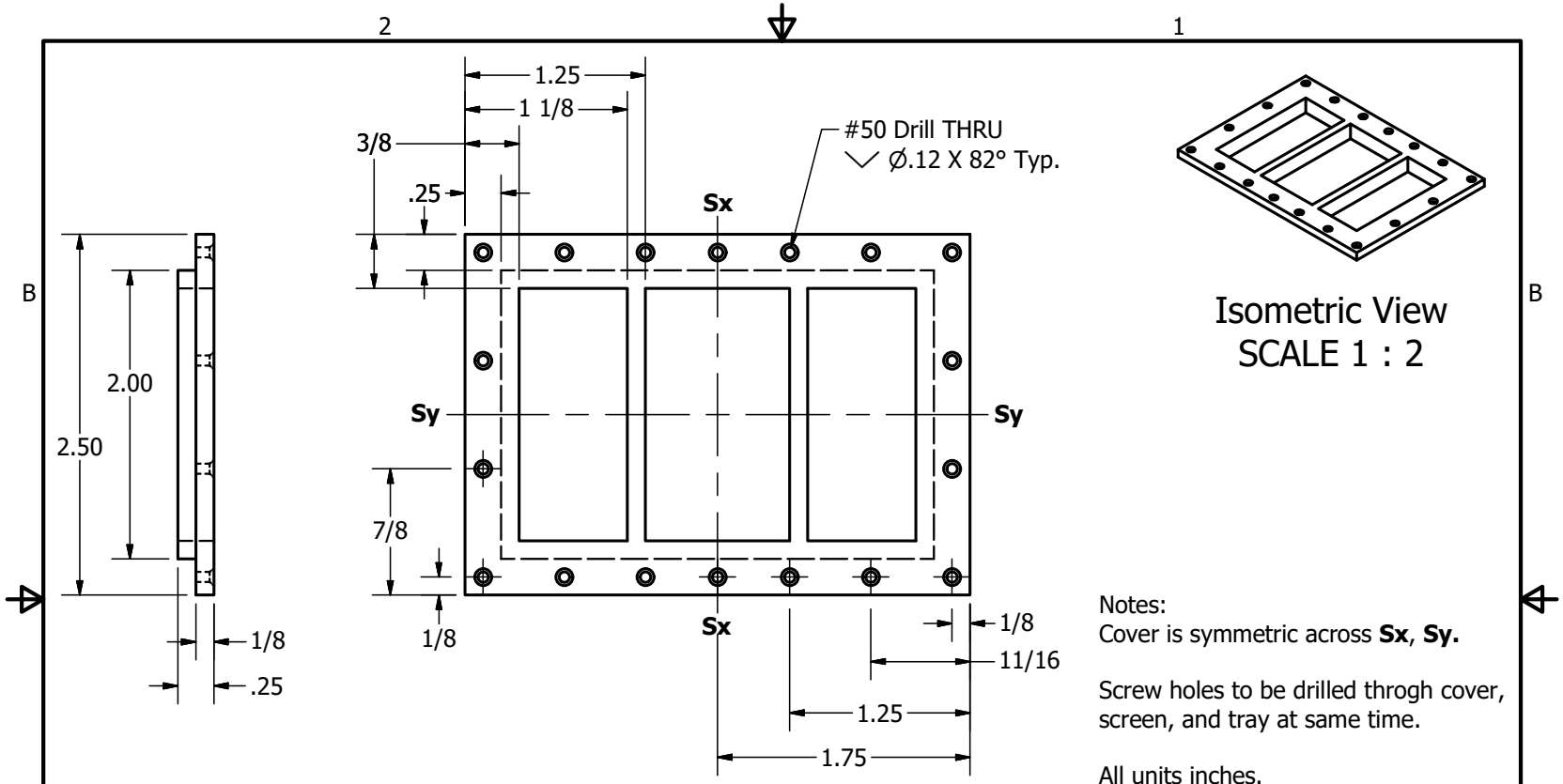

Isometric View
SCALE 1 : 2

Notes:
Cover is symmetric across **Sx**, **Sy.**

Screw holes to be drilled throgh cover, screen, and tray at same time.

All units inches.

DRAWN Jordan Argyle	11/27/18	University of Idaho
CHECKED		TITLE: Large Screen Cover - Tops x2
QA		
MFG		
APPROVED		
SIZE A		DWG NO Screen Cover - Large / REV 2
SCALE 1 : 1		7 of 10

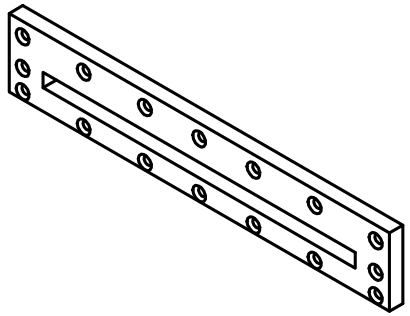

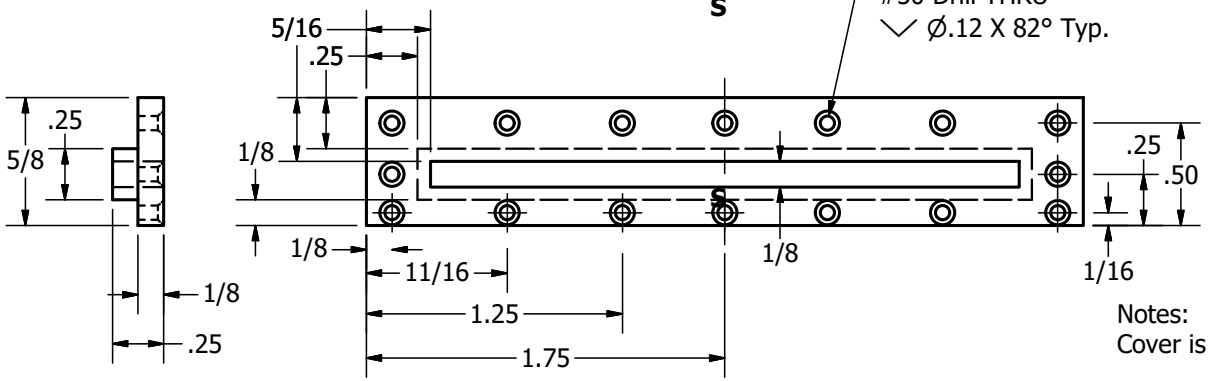

Isometric View
SCALE 1 : 1

Notes:
Cover is symmetric across **SS.**

Screw holes to be drilled throgh cover, screen, and tray at same time.

All units inches.

DRAWN Jordan Argyle	11/29/18	University of Idaho
CHECKED		TITLE: Small Screen Cover - Fronts, Tray Back x3
QA		
MFG		
APPROVED		
SIZE A		DWG NO Screen Cover - Small
SCALE 4 : 3		REV 2
		8 of 10

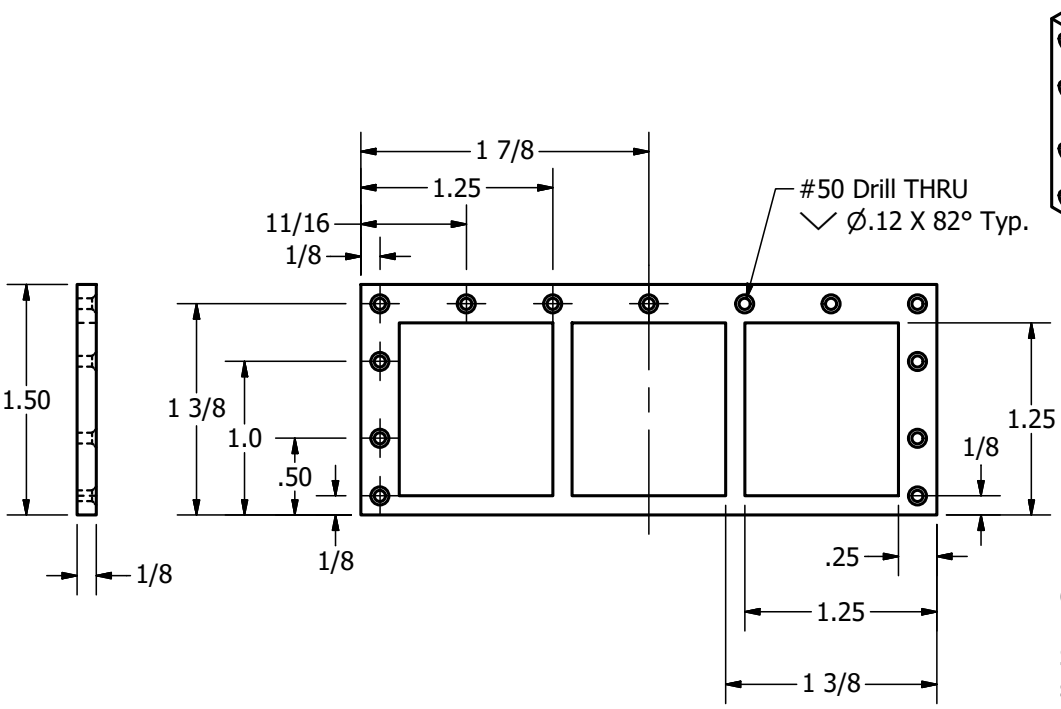

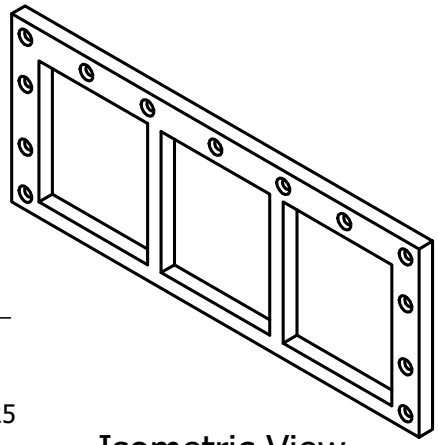

Isometric View
SCALE 1 : 1

Notes:
Cover is symmetric across **SS.**

Screw holes to be drilled throgh cover, screen, and tray at same time.

All units inches.

DRAWN Jordan Argyle	11/29/18	University of Idaho
CHECKED		TITLE: Medium Screen Cover - Box Back
QA		
MFG		
APPROVED		
SIZE A		DWG NO Screen Cover - Medium / REV 2
SCALE 1 : 1		9 of 10

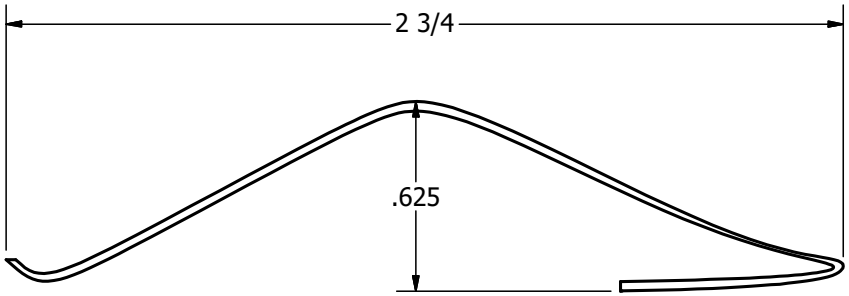

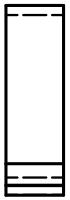

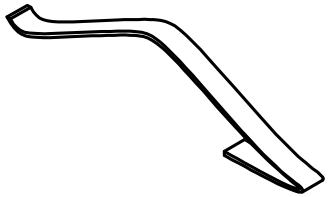

Isometric View
SCALE 1 : 1

Notes:
Purchased. Based on corner-mounted tension spring model #L 5794 at
https://www.homedepot.com/p/Prime-Line-3-16-in-Corner-Mounted-Tension-Spring-L-5794/100536660

All units inches.

DRAWN Jordan Argyle	11/29/18	University of Idaho
CHECKED		TITLE: Leaf Spring
QA		
MFG		
APPROVED		
SIZE A	DWG NO Leaf Spring	REV 2
SCALE 2 : 1		10 of 10

Appendix D: LabVIEW Code

This appendix documents the Laboratory Virtual Instrument Engineering Workbench (LabVIEW) code written for data collection for the simplified system as it was built. The LabVIEW code, from National Instruments, was chosen for data collection because the team already had experience working with it and because much of the hardware was already owned by the department. The data acquisition (DAQ) was set up for a four-slot cDAQ-9174 with two NI-9211 thermocouple (TC) modules and an NI-9205 voltage module for the pressure transducer. A Tempco TEC-9100 temperature controller in a TEC-1000 chassis provided the power for the heaters, using a K-type TC directly connected to the getter tank flange.

The front panel shows the piping and instrumentation diagram (P&ID) of the as-built system with readouts for the instrumentation positioned where it would sit on the P&ID. Below this is a grid of data to assist the experimenter, including expected pressures and gas purity. The program starts by pre-computing the experimental parameters to populate the grid, which assists the experimenter in knowing when steps in the procedure have reached their conclusion. After these are computed, the program reads in four TCs (T1 in the fill tank, $T2_a$ and $T2_b$ in the bottom of the getter tank, and $T2_{check}$ on the getter tank flange to check what our controller TC should have seen) and the pressure transducer every two seconds. It displays the data read in on the P&ID, tracks them on a chart, and writes them to a file. The $T2_{aandb}$ have their signals averaged.

What follows is a replication of a text document meant to explain the code to other members of the research team. Specifically:

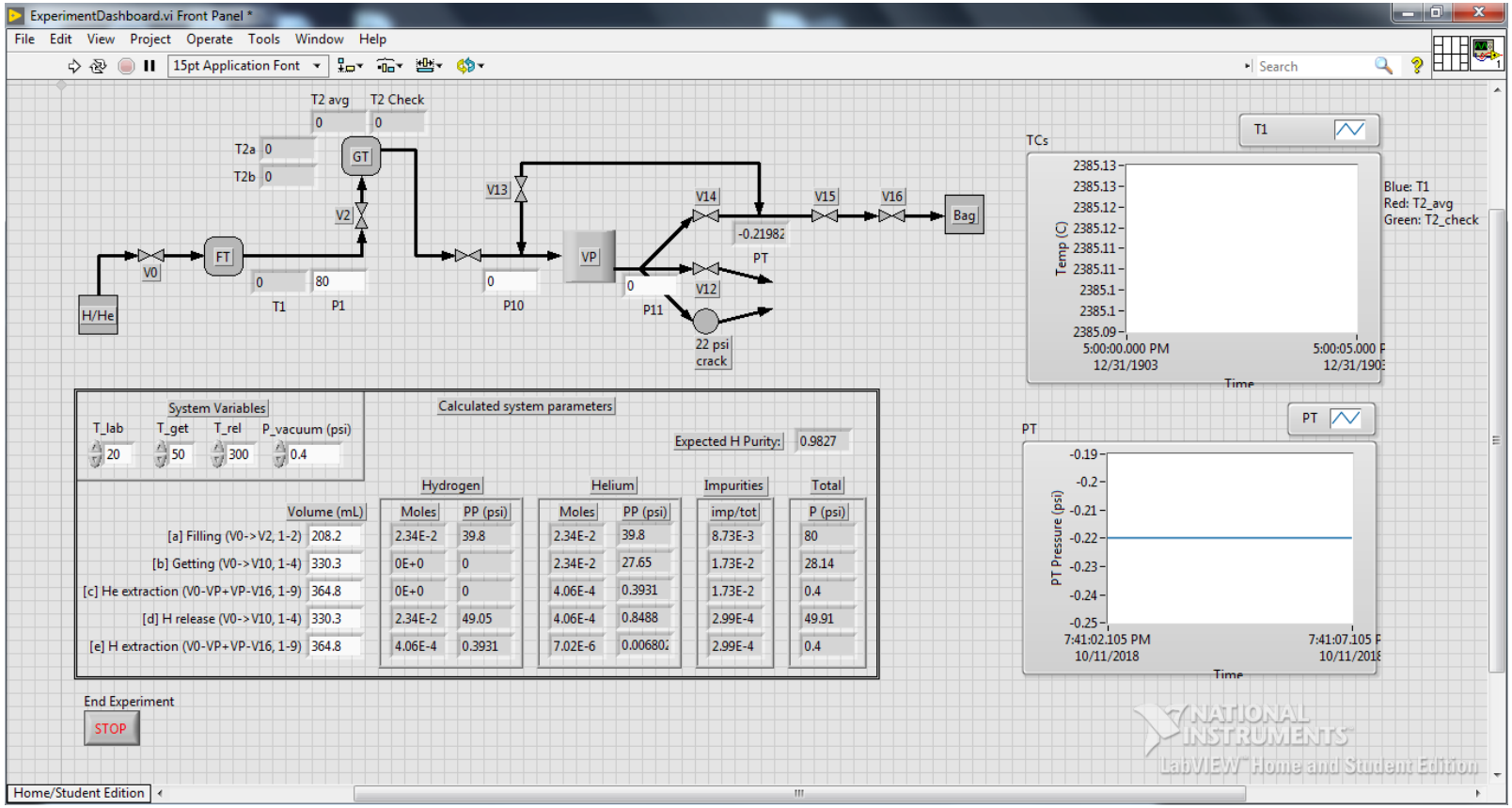

A P&ID of the system with indicators for the thermocouples and pressure transducer, as well as the locations of the pressure gauges. I will probably add some logic to take values entered in those and tell you something about the program's run, but for now, they don't do anything. Below the P&ID is a pre-calculation of the system parameters. It takes P1 (fill pressure), as well as the lab temperature (T_{lab}), temp of heater during getting phase (T_{get}), temp the getter will be heated to release the H (T_{rel}), and the pressure when pulling a vacuum (P_{vacuum}). It also takes all the volumes entered in mL, and then computes the moles and partial pressures using known values. To the right are the charts so you can see the recent histories of the thermocouples and pressure transducer. At the very bottom is a button to stop data collection.

The pre-calculated values, for some reason I can't find, require that the code be run 3 times to fully compute, but otherwise it's a nice way of knowing about what can be expected during the run. Massive deviations from these values should be carefully evaluated, and could indicate problems with volume measurements (most likely), leaks, or failure to get/release. Following this page is the code behind these front-panel objects.

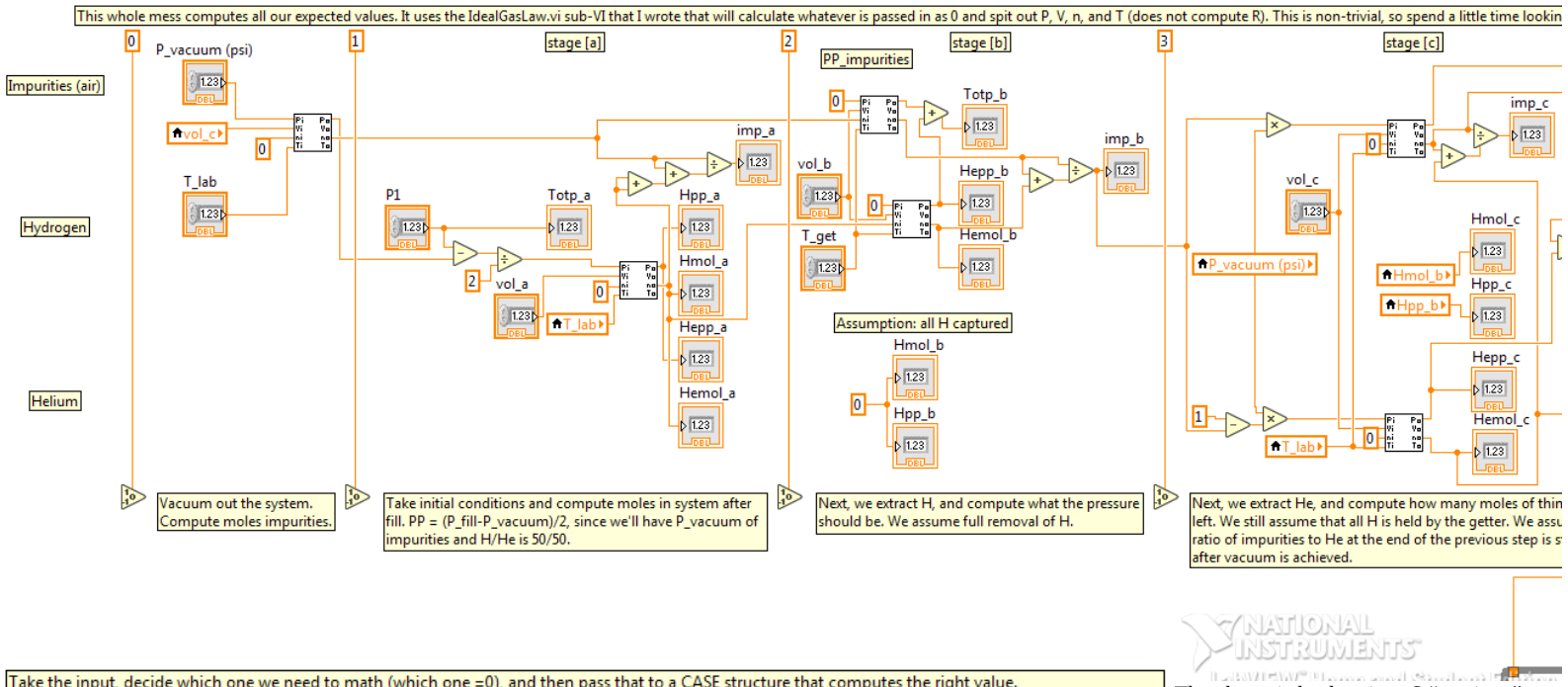

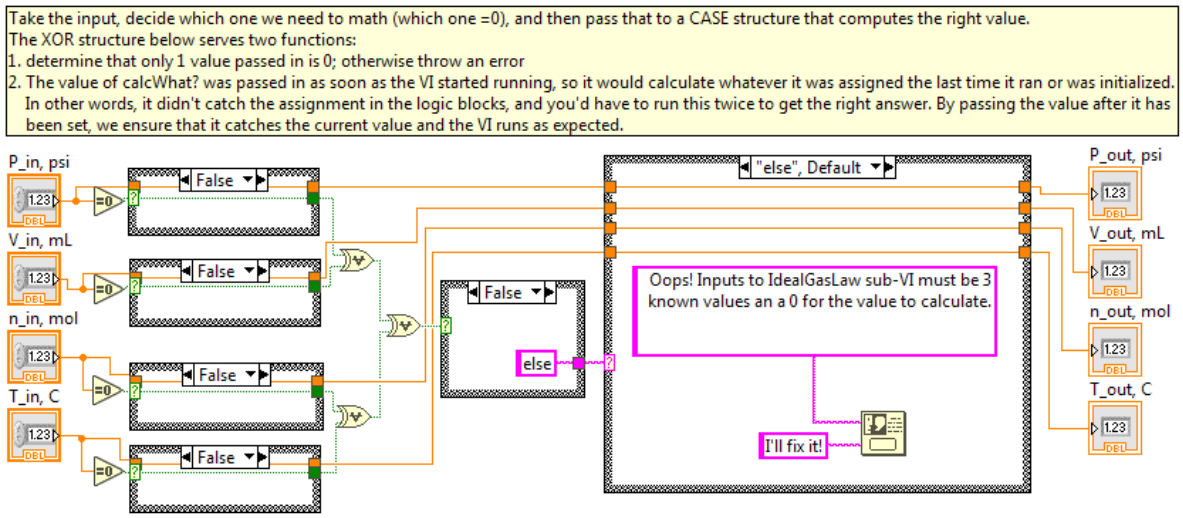

The above is broken into 6 “sections” using +/- checkers and the number of segments passed. I tried to type below what each segment does, so hopefully that tells you.

To the right is the code for the ideal gas law (the block with P, V, n, T in on left and out on right. The logic here is that it looks at which one is 0, and uses that to figure out what to compute. If not 0 (shown), it passes the value right through and to the main computation block. However, if there were no 0’s or multiple 0’s (shown), then “else” is passed into the computational block, and it shows an error. In this case, the values passed in are passed back out to make debugging easier.

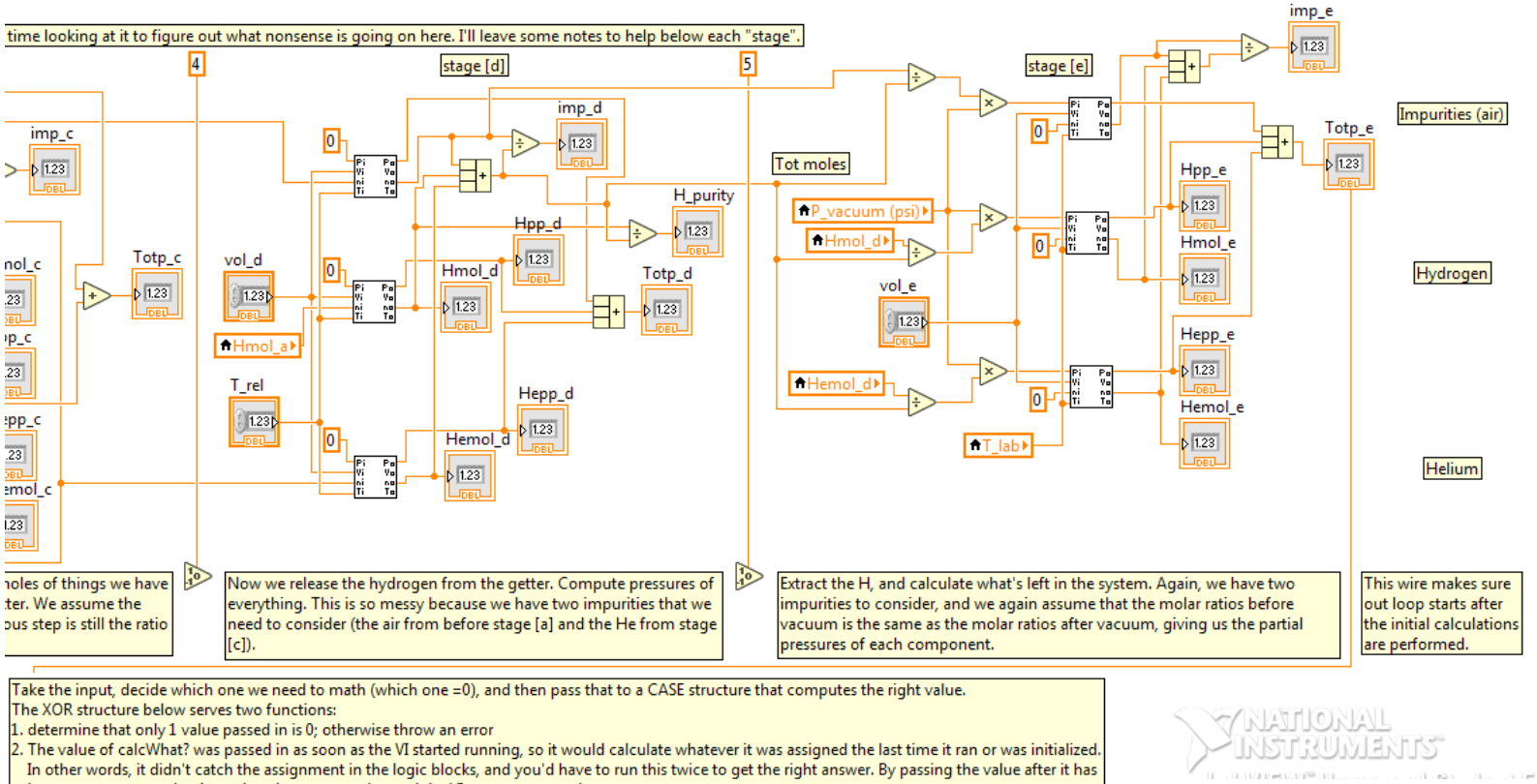

Again, above is the rest of the pre-calculation logic.

To the right, if any value is 0 (shown for all inputs), then the picker is set to a value that will compute that variable. Assuming only one 0 is passed in (shown), the value to compute is passed as the selector to the case block. Calculation for pressure is shown to the right. The values not computed are passed straight through.

The other computational blocks (for V, n, and T) are on the next page.

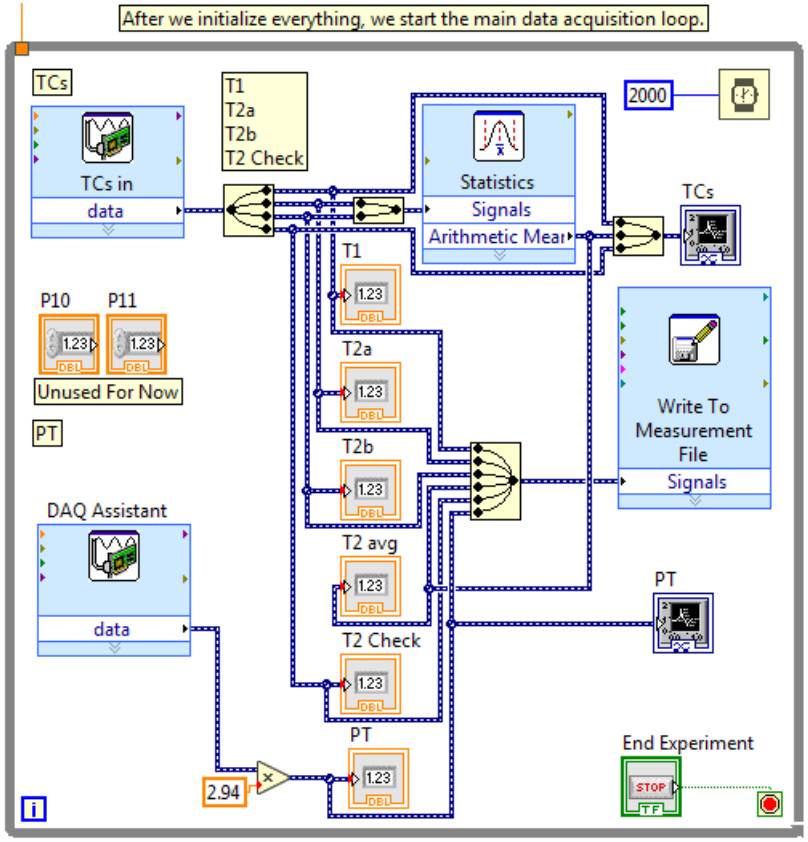

Above: after the pre-calculations are completed, a wire passes into this loop. By wiring it this way, it forces LabVIEW to run all calculations before it starts this loop. The loop runs every 2 seconds, and reads in 4 thermocouples (T1, both T2's in the bottom of the tank, and the one lashed to the top of the flange where heat transfer is more favorable to controlling the heater), and the pressure transducer.

The transducer (DAQ Assistant at the bottom left) is a raw voltage, so we multiple by 2.94 to convert to PSI. It's values are passed to the PT indicator, the PT chart, and a merge for writing to a file.

The TCs are less straightforward. T1 is passed straight to the chart, indicator, and merger for file writing. The two internal T2's are averaged together, and the mean is written to the chart, while both individual values are written to their respective indicators and merged for writing to the file. The T2 lashed to the flange is passed unaltered to the chart, indicator, and merged for output.

All 5 measurements + the calculated average are smashed into a single data stream that is written to a row of the measurement file (a .cvs file for easy access in Excel or through Python). Each row, therefore, will be: Timestamp, T1, T2a, T2b, $T2_{avg}$, $T2_{check}$, PT. An example might be 10/19/2018 13.05.24, 35, 60, 61, 60.5, 90, -13.9

Right: The blocks for calculating V, n, and T. Note that, again, the values not being computed are passed through unaltered (straight lines on top).

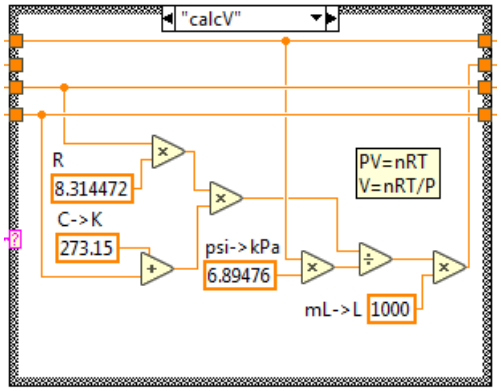

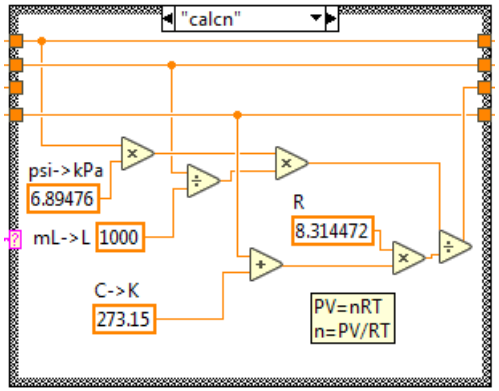

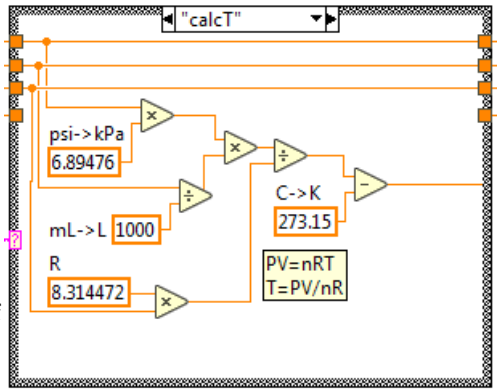

Appendix E: Redesigned System Analysis

This appendix explains the thermal analysis of the getter tray system using the **An**alysis **Sys**tem (ANSYS) code package, version 19.1. Discussion will cover the geometry and data used to run the simulation, details of the model parameters and setup, and analyses the results with the goal of determining how long the new design should take to get to temperature, and how that temperature will be distributed. This analysis verifies that the getter tray design will not suffer from the same problems the vertical getter tank had, and provides the confidence that the tray design will meet the sponsors needs.

E.1 Setup

The different steps of setting up the problem will be discussed in the order that they appear in the Transient Thermal block used to set up the problem in ANSYS (see Fig. E.1 below).

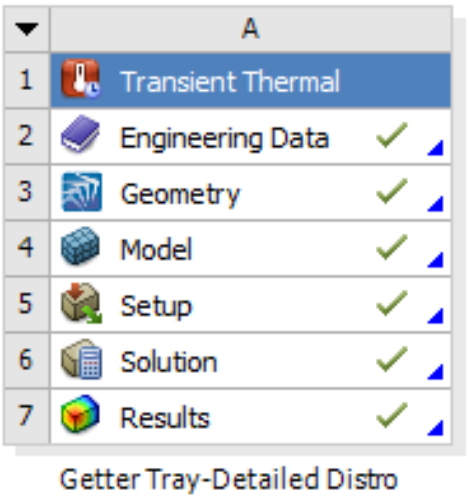

Figure E.1: *Transient thermal analysis block as shown in the Project Schematic of ANSYS Workbench R19.1.*

E.1.1 Engineering Data

The Engineering Data section is where the materials to be used in the analysis are built into a project material library containing all the necessary thermophysical properties ANSYS needs to solve the model. Pre-configured libraries have common materials, and there are provisions for building custom libraries with user-defined materials.

Since this is a thermal analysis, the material Aluminum was chosen from the Thermal Materials library. It specifies a density, ρ_{Al}, of 2.689 $\mathrm{g\,cm^{-1}}$, an isotropic thermal conductivity, k_{Al} of 237.5 $\mathrm{W\,m^{-1}\,K^{-1}}$, and a specific heat, $\mathrm{C}_{p,Al}$, of 0.951 $\mathrm{J\,g^{-1}\,K^{-1}}$. The ZrCo getter powder, being a non-standard material, was manually added using data from Sei-Hun *et al.* [55], who had values for the same getter that we purchased. Sei-Hun *et al.* measured true density, ρ_{ZrCo} of 7.6238±0.0093 $\mathrm{g\,cm^{-3}}$, and temperature dependent thermal conductivity and specific heat values, shown below in Table E.1.

Table E.1: *Heat capacity and thermal conductivity of ZrCo powder over the temperatures expected during the experiment.*

T (°C)	k_{ZrCo} ($W\,m^{-1}\,K^{-1}$)	$C_{p,ZrCo}$ ($J\,g^{-1}\,K^{-1}$ J/gK)
25	0.139	0.328
100	0.125	0.339
200	0.108	0.308
300	0.081	0.299
400	0.122	0.314
500	0.133	0.330

These properties are sufficient for ANSYS to solve a transient thermal model.

E.1.2 Geometry

The CAD model imported included a simplified holding box, the heating plate, the getter tray, and powder to fill the tray wells. This simplified geometry is shown in Fig. E.2. Screens, the front door, screws and bolts, holes for screws and bolts, and the leaf springs were not included in the model. Together, it consisted of 78 bodies total, with 75 of those being powder in the wells.

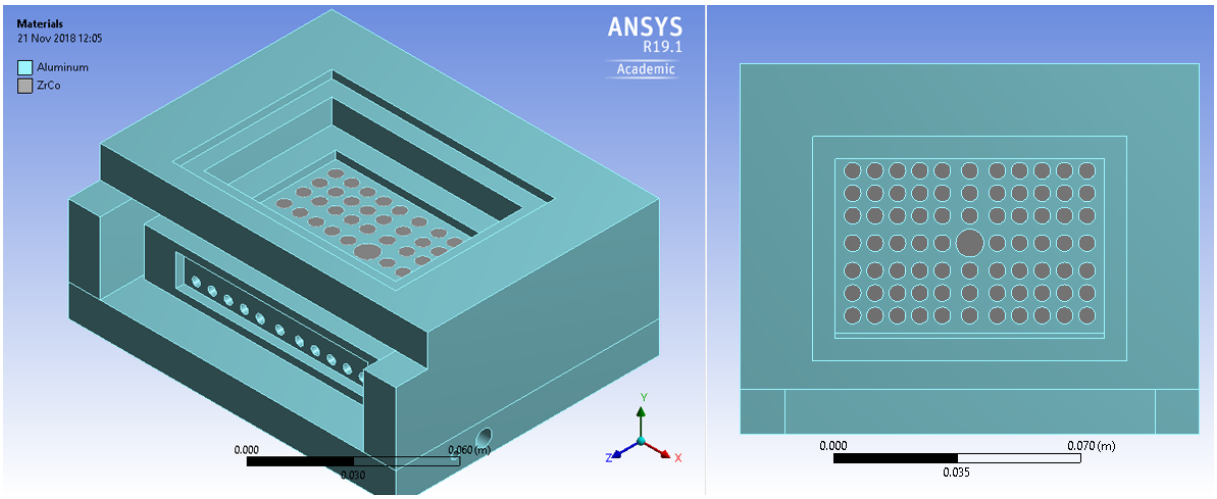

Figure E.2: *Material arrangement for the analysis of the new design where green is aluminum and grey is ZrCo powder; Left: Orthographic view, Right: View from directly overhead. This image is a replication of Fig. 4.2.*

E.1.3 Model

The Model section defines connections, mesh, and selections. The most important connections are the bottoms of the getter tray and holding box with the top of the heater plate. Connections between the powder and the getting tray were also established. These connections provide boundary conditions

for the solver as it moves from mesh nodes on one body to nodes on another body.

Because the geometry is simple, the automatic meshing tools in ANSYS were used, specifying the Transition Speed (fast or slow) and the Span Angle Center (coarse, medium, or fine). According to the ANSYS user guide [56], the Transition Speed affects the rate at which adjacent elements will grow, and the Span Angle Center sets the goal for the refinement of curvature, *i.e.*, the mesh will subdivide in curved regions until the individual elements span an angle as close to the goal as possible. The user guide specifies that a setting of "Coarse" results in angles from 91° to 60°, while "Medium" results in angles from 75° to 24°.

A fast Transition and coarse Span Angle Center were first used, resulting in 101,898 nodes and 39,533 elements. This meshing was used for the first few simulations to understand the time steps needed to understand how the system behaves. After this behavior was estimated, a medium Span Angle Center with slow Transition was used, generating 562,955 nodes and 361,599 elements, which is 5.53 and 9.15 times more, respectively, than the coarse mesh. The results from the two mesh configurations were within 5% of each other.

E.1.4 Setup

The Setup section is where boundary conditions are applied and solver settings, such as the time steps, are set. Generally, the larger amount of time spanned over a time step, the larger the sub-steps are. For this reason, 23 major time steps were used to divide one hour of heating and one hour of cooling. In both cases, the first few time steps for each hour were short (a minute or so), with the steps increasing in length over the hour.

Radiation to lab temperature (20 °C was applied over all exterior surfaces, correlated to ambient with an emissivity of 0.25 over both simulated hours (typical for aluminum, [57]). An assumption was made that a flow of mixed H and He would be established, producing a convection film coefficient, h, over the same external surfaces of 32.18 at a temperature of 22 °C. This coefficient was calculated with averaged properties (*e.g.*, dynamic viscosity, thermal conductivity, *etc.*), using equations from a heat and mass transfer textbook [57]. This approximation of covection was applied for the full two hours of the simulation. Because this is a scoping analysis, this approximation of convection was sufficient.

Finally, a heat flow was applied to the inside surfaces of the heater holes on the heater plate to a total of 800 W over the first hour, and all heating was cut for the second hour. The heating was chosen assuming the use of two of the same 400 W heater rods that were originally planned for the system.

E.2 Results

The results showed a heating to activation temperatures of 450 °C within 7 minutes in a vacuum, and would require nearly 25 minutes with convective flow of a purge gas. After the powder was activated, the recommended getting temperature could be obtained in less than two minutes for 100 °C, and less than five minutes for 200 °C assuming convective and radiative cooling. The system required 42 minutes of cooling to reach a safe removal temperature, assumed to be 40 °C.

The temperature distribution in the getter powder at capturing temperature is shown below in Fig.

E.3. To determine how close the individual getter well temperatures were to each other, individual temperature probes were generated in the corner wells, the center wells along each edge, and the center well (see Fig. E.3; tracked wells marked in green). The other side of Fig. E.3 is a plot of the temperature of the 9 wells over the full two hour simulation. Because the spread between the wells is not easy to see with a full ranged plot, a subset of Fig. E.4 showing the average well volume temperature from start to 100 °C is also shown (Fig. E.5). The standard deviation (σ) between the temperatures of the wells over the run is plotted in Fig. E.6, and is interpreted as $T_{well} = T_{mean} \pm \sigma$.

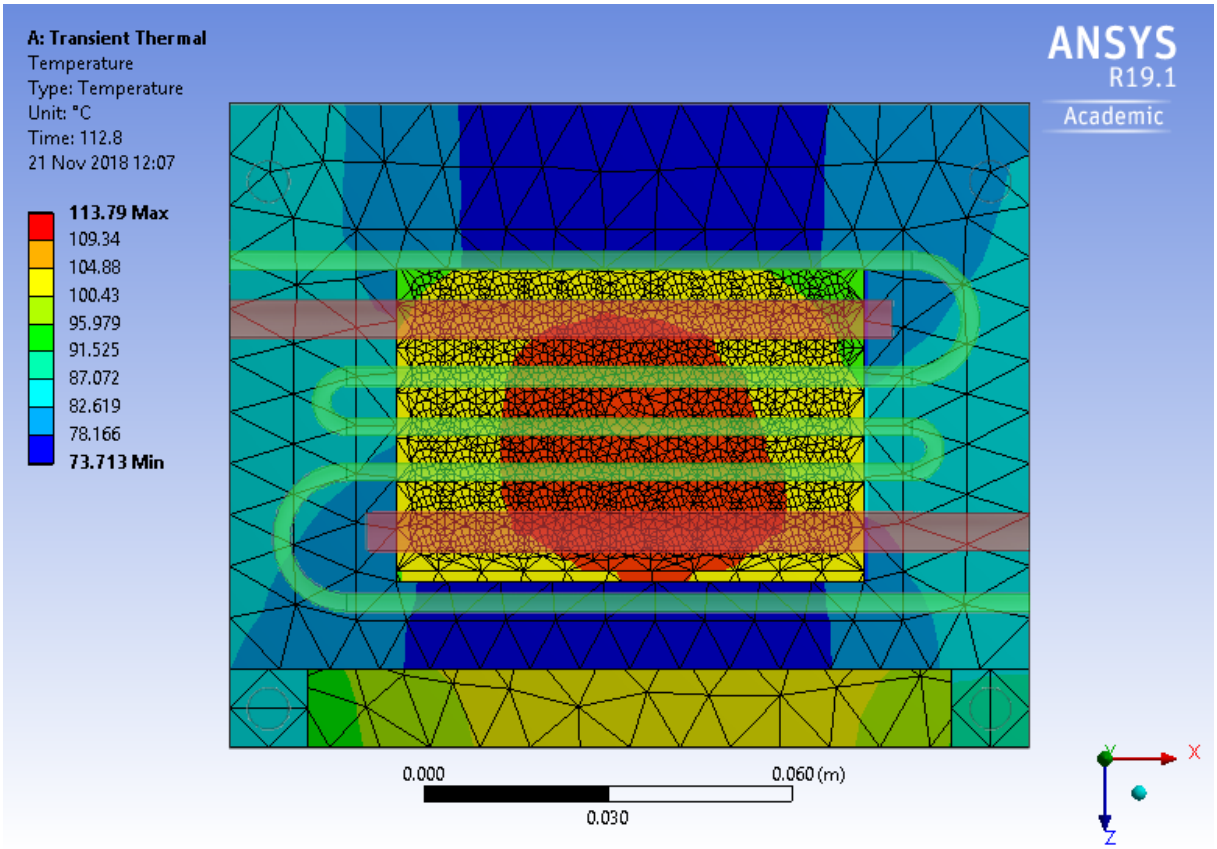

Figure E.3: *Temperature distribution in getter tray around the time that getter powder in all wells reaches 100* °C*, with location of heaters (light red) and the cooling channel (light green) superimposed. The heating and cooling both are supplied below the getter tray. Colors for the getter bed (center) exaggerated for clarity. The red region was orange, the yellow region remained the same, and the vivid green in the corners was the pale green under yellow in the key. This image is a replication of Fig. 4.3.*

While the distribution is not uniform, the deviation was less than 3 °C during heating. The standard deviation would be smaller (*i.e.*, well temperatures more uniform) if (1) the temperature was held constant, *i.e.*, controlled, as it would be during an experimental run; (2) the tray was made of a more conductive material, *e.g.*, copper; or (3) copper or aluminum beads were mixed into the powder to increase its thermal conductivity.

The final important fix to verify for this new design was what the TCs read during the process. Temperature probes over the surface of the TC holes revealed that the powder mean temperature was,

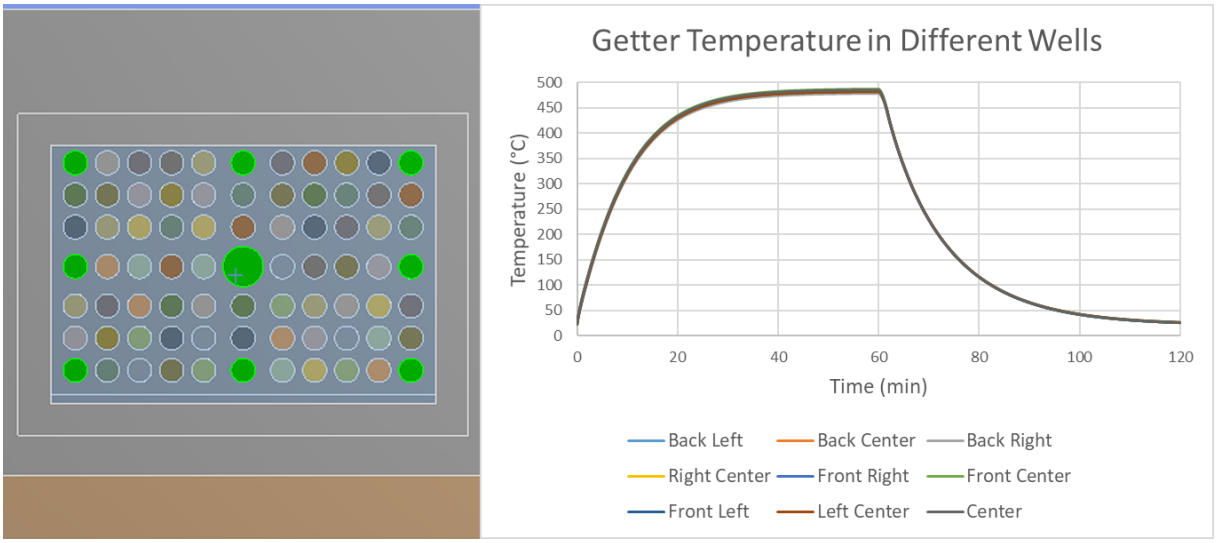

Figure E.4: *Temperature profile of the tracked wells over the full two hour run; Left: The nine wells where average volume temperature was tracked, marked in green; Right: Temperature profiles of the nine wells over the full two hour run. This figure is a replication of Fig. 4.4.*

on average, +0.21/-0.047 °C off from what the TCs showed and +0.57/-1.34 °C when furthest off. The closer positioning of the TCs to the powder and in the path of conduction, yielded the benefit of accurately measuring the powder temperature. Even when furthest off, it showed the mean powder temperature to less than the standard deviation between wells.

This analysis demonstrates that the redesign solves the problems encountered with the vertical getter tank presented in Appendix B. Furthermore, the same manufacturing team that made the vertical getter tank noted the ease with which the getter tray system could be produced, going so far as to say it would take only one day to build. Upon seeing the results of this analysis, all others involved in this project (including the project sponsors) concluded that the tray could meet the objectives originally set for the project.

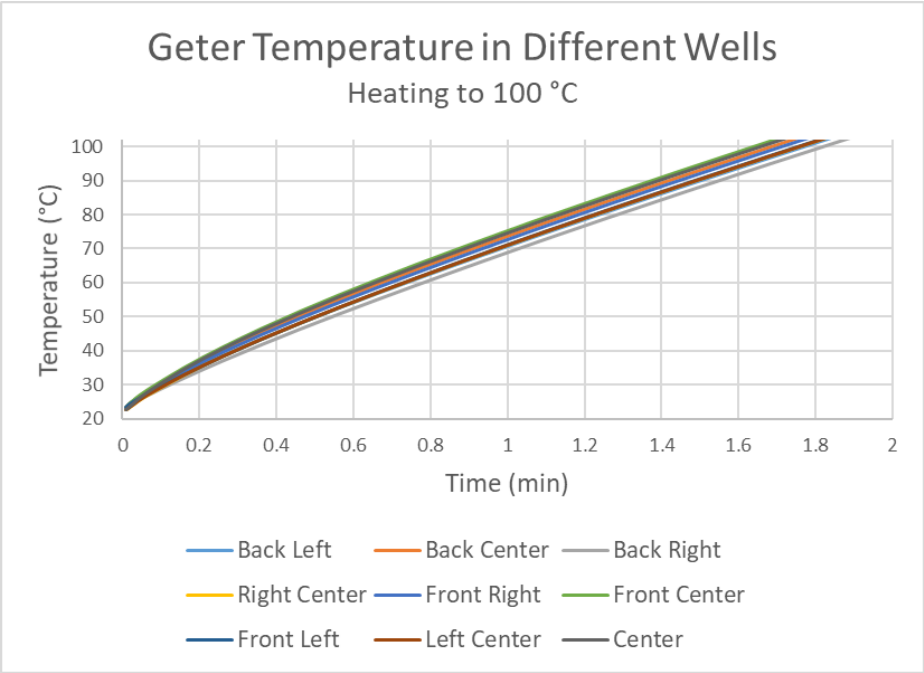

Figure E.5: *Temperature profiles of the nine wells in the first two minutes up to 100* °C*. Note the slight spread between different wells, with the back right coldest (102* °C *at 112.8* s*) and the front center the hottest (109* °C *at 112.8* s*).*

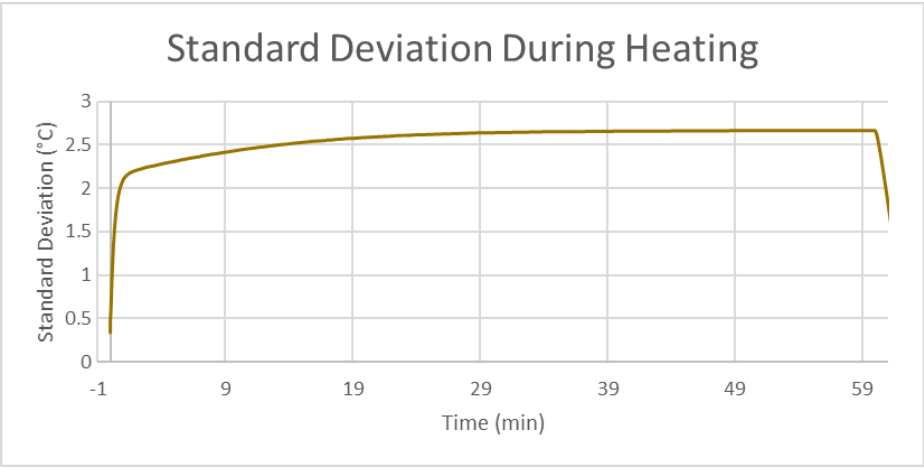

Figure E.6: *Plot of the standard deviation between the tracked well temperatures over the heating portion of the run. During cooling, the deviation rapidly plummets from a high of 2.665 at 58 minutes of heating to less than one after 2 minutes of cooling.*